A Strategy for the Use of Light Emitting Diodes by Autonomous Underwater Vehicles

by

Joseph R. Curran

S.B. Ocean Engineering
Massachusetts Institute of Technology (1999)

Submitted to the Department of Ocean Engineering
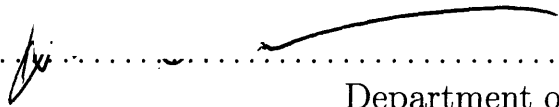in partial fulfillment of the requirements for the degree of

Master of Science in Ocean Engineering

at the
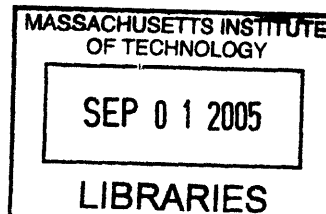
MASSACHUSETTS INSTITUTE OF TECHNOLOGY

June 2004

Author . . . .
Department of Ocean Engineering
May 24, 2004

Certified by . . . .
Chryssostomos Chryssostomidis
Henry L and Grace Doherty
Professor of Ocean Science and Engineering
Thesis Supervisor

Accepted by . . . .
Michael S Triantafyllou
Professor of Ocean Engineering
Chairman, Department Committee on Graduate Students

A Strategy for the Use of Light Emitting Diodes by Autonomous Underwater Vehicles

by

Joseph R. Curran

Abstract

Light Emitting Diode (LED) technology has advanced dramatically in a few short years. An expensive and difficult to manufacture LED array containing nearly 100 individual LEDs and measuring at least 5 cm^2 can now be replaced by a single 5 Watt LED smaller than a quarter. As the light output for a given package size continues to increase, doubling every two years, it is possible to consider using these new LEDs to improve existing lighting systems and to explore non-traditional methods of underwater photographic illumination.

So, can these high-output LEDs be used for underwater illumination, under what circumstances are they a good choice, and what is the optimal way to deploy them for a given set of conditions? In this thesis I attempt to answer these questions.

In this thesis, I tested these 5W LEDs in a number of conditions and orientations in order to simulate the lighting conditions experienced by autonomous underwater vehicles (AUVs) illuminating and imaging targets on the ocean floor. These LEDs were characterized and compared to existing lighting systems and methods. Their suitability for use both as vehicle-carried illumination and off-the-vehicle lighting packages was examined. Finally, conclusions were drawn as to the effectiveness of the 5W LEDs for underwater illumination and a guideline for LED illumination is presented to help AUV researchers determine the optimal lighting package for use on their missions.

Acknowledgments

To Gini, Nana and Bub.

Contents

List of Figures

7

10

List of Tables

15

Chapter 1

Introduction

Like photography in air, underwater photography depends greatly on good illumination. Unlike traditional photography, however, as much depends on the illuminated water volume as on the illumination of the actual subject. Water is much denser than air, and even most pure natural water contains suspended and dissolved material. This extra material and the water itself present unique problems to the underwater photographer. As light travels from the source to the target and then back to the camera, it is absorbed, scattered, and sometimes reflected directly at the camera without first illuminating the target. In most cases, this *backscattered* light presents the greatest challenge.

Absorption, scattering, and especially backscattered light all reduce the contrast of images taken by underwater cameras. This reduction in contrast means that what would otherwise be black and white in air is now two shades of gray. To reduce the contrast loss due to backscatter, the source/receiver separation is critical. That is to say, with all other things being equal, the greater the distance the light source is from the camera (receiver), the better, generally, the image will be.

Be it an autonomous underwater vehicle (AUV), remotely operated vehicle (ROV), submarine, or diver, a light source for the underwater camera traditionally had to be carried by the vehicle itself. The lateral source/receiver separation is then limited by the size of the vehicle. By using the concept of off-the-vehicle lights, which place the light source either on the bottom or on a separate vehicle, greater lateral separations are possible. Source/receiver geometries that take advantage of vertical separations, which minimize the total illuminated

water volume, are possible as well.

Of course, with greater source/receiver separations, more powerful light sources are required because the water tends to attenuate the light and reduce its illumination effectiveness. For small AUVs, which operate without a tether and are dependent on batteries for power, power consumption is of critical importance. A balance must be found to maximize light output, minimize power consumption, equipment size and weight, and reduce costs.

This is where LEDs come in. While no perfect system exists for all cases, I will show that LEDs have developed to the point that they are now very efficient in terms of size and power usage compared to other traditional light sources. As costs drop, new methods of deploying off-the-vehicle lights can be considered. If the light source can be made independent of the vehicle, and can be thought of as disposable, a new model of lighting may be developed which places light source on the ocean floor closer to the target than the imaging vehicle. This geometry takes advantage of vertical source/receiver separation and can increase lateral separation beyond the bounds imposed by the size of the AUV.

Systems called *lighthouses* in this work place large, focused light sources behind the vehicle. Systems I choose to refer to as *candles* place small, diffuse light sources very close to the target, in front of the camera. By using off-the-vehicle lights independent of the AUV, power consumption is no longer a concern of the AUV (it is still a concern, of course). Lighthouses can take advantage of larger lateral source/receiver separation and can further reduce backscatter by placing the most highly illuminated water volume, immediately surrounding the light, behind and away from the camera. Candles can minimize the total illuminated water volume to a small conical patch in front of the camera.

By simulating the geometry, LED candles, LED lighthouses, and AUV carried LEDs were tested experimentally and compared to other existing lighting systems. The effectiveness of LED lighting for underwater photography was analyzed for a variety of water conditions, light and camera locations, LED wavelength, and source illumination intensities.

After careful contrast and image quality analysis of the resulting images, it is possible to generate a set of guidelines for the optimal use of LED lights for underwater photographic illumination by AUVs. Taking into account the power and size limitations of AUVs, LED light sources show great promise for underwater photographic illumination.

Chapter 2

Background

This chapter provides an overview of the interactions of light and water as they pertain to underwater photography. It begins with a review of the scientific terms of light and illumination, followed by a detailed explanation of light transmission in sea-water. Existing illumination sources are described, with a metric to judge the efficiency of a given light source. How camera systems capture images is detailed with emphasis on the relationship between light and an image. All of this is tied together in the final sections detailing the current state of real and simulated underwater photography.

2.1 Light Measurement

This thesis deals with light in an underwater environment. Before addressing the characteristics of water that make this challenge unique, it is important to review certain properties shared by light propagating in all mediums.

2.1.1 Solid Angles

First, a quick geometry lesson. In the study of light, it is often useful to employ the geometry of three dimensional solids. Rather than two lines describing a 2D plane angle, a conical surface encloses a *solid angle*, represented by the Greek letter ω. The conical surface may be of arbitrary shape, that is to say cross sections need not be circular. When a cone of height

r encloses a region on a sphere of radius r of area equal to r^2, the associated solid angle is said to be equal to one *steradian*. For other enclosed surfaces of area S, the solid angle is define as

$$\omega = \frac{S}{r^2} \tag{2.1}$$

Note that a sphere of radius r and surface area $4\pi r^2$ would contain 4π steradians, or 4π sterad.

Now imagine a spherical onion is parallel sliced to make onion rings. The surface of one resulting onion ring, which could be described as the area enclosed by two concentric conical surfaces sharing an apex, would describe a special solid angle

$$\omega = 2\pi(\cos \alpha_1 - \cos \alpha_2) \tag{2.2}$$

Angles α_1 and α_2 represent the half-angles of the cones, from their axes to their sides. If the onion is the Earth, angles α would start at $0°$ at the north pole, and go to $90°$ at the equator. For example, for $alpha_1 = 10°$ and $alpha_2 = 40°$, the onion slice described by the corresponding solid angle would lie between $50°$ and $80°$ north latitude. For conditions where $\alpha_1 = 0°$, i.e. for a simple cone, equation 2.2 reduces to

$$\omega = 4\pi \sin^2 \frac{\alpha_1}{2} \tag{2.3}$$

Solid angles are the basis of the conversion between various units of measure, and will prove to be very useful when determining the total light output of a source in Chapter 4. A derivation of these equations is presented in Keitz [2].

2.1.2   Units of Measure for Light

Before defining the actual units of measure used to describe light, Table 2.1 summarizes the units and their symbols. These are the photometric units, which are used to quantify light as percieved by humans.

Quantity	Units (abbrev.)	Symbol
Wavelength	nanometer (nm)	λ
Luminous Intensity	candela (cd), SI defined	I
Luminous Flux	lumen (lm), 1 cd over 1 sr	P
Illumination	lux (lx), lm/m^2	E
Luminance	nit, $lm/m^2/sr$ or cd/m^2	B
Luminous Energy	lumen-second (lm-sec)	N/A
Exposure	lux-second (lx-sec)	N/A

Table 2.1: Table of photometric units (as the human eye percieves light). The abbreviation *sr* refers to the solid angle *steradian* (there are 4π steradians in a sphere). Units referenced in equations are denoted by the given symbols or not-applicable (N/A).

Wavelength: Nanometer

Electromagnetic radiation is measured by its characteristic wavelength, denoted by the Greek letter lambda, λ. Humans are only sensitive to a narrow range of wavelengths. This range is roughly from 400 (violet/blue) to 700 (red) *nanometers* (nm), with a nanometer being 10^{-9} meters. Many things, from camera response to light transmission in water, are wavelength dependent, so many characteristics will be displayed as $f(\lambda)$, with λ in nanometers abbreviated nm.

Intensity: Candela

Lights are often described by how bright they are. This *luminous intensity*, is most useful for describing the brightness of, for example, indicator lights, and as such is used to characterize many commercially available LED lights. The standard unit of luminous intensity is the *candela* (cd). It is one of the seven base units in the International System of Units (SI), and has been defined, since 1979, as *the luminous intensity, in a given direction, of a source that emits monochromatic radiation of frequency $540 \times 10^1 2$ hertz and that has a radiant intensity in that direction of 1/683 watt per steradian.* It is, of course, roughly equivalent to a wax candle, but without the variation unavoidable in a flame-based light standard.

Flux: Lumen

More useful to the study of light and illumination is a quantification of the amount of light output. Analogous to the flow of water through a pipe (or from a potential flow source), this is known as the *luminous flux*. Using solid angles, it is possible to define a *lumen* (lm) as a unit of luminous flux in terms of candelas: For a light source of uniform luminous intensity equal to one candela, the luminous flux through one steradian is equal to one lumen. Since there are 4π steradian in a sphere, a uniform point light source of 1 cd intensity would have a total luminous flux or total light output of 4π or 12.57 lm.

Uniform point sources of light don't exist, of course, but this conversion from candelas to lumens becomes useful when attempting to determine the total luminous flux of a light source that is given in candelas, usually with an accompanying diagram specifying the light intensity at certain angles. By integrating the intensity over the onion ring shaped slices of the light source's range of output, it is possible to determine a total luminous flux in lumens, often referred to in this work as the total lumen output of the light source.

Illumination: Lux

When determining correct exposure time for a camera it is useful to define the incident light on a target, i.e. the illumination level, measured in *lux* (lx). Lux, which is lumens per square meter, or lm/m^2, is a common output of photographic light meters, and is used extensively in this thesis to quantify available light for photographic purposes. A target or scene of interest can be abstracted as an area. For a particular light source of given lumen output, the average illumination level can easily be estimated by assuming uniform illumination. A camera's exposure time can be estimated based on the illumination of the target in lux, and the exposure can be scaled linearly by adjusting the illumination level. In general, a scene illuminated at 10 lux will require half the exposure time to photograph as the same scene illuminated at 5 lux from a light source in the same position. By varying the illuminated area, the lumen output or flux of the light source, and other factors, it is possible to change the illumination of the target as measured in lux. It is ultimately the lux reading at the target and details of the target itself that primarily account for the quality of the image

produced.

Luminance: Nit

For most cases, and especially for LEDs, a light source may be modeled as a point. As in the case of indicator LEDs, a measure of the brightness, or luminous intensity, is sufficient. For illumination LEDs or light bulbs, a measure of the total luminous flux is most convenient. However, if the light source has a substantial surface area, the intensity divided by that area is known as the *luminance*, and is measured in *nits*. One nit one candela per meter squared (cd/m^2), which is equivalent to one lumen per meter squared per steradian $(lm/m^2/sr)$.

This measure may come into play, for example, to describe a light-box used to view X-ray slides. Of greater importance, however, is the use of luminance to describe illuminated targets. A perfectly reflective flat surface that acts as a lambertian diffuser (defined in 2.1.3), illuminated at a level of 1 lux, will have a luminance of $1/\pi$ cd/m^2. In actual practice, this value decreases for off-axis illumination and for real world materials, but similar targets with similar illumination geometries will have the approximately the same luminance at the same illumination level.

Luminous Energy: Lumen-second

For a constant light source, it is sufficient to measure light output in lumens, and measure lux at the target. However, the output of some light sources is not constant. For these cases, a measure of the *luminous energy* or total light output is desired. This is the variable lumen output integrated over time, measured in *lumen-seconds*. For example, an LED may have a constant output of 100 lm. Another LED may have a 50% duty cycle square-wave output with a peak of 200 lm. A small strobe may have an output of 2000 lm for a period of 50 milliseconds. All three of these light sources would output a total light quantity of 100 lumen-seconds. For a one second exposure, and assuming all other variables are constant (beam pattern, light wavelength and location, etc.), the image generated by the three light sources would be indistinguishable. With a high enough frequency for the pulsed LED, shorter exposure images taken with either LED light source would likewise be indistinguishable, with the total lumen output being 100 lm times the exposure time.

Exposure: Lux-second

To quantify the *exposure* of an area of film, for example, or a digital camera's CCD array, it is useful to quantify the total light input over time divided by the area of the film in question. Using the unit *lux-seconds* (lx-sec), or $lm - sec/m^2$, the total time integral of illumination of a film slide or digital camera CCD array can be described. This is the exposure of that camera (not just the exposure time).

2.1.3   Reflectance and Lambert's Cosine Law

As stated in the definition of *luminance* above, under perfect conditions, the luminance of a subject, $B = E/\pi$, where E is the illumination in lux. This assumes that illuminated object is both perfectly reflective (no light energy is absorbed) and all light is reflected in all directions equally. It is useful to define reflectance and lambertian diffusers and point out how neither assumption is matched in the real world.

Reflectance

In the real world, perfectly reflective surfaces do not exist. The material will always absorb some, but not all, light energy. The ratio of reflected power (or flux) to the incident power is called the *reflectance* (R). Reflectance is a non-dimensional quantity which will always range from zero (for a perfect absorber, like a black hole), to one (for a perfectly reflective mirror). In practice, $0 < R < 1$. Naturally, for any real material, R is also dependent on the wavelength of light.

Not counting geometry, (assuming that the angle of incidence, α, and the angle of observation, β, both equal zero), the luminance of a subject becomes

$$B = \frac{RE}{\pi} \tag{2.4}$$

with B the luminance measured in candelas per square meter and E the illumination in lux.

23

Lambert's Cosine Law

A lambertian object is defined one which obeys Lambert's cosine law. This law states that the luminous intensity in any direction from an element of a perfectly diffusing surface is proportional to the cosine of the angle between the observing path and line perpendicular to the surface, which we call β, the angle of observation. For a lambertian object

$$I_{observed} = I_{actual} \cos \beta \tag{2.5}$$

where I is a measure of the luminous intensity in candelas.

For a lambertian object, the luminance is the same in all directions. Light emitted from a lambertian object, whether it be reflected light from a surface or radiated light from a light source, is emitted equally in all directions regardless of the observation angle. The $\cos \beta$ effect is due solely to the fact that a flat object viewed off-axis visually occupies less area.

LEDs, for example, which have flat emitting surfaces, are Lambertian *sources*, neglecting the effect of any plastic lens they may be placed inside. A newspaper, or other matte surface for example, is a reasonable approximation of a lambertian *surface*, and is said to be *diffuse*. A mirror, of course, is not lambertian at all but rather *specular*, with light entering from an angle of incidence α, reflecting off the surface, and continuing in the $-\alpha$ direction. Incident light striking a lambertian surface at angle of incidence α will cause an effective illumination according to

$$E_{effective} = E_{incident} \cos \alpha \tag{2.6}$$

where E is the illumination in lux, and $E_{incident}$ is the measured illumination in the direction of the light source. As α increases, less of the surface is "visible" to the light source to illuminate.

Effective Luminance

Putting Equations 2.4 and 2.6 together, the resulting luminance of the target is governed by the following equation, with the angle of incidence α measured from perpendicular

$$B = \frac{RE \cos \alpha}{\pi} \qquad (2.7)$$

which accounts for the $1/\cos \alpha$ effect due to the loss of effective target area due to α[1]. For R that has an angle dependence (for a non-lambertian surface), this becomes

$$B = \frac{R(\alpha)E \cos \alpha}{\pi} \qquad (2.8)$$

Luminance is most fundamentally responsible for the required exposure time of a camera imaging a target, so this relation becomes very important for off-angle illumination.

2.1.4 Eye vs. Camera Response

If only human observers were used, this would almost be the end of the story. The above units represent the photometric system, i.e. based on the human response to light. This response is, of course, dependent on the particulars of the individual human eye. Visible light is percieved roughly in the wavelength range of 400 nm for violet/blue light, to 700 nm for red.

Cameras, and other light detectors, have their particular wavelength-dependent responses measured in radiometric units. That is, their response is dependent on the actual light power based on the SI unit *watts* (W), rather than candelas (cd) which remains based on an assumption about the human eye response. A conversion between radiometric power (watts) and the analogous photometric or photopic units (lumens) is possible using the International Photopic Luminosity Function (IPLF)

$$P_p = C\Sigma V_\lambda P_r(\lambda) \qquad (2.9)$$

where P_p is photopic power (sub-script p) in lumens, C is the conversion, assumed[2] to be 650

---

[1]Note that there is no $\cos\beta$ term here for an off-axis observer. That is because the luminance of a lambertian surface does not change. Additionally, the exposure required to accurately image that surface with a camera does not change even for off-axis observation. As the intensity of the surface decreases by Equation 2.5, so does the viewed dimension of the surface. The effects cancel out [12].

[2]This number comes from Rosser [13], and varies depending on the source. The International Light handbook [14], for example, lists a value of 683 lm/W at 555 nm, the peak of the curve in Figure 2-1
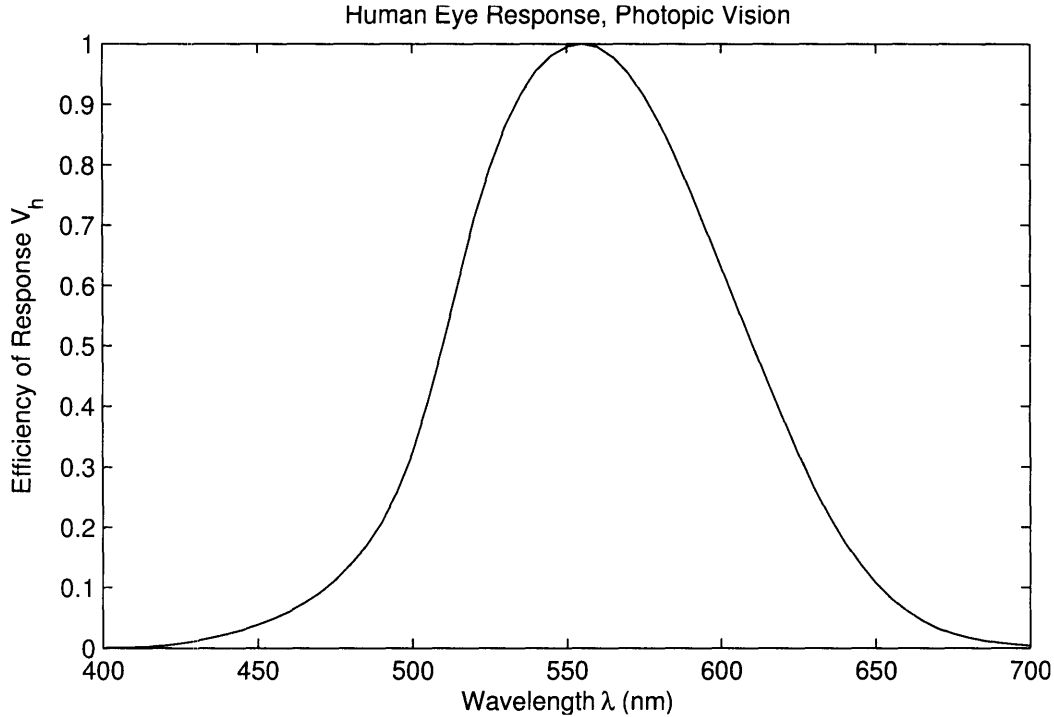
Figure 2-1: International relative luminous efficiency of radiation for photopic vision, human eye response, CIE 1931, adapted from Keitz [2]

lm/W, V_λ is the wavelength dependent human eye response, and $P_r(\lambda)$ is the radiative power (sub-script r) in watts at a given wavelength (Σ denotes summation). A standard model for the human eye response was adopted by the Commission Internationale de l'Eclairage (CIE) in 1931 and is presented, in the spectral range of interest in this work, in figure 2-1.

For cases where the light output of the source is restricted to a single wavelength, or where the energy output is desired for a specific wavelength, it is possible to simplify and reverse equation 2.9 to convert from lumens to watts

$$P_r(\lambda) = \frac{P_p}{CV_\lambda} \qquad (2.10)$$

This conversion is especially useful for LED lights. Their output is often given in lumens (or can be converted to lumens from candelas), and is restricted to a narrow range of wavelengths. By either making the assumption that the total light output is at a single wavelength, or picking particular discreet wavelengths and integrating, it is possible to easily determine the radiometric output of an LED, which will in turn affect the response of a

26

camera imaging a scene illuminated by that LED.

Equation 2.10 may also be used to integrate the total radiative output when the luminous output is known for each wavelength.

2.1.5 Blackbody Radiation

Radiation emission due to heating is the most common method of generating light. Everything from incandescent light-bulbs, to electric stove burner elements, to the sun, gives off light as it is heated. In order to understand the output of lights using this principle, it is useful to describe the concept of blackbody radiation.

Imagine a material whose reflectivity, R, is zero for all λ. In other words, all radiation at all wavelengths is absorbed by that material. Such a material would have an emissivity, e, of one. All radiation generated by the material would be emitted. Such a material is known as a blackbody.

As a blackbody is heated, it emits radiation in a pattern that is characteristic of it's absolute temperature, T, measured in degrees Kelvin. The radiated power, P, of the blackbody is given by the Stefan-Boltzmann law [15]

$$P = \sigma A T^4 \tag{2.11}$$

and is measured in watts on the blackbody's surface. The Stefan-Bolzmann constant, σ is given as $\sigma = 5.6705 \times 10^{-8} W/m^2 \cdot K^4$ and A is the surface area of the body. The wavelength at which the peak intensity occurs is given by the following relationship

$$\lambda_m T = constant = 2.90 \times 10^{-3} \ m \cdot K \tag{2.12}$$

As the temperature of the blackbody rises, the λ_m moves into shorter, and higher energy, wavelengths. Planck, in 1900, derived the Planck radiation law which defines the distribution of radiation intensity

$$P_\lambda(T) = \frac{2hc^2}{\lambda^5} \frac{1}{e^{\frac{hc}{\lambda \kappa T}} - 1} \tag{2.13}$$

where P_λ, a function of the temperature in Kelvin, is the radiated power per unit area of the blackbody, Planck's constant, h is 6.626×10^{-34} $J \cdot sec$, the speed of light, c, is 3.0×10^8 m/s, and Boltzmann's constant, k, is 1.381×10^{-23}.

For temperatures T beginning at around 2000 K, this radiation distribution reaches into the visible light region of 400 nm $\leq \lambda \leq$ 700 nm. Because of this, T is often referred to as the *color temperature*, as its value determines the perceived color of the resulting visible light radiation spectrum. Figure 2-2 shows radiation distribution for three color temperatures commonly used for incandescent lighting.
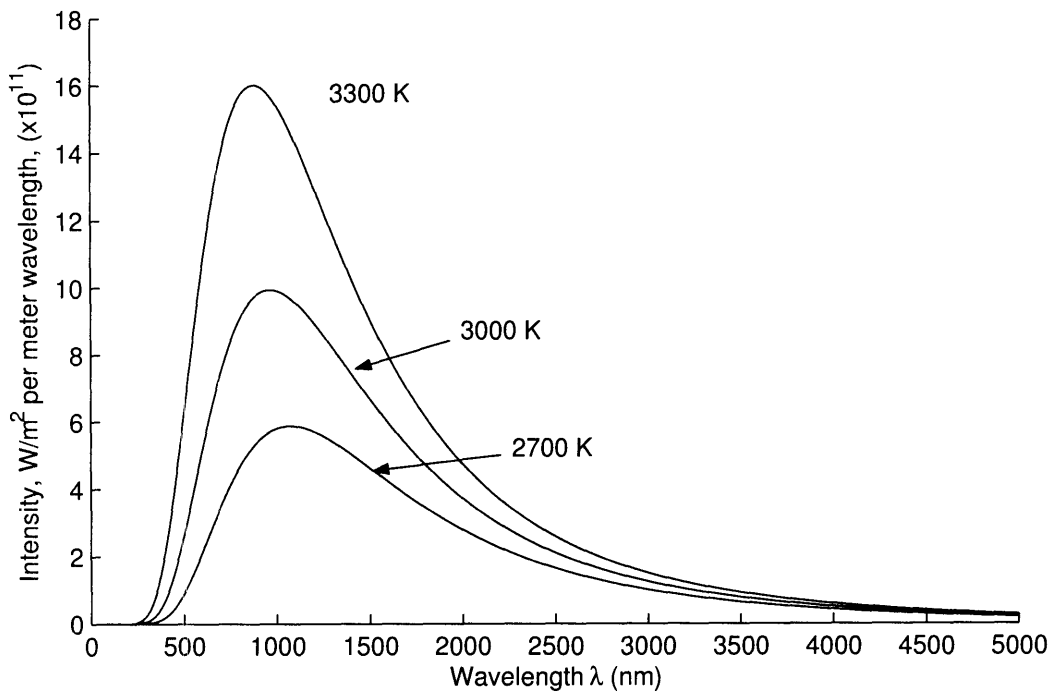
Figure 2-2: Intensity distribution for continuous spectrum blackbody radiation at color temperatures $T = 2700$ K, $T = 3000$ K, and $T = 3300$ K.

Because of it's relatively low color temperature, and resulting red bias, incandescent lights are often described as producing "warm" light. The sun has a surface temperature of 6000° K and is often used as the standard of "white", or full-spectrum light. However, due to absorption and scattering by the atmosphere, the sun may be percieved as anything from about 2000 K at sunrise and sunset (very red), to about 5400 K on a summer day. A deep blue sky may be anywhere from 12,000 K to 20,000 K.

2.2 Optical Properties of Sea-water

Whereas still, homogeneous air can be treated as a vacuum for most light measurements over moderate ranges (up to 100 meters), water cannot. Water has three properties that make the use of light in water, and especially sea-water, challenging: water's index of refraction, its ability to dissolve certain chemicals, and to suspend particles. Additionally, the ocean is a much more hostile environment in which to work. Water and salt corrode electronic equipment, and any devices sent into the sea must be designed to work under pressure, or be placed in a pressure housing. While pressure and corrosion are primarily operational concerns, the ways these challenges are met often influence the performance of the optical system.

2.2.1 Index of Refraction

As light passes from one medium to another, the light's angle of incidence α, measured perpendicular to the surface interface, is governed by Snell's law

$$n_1 \sin \alpha_1 = n_2 \sin \alpha_2 \tag{2.14}$$

where n_1 and n_2 are the respective indices of refraction of the materials.

The index of refraction, n is an intrinsic property of any transparent material. The lowest possible is $n = 1.0$, which is true for a vacuum. Air has an index of refraction of 1.0003.

In order for a lens to work, it must have a different index of refraction than the medium it is operating in. Most optical glass has $n \approx 1.45 - 1.55$. So an inexpensive glass lens will work well in air. However, that inexpensive lens will not work as well in a medium with a similar index of refraction

The index of refraction of sea-water is given as $n = 1.34$ [16]. This is very close to that of typical optical glass, or for that matter many clear plastics. Due to Snell's Law (2.14), this similarity means that light will not change direction very much as it passes from glass into water. This greatly changes the effect of any optical system and has two implications for underwater photography.

First, optical systems with an air gap must be designed properly. A flat glass plate (for

29

example, the lens of an inexpensive pressure housing) with water on one side and air on the other will act as a lens, distorting the image and narrowing the viewing angle. This is most important for cameras, though many underwater lights encounter and correct for this problem as well. Some expensive off-the-shelf camera and light housings use a spherical glass aperture to eliminate this effect. Placing the camera or light source at the radial center of this spherical dome will minimize the distortion caused by the water/air transition, and will enable the camera to take images as if in air.

More important to this work is the effect on lenses without an air gap. Most lenses completely submerged in water will have little or no effect. With a refraction coefficient very close to that of water, the lens is effectively invisible. The implication for LEDs is clear; the clear epoxy lens that is molded onto most LEDs to focus the light into a beam is rendered ineffective. Additional lenses placed in front of the LED in water will similarly be ineffective. Short of placing the LED in a pressure housing (which is prohibitively expensive), or using very expensive exotic material for the lens, the only way to focus an LED in water is by using reflectors, which are governed purely by geometry and not by refraction coefficients.

2.2.2 Absorption

When photons of light strike an atom, their energy can be absorbed. In air, atoms are sparse, and the effect is hardly noticeable in the visible spectrum. In water, however, the increased density increases the probability of absorption. Assuming homogeneous water where the rate of absorption over propagation is constant, light intensity decreases exponentially as a function of a coefficient of absorption, a, which has units of 1/length, m^{-1} for all data contained in this work.

$$P_2 = P_1 e^{-ax} \qquad (2.15)$$

P is a measure of luminous flux or total light power, measured in lumens, though the equation may be applied to illumination (lux) as well. The light propagation distance is given as x. The coefficient of absorption, a, is wavelength dependent, and sometimes symbolized as $a(\lambda)$. It is also dependent on the purity of water, as dissolved chemicals such as salt, tannin

(common in the Charles River), chlorophyll, and other chiefly organic substances tend to raise the value of a, especially for longer (red) wavelengths.

Much work has been done with pure water. Figure 2-3 shows a commonly cited example of the wavelength dependence of the absorption coefficient for pure water.
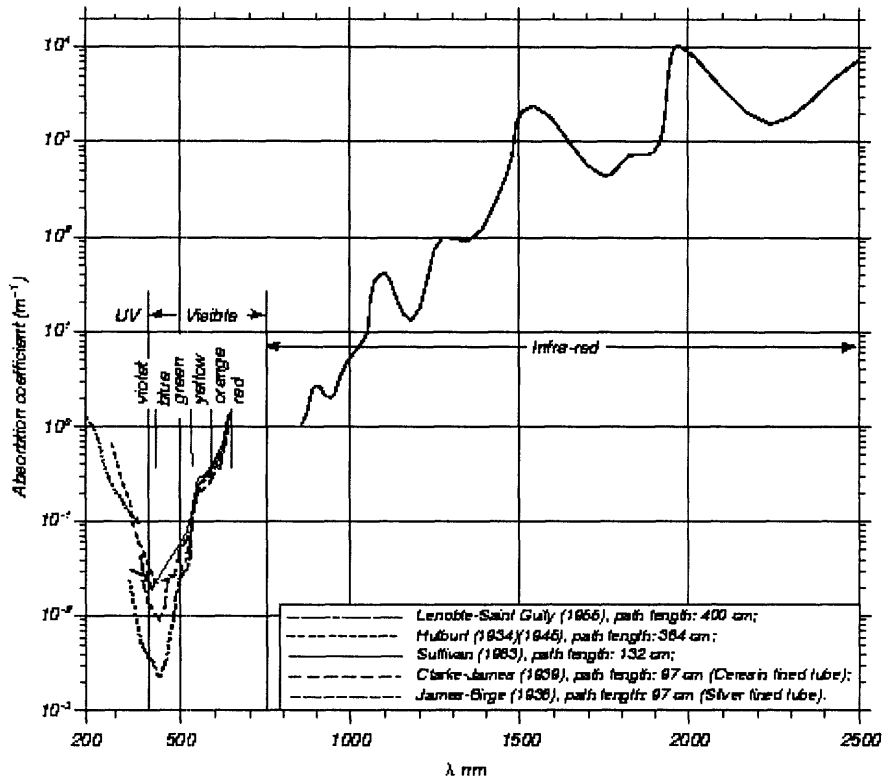
Figure 2-3: Absorption coefficient for pure water as a function of wavelength λ of the radiation. Taken from Morel [3] by way of Stewart [4].

More contemporary data showing absorption coefficients for pure water is presented in Figure 2-4. Note that while the shape of the curves are quite similar, the actual wavelength of the absorption coefficient minimum varies.

Some absorption coefficients of sea-water were also tabulated by Shifrin [8]. Several surface and 10 meter depth values of $a(\lambda)$ from potential AUV operation areas are presented in Figure 2-5. Note that the absorption minimum shifts nearer to the green wavelengths ($\approx 500 - 550$ nm) for actual sea-water, whereas it was well into the blue wavelengths for the various pure water experiments.

Methods of measuring a directly have been developed which take into account scattered

31
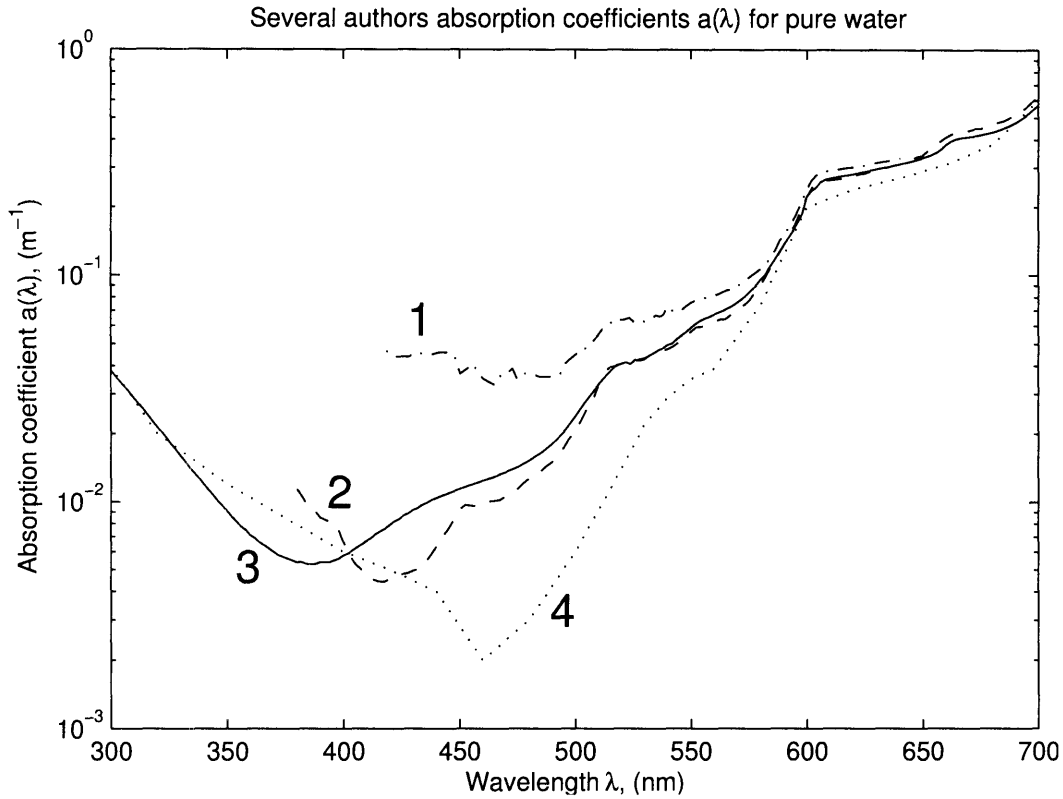
Figure 2-4: Experimentally determined absorption coefficients for pure water. Adapted from data collected by: 1, Querry [5]; 2, Pope [6]; 3, Buiteveld [7]; 4, Shifrin [8].

light. However, instruments to measure a tend to be bulky and expensive. Jerlov [17] shows that there is a close correlation between a and the attenuation coefficient α, defined in Section 2.2.4. The effect to remember which is shown in the Figures is that even for very clear water, absorption rises tremendously near 700 nm.
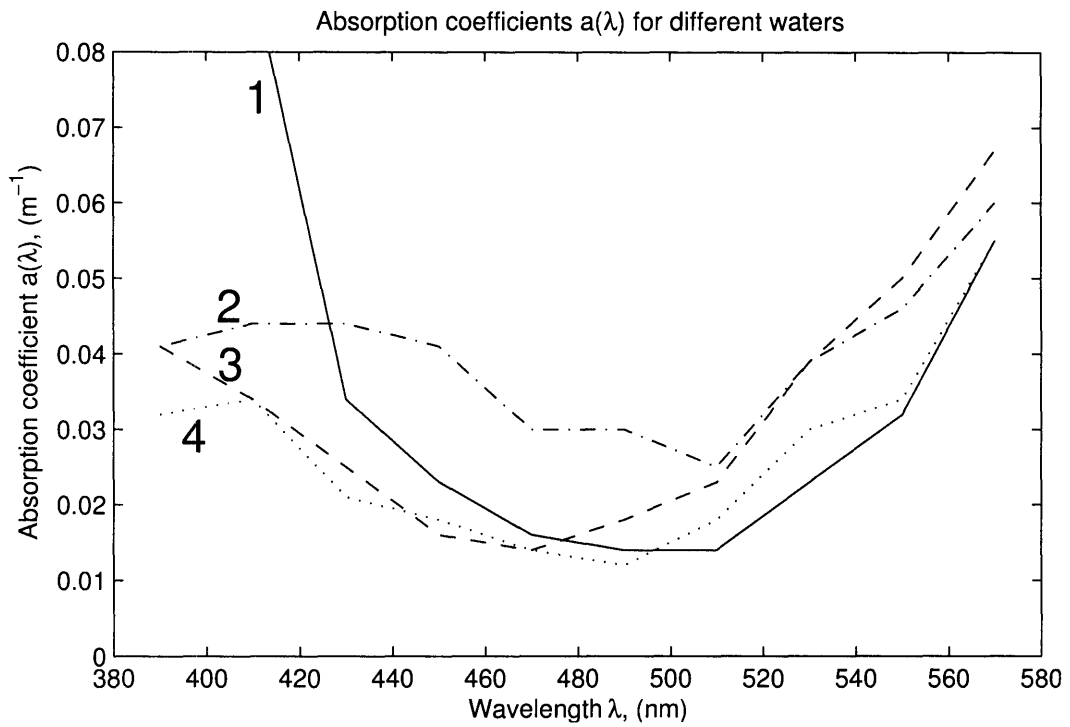
Figure 2-5: Values of the absorption coefficient $a(\lambda)$ in different oceanic regions. 1, Caribbean Sea; 2, Gulf Stream; 3, Sargasso Sea; 4, North Trade Wind current. Adapted from Shifrin [8]

2.2.3 Scattering

Light that is reflected off of particles in the water and sent on a different path is said to be "scattered". This can be due to any suspended particle larger than the wavelength of light, but is typically due to small mineral particles (silt) or larger biological matter (single celled organisms, biological detritus, algae, etc.). The total scattering coefficient, which is wavelength dependent, is called s, which describes the attenuation of light due solely to scattering. It is related to the volume scattering function, $\sigma(\theta)$ by

$$s = 2\pi \int_0^\pi \sigma(\theta) \sin\theta d\theta \qquad (2.16)$$

where $\sigma(\theta)$ describes the angular dependence of light scattered from a small volume element (Funk, *et al.* [9]).

The backscattering coefficient, b, describes the amount of light scattered in the interval $\pi/2 \leq \theta \leq \pi$. This is again related to the volume scattering function

$$b = 2\pi \int_{\pi/2}^\pi \sigma(\theta) \sin\theta d\theta \qquad (2.17)$$

The backscattering coefficient is perhaps the most useful as it is typically backscattered light that causes the most problems for underwater photography. Determining $\sigma(\theta)$ in situ, from which s and b can be derived, requires a complex, expensive instrument. Fortunately it is usually sufficient to determine s implicitly, which can be estimated by measuring the total attenuation coefficient of the water.

2.2.4 Attenuation

It is difficult and expensive to uncouple scattering from absorption in measurements of dirty water. It is much easier to obtain a measure of the optical properties of typical ocean water by combining the two effects into a single attenuation coefficient, α. Similar to absorption, it acts exponentially over propagation distance where scattering and absorption are constant.

$$P_2 = P_1 e^{-\alpha x} \qquad (2.18)$$

where P_1 is the total flux content of the source as it leaves the emitter, P_2 is what remains at after the propagation length x [18], and α is the sum of the absorption and scattering coefficients:

$$\alpha = a + s \tag{2.19}$$

which has units 1/length, m^{-1}. Figure 2-6 illustrates the wavelength dependence of α for varyingly dirty water.
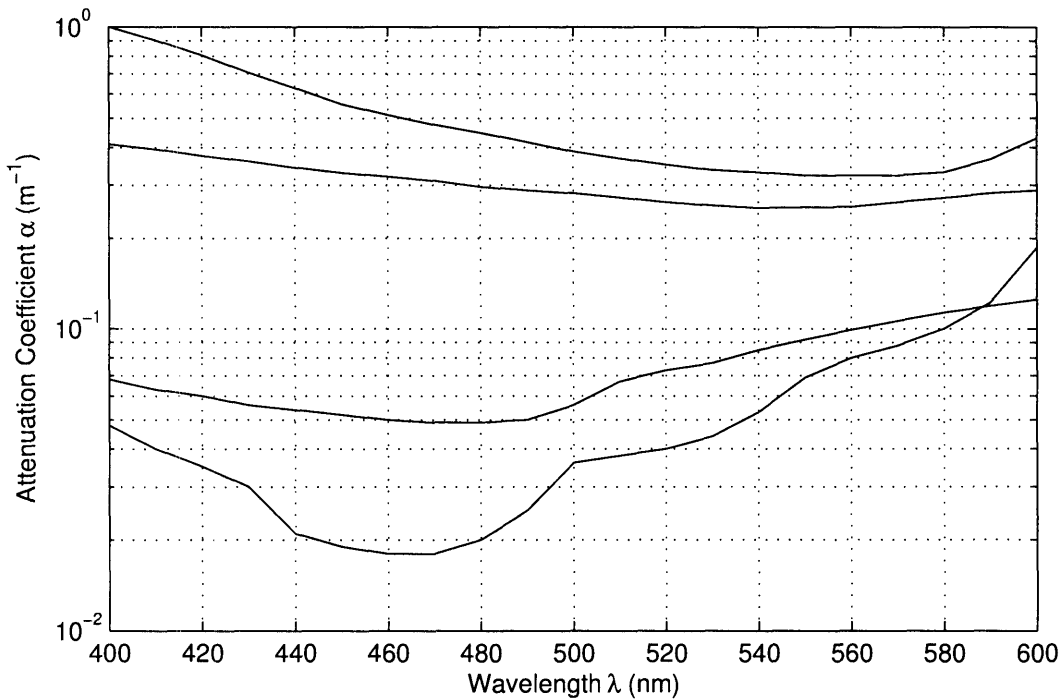
Figure 2-6: Attenuation coefficient for different water conditions adapted from Funk, *et al.* [9]. From top to bottom (dirtiest to cleanest) the curves correspond to bay water, coastal water, deep ocean water, and distilled water.

An important characteristic of α to note is that as water becomes less pure (i.e. as dissolved substances and suspended particulate matter increase), the wavelength corresponding to the minimum attenuation coefficient increases and shifts towards the red end of the spectrum. For coastal and bay water, the "optimal" wavelength for which α is the least is well into the green region of the spectrum. The implication of this is that for clear water, blue light will propagate the furthest, whereas in typical dirty water, green light will propagate

the furthest (but for far shorter a distance than blue light would in clean water).

One additional important observation is that because of Equation 2.19, the absorption seen in pure water will still be present in dirty water. Therefore, although scattering tends to raise the attenuation coefficient across the spectrum, the sharp peak in absorption as wavelenghts approach 700 nm will still be present in attenuation.

2.3   Underwater Light Sources

The most common source of light underwater is, of course, the sun. Under certain circumstances, sunlight may provide sufficient illumination for photography. However, in murky water, at night, or at great depth, artificial light is required. Because of the diffuse nature of ambient sunlight, artificial illumination is often preferable when available, as the artificial light can bring out textures in surfaces and shadows in objects, yielding better images.

Many light sources that are commonly used on land have been adapted to work underwater. What follows is a review of many available lighting options, with special emphasis on persistent light sources and their suitability for AUVs.

2.3.1   Persistent Light Sources

A persistent light source is one which, when turned on, emits a relatively constant quantity of light. Operating temperature, input voltage, length of operation, and other variables may affect the total luminous output, but the light itself can be regarded as either "on" or "off". In general terms, time is not a variable that has any bearing on the total scene illumination provided by the light source.

Incandescent

Incandescent lights have been used for many years for underwater illumination for divers and for photography. Figure 2-7 shows an incandescent light used during World War II. Basically the same light source that has been used in houses and automobiles for nearly a hundred years, incandescent light relies on a tungsten filament that emits blackbody radiation when heated to about 2700°K (which corresponds to its blackbody color temperature) inside an
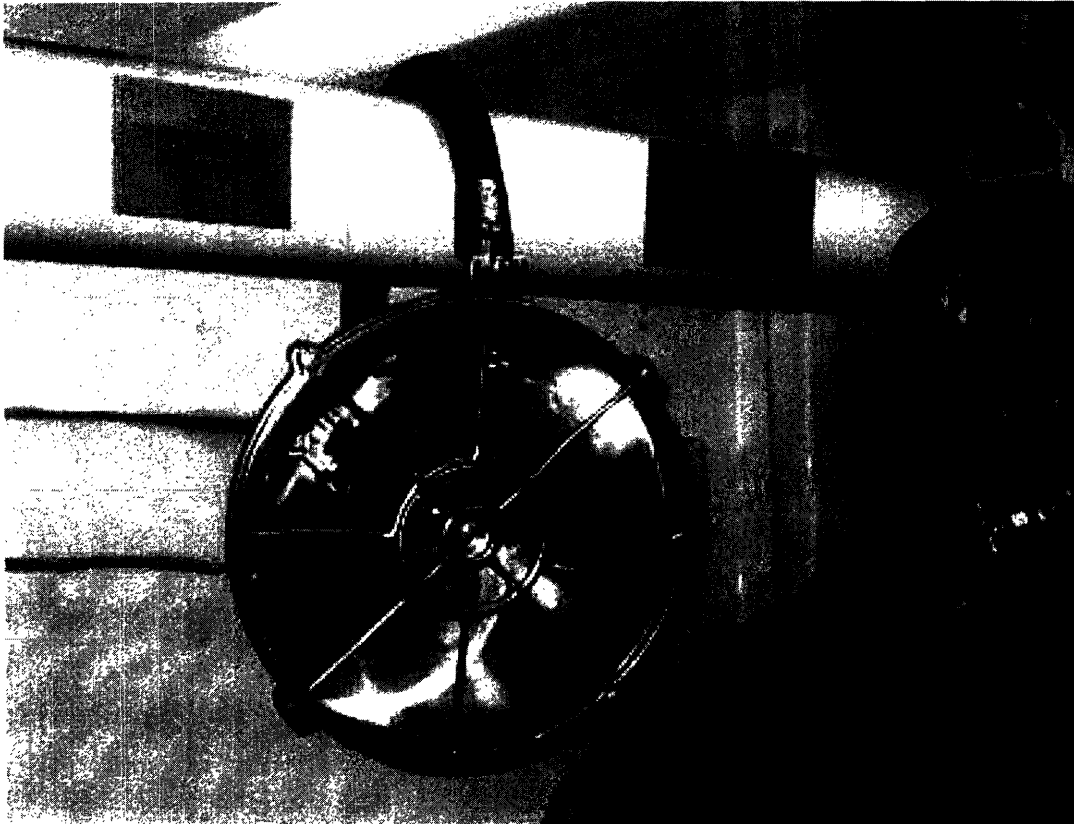
Figure 2-7: This 1000W underwater work light was used by divers during WWII. The light is on display at the Charleston Naval Shipyard Museum on the USS Yorktown, Patriot's Point, Mt. Pleasant, SC. Photo by the author.

inert argon-filled glass bulb. To operate underwater, a pressure housing with a clear lens is used to prevent the bulb from being crushed. An integral reflector is often added to direct the light.

Incandescent lights, though very common, require a lot of power for a given quantity of light. This is due to the nature of blackbody radiation. At the temperature of incandescent lights, most of the energy falls in the infrared range of the spectrum and is lost as heat. Additionally, some of the tungsten of the filament is deposited on the inside of the glass as the bulb is used. The black sooty deposit is easily visible in an old household light bulb, and tends to slightly degrade the light bulb's performance over time.

Halogen

Halogen lights are an evolved form of incandescent lights. They use a halogen gas, such as iodine, as a small component of the gas surrounding the filament. The gas remains about 99% argon, and only 1% halogen. They operate at higher temperatures and must use a smaller, quartz or hard glass bulb enclosure. As the tungsten evaporates from the filament, it condenses on inside of the bulb where it reacts with the halogen gas, forming a tungsten halide. This tungsten halide evaporates easily, and eventually redeposits the tungsten back on the filament. This acts to keep the inside of the bulb clean and to lengthen the lifetime of the bulb. Additionally, the extra-strong bulb can withstand higher internal gas pressure, which enables a higher filament temperature. This corresponds to a higher color temperature of about 3000 to 3300 K. This moves the peak of the blackbody light output curve further into the visible spectrum, providing a "whiter" light and greater lighting efficiency. Most light bulbs labeled as "xenon" or "krypton" bulbs are simply halogen bulbs that use xenon or krypton as their inert gas rather than argon. The exception is for xenon metal halide lamps, which are described separately.

Halogen lights are a common choice for underwater applications. They have the same pressure vessel requirement, and often cannot be operated in air without overheating (submerging the pressure vessel in water is required to keep the bulb inside cool). Basically, they may be thought of as incandescent lights with a higher color temperature, which results in a slightly more optimal output radiation curve.

Other Light Sources

Certain light sources require high voltages or special power supplies to operate. Fluorescent lights require a large, heavy ballast (relative to the size of the bulb) to operate. High intensity discharge (HID) lights, for example xenon metal halide and high pressure sodium lamps, require high voltage power supplies which are often far more expensive than the bulbs. They are gaining wider acceptance when cost is not a primary concern. For example, the blinding blue lights on some newer German cars are HID lights. Halcyon makes a diver carried HID lighting system for $580.00 which may be a good system for a medium-sized

AUV, but certainly not for a disposable system.

2.3.2 Intermittent Light Sources

Chemical Reaction Light Sources

Light sources such as underwater magnesium torches and chemical light sticks can provide light without electrical power. However, they are difficult to control from a small AUV and output a non-constant quantity of light.

Strobes

Strobe lights are often used in an underwater environment to provide additional light for still photography. When timed to flash while the camera's shutter is open, strobe lights can output a lot of effective lumens for their size. Total power draw is relatively small, dependent on flash frequency. For a camera imaging only select targets every few seconds, a strobe is far and away the best choice from a power standpoint.

However, strobe lights are not persistent. They can be made to flash continuously, but without flash/camera synchronization, they are of limited use for photography. Synchronization can easily be achieved electronically, but for a bottom mounted light operating independent of an AUV, acoustic or optical synchronization would be difficult and/or expensive.

Laser Range Gating

This method takes the concept of the strobe light one step further. Rather than merely timing the flash to occur during the period that the camera's shutter is open and exposing, the exposure time is a very short window that only admits the fraction of the light that has been reflected off of the target.

By knowing the range to the target and the speed of light in water, the camera images only the light that arrived in the time window equal to that required for the light to leave the source, reflect off the target, and return to the camera. Light that backscatters off of particles in the water column and effectively takes a shortcut to the camera is not imaged,

as the shutter has not yet opened when that light arrives. Light that has mulitiply reflected and takes too long of a path arrives after the shutter is closed and is also not imaged. Backscatter can be greatly reduced using this process as very little of the water volume is actually imaged, only light reflecting from the target.

Naturally, This method requires a very complex control system, and is absolutely not suited for an independent source/receiver situation, like that of a bottom mounted light and an AUV. However, this method does show much promise for an AUV mounted package system.

2.3.3   Light Emitting Diodes (LEDs)

Light Emitting Diodes, or LEDs, have been around for forty years. They were first developed using a gallium arsenide phosphide semiconductor alloy. As a current is passed through the semiconductor, electrons move about and release photons directly. As a result, LEDs can be much more efficient than incandescent light sources, as less wasted heat is generated. The diode itself is typically encased in a small plastic bulb, which helps reflect and direct the light, as well as protect the semiconductor material.

Advances in semiconductor material led to the profusion of LEDs being used for indicator lights in electronic devices. Analogous to Moore's Law (which states that the number of transistors on a computer chip will double every two years or so), Haitz's Law [19] predicts a doubling of the luminous ouptut of a single LED package every 18-24 months. This law has been followed for 36 years. The semiconductor chemistry has steadily evolved over that time as new processes are developed.

Indicator LEDs were typically red, as the chemistry of the semiconductor material dictated. The Japanese company Nichia first pioneered blue-green LEDs [20]. Other companies have followed suit. By taking advantage of the human eye's higher response to green light, these LEDs made possible the use of LEDs as sources of illumination (indirect viewing) rather than as indicators (direct viewing).

One of the areas of greatest interest for LED manufacturers is in reproducing white light. Fluroescent lights make use of phosophors, though they are often criticized for having too "cold" an output, with wavelengths in the blue end of the spectrum which tend to make skin

look pale. "Warmer" incandescent lights, which have a more pleasing yellow tint, are much more inefficient. LEDs emit photons in a very narrow spectral range. Two methods are available to reproduce a more visually pleasing broad spectrom of light. First, by combining red, green, and blue LEDs in the appropriate proportions, white light can be simulated (this is what digital color cameras do in reverse). Or, by adding phosphor material to the LED lens, which absorbs short wavelength photons and re-emits longer wavelength photons, high energy LEDs in the blue and ultraviolet range can be used to produce white light.

With the efficiencies available from LEDs, both in power and operational lifetime, it is predicted that LEDs will move into consumer's homes within the next five to ten years [20]. Many cars are now available with red and amber LED arrays powering tail-lights, and LEDs are steadily replacing incandescent light bulbs in traffic signal lights. Based in part on Dodge's use of their LEDs for the headlights in it's V-10 powered Tomahawk concept motorcycle, the LED manufacturer Lumileds, makers of the 5 watt Luxeon LED line, is predicting a full-spectrum automotive emitter package that will compete with halogen and HID headlights in the near future while being more efficient and much more versatile [21].

As LEDs continue to shrink in package size, while maintaining efficiencies greater than that of incandescent light sources, many additional applications can be imagined. Taking advantage of an attenuation coefficicient minimum at the Nichia blue-green LED's emitted wavelength, Rosser [13] created an array of LEDs for use by the Odyssey IIc vehicle for photographic illumination. Taking advantage of the nearly instantaneous on-off ability of LEDs, which enable serial signals to be transferred at rates similar to a computers's modem, and based in part on the justification of Bales [22], Sanoner [23] used Nichia blue-green LEDs as well as Lumiled's 5W Luxeon cyan LEDs to investigate underwater light communication.

2.4   Underwater Vehicle Light Applications

2.4.1   Vehicle Mounted Lighting Systems

Any and all of the above mentioned lighting sources can and have been mounted on underwater vehicles at one point or another. Most often, complicated sources requiring high

voltages are used on ROVs. Both ROVs and AUVs commonly make use of halogen lights. The Odyssey IIc vehicle operated by the MIT Sea Grant AUV lab has been through many lighting revisions including strobes, a 50W DeepSea Power & Light (DSPL) halogen unit, and at least two LED array sources.

Power consumption and package size are typically the primary constraints on AUV mounted lighting systems. Using the Odyssey vehicle as an example, the 50W DSPL light source, when turned on, consumed approximately 20% of the vehicle's total operating load, which includes all other sensors, computers, and propulsion. The approximately fist sized light, while not large by industry standards, still required some effort to fit inside the vehicle. The new Hovering AUV (HAUV) has much smaller dimensions and the same light would pose a greater operational challenge.

2.4.2 Off-the-Vehicle Systems

Any remotely deployed lighting system that is independent of the AUV or other imaging vehicle is referred to in this work as an *off-the-vehicle* lighting system. This hypothetical system is physically and electrically independent of the imaging platform, regardless of how it is controlled. Special kinds of off-the-vehicle systems, differentiated by their size, application, and level if independence, are described by the following models.

Droplight Model

In a garage or construction site, a *droplight* or trouble-light is often used to provide extra illumination. The droplight is plugged into a wall socket, and hung near the work area. In an underwater environment, an example of such a system is the HPS-Droplight made by Remote Ocean Systems. Designed for inspection of nuclear reactors, the system consists of a high-pressure sodium light head unit, a spool of cable to lower the head unit, and a ballast to provide the appropriate voltage to the bulb. The light shown in Figure 2-7 is an example of a remotely powered, diver manipulated light.

Any droplight requires at least one controller to either lower the light into position, or aim it while in the water. As is often the case for deep-diving ROV systems, the droplight

could take the form of a sled lowered to near the ROV's position which allows the ROV to operate on a smaller, more flexible tether.

Lighthouse Model

I will use the term *lighthouse* to refer to self-powered off-the-vehicle lights that have high-output sources that can be aimed at a particular target. A lighthouse would have a large supply of batteries to run the light source, and a way of communicating with a surface support ship (perhaps via an ROV) or an AUV.

The term *offload* light was used by Coleman, *et al.*, [24] to describe a 1200 W HMI lamp designed to sit on the bottom and illuminate an underwater archaeological site. To take advantage of greater source/receiver separation, and to reduce the power load on the primary vehicle (in this case an ROV), the Institute for Exploration developed this offload light or lighthouse. It carried its own batteries, hae its lighting head elevated off the bottom, and was acoustically controlled pan and tilt ability. The idea was conceived by Dr. Robert Ballard [25]. A working light was built and taken on an expedition, but it was never used.

An LED lighting head unit is currently being built at WHOI by Dr. Hanumant Singh. It has 47 focused 5W Luxeon LEDs, 7 by 7, arrayed in on a convex aluminum fan [26]. This arrangement could be used in an LED lighthouse as a well-focused, very powerful light source.

Candle Model

The term *candle* will be used to refer to smaller off-the-vehicle lights that illuminate a patch of ground directly beneath them. They may have communications ability to turn on or off, but no ability to aim anywhere other than where they are placed.

Examples close to this model of lighting include underwater magnesium torches, glow-sticks, and even flashlights. However, all of these light sources require a diver's intervention. They can't aim themselves, but they can be manipulated by a diver. To the best of my knowledge, no type of underwater candle has yet been deployed by an AUV for the purpose of underwater illumination.

Autonomous Partner Model

Much like a friend holding a flashlight to illuminate a scene, it is possible to envision an *autonomous partner* that can act as an intelligent light source, illuminating regions of interest. Rather than an operator aiming the light, one AUV could direct a second into position. Though the mechanism to control such a pairing is beyond the scope of this work, it is important to consider that such a pairing would offer virtually unlimited source/receiver geometry possibilities. The light source could be placed anywhere, and in fact more than one light source could be used.

2.5   Light Efficiency

There are two commonly accepted methods of gauging the efficiency of a light source. One is to compare the total luminous output to the light's power usage. The other is to compare the light's radiative output to its power usage.

The measure of luminous efficiency is most useful comparing light sources for use by humans, for example overhead lights in an office. For this measure, the total luminous output is divided by the power used by the light. For example, a 100 watt incandescent light bulb may have a rated luminous output of 2000 lm. This bulb would have a total luminous efficiency of 20 lm/W.

The luminous efficiency rating assumes that the observer will respond according to the photopic response curve. For situations where this is not the case, for example for digital cameras which have a relatively flat response curve, a much better metric is radiative efficiency. The light's total radiative energy output is measured in watts. This is unfortunate, as a light's radiative efficiency is then given as watts per watt, or W/W. To differentiate between electrical power watts and radiative power or "light watts", I will use the subscript r for radiative, and denote light watts as W_r. Even better is to denote light watts in milliWatts, or mW_r. As an example, a light source that has a radiative power output of 500 mW_r and uses 5 watts of electrical power will have a radiative efficiency of 100 mW_r/W.

2.6 Imaging Details

In this section, the two principle types of still cameras, film and digital/CCD, are reviewed. Though video cameras are more traditionally used with persistent light sources, video cameras are dependent on either film or a digital sensor to encode sequential images. Still cameras are more easily quantified and analyzed. Their outputs may be analyzed directly, without any of the compression losses involved in either capturing still images from analog or digital video format.

After a background discussion of film cameras and digital CCD cameras, a method of predicting exposure times based on illumination is presented.

2.6.1 Film Cameras

Traditional photography is conducted using cameras which use film. A sheet of gelatin film with a layer of light-sensitive silver halide particles is placed at the focal plane of a lens. In the case of black and white film, only one kind of particle is used. For color film, three different layers that are responsive to red, green, and blue light are used. A shutter is opened for a calculated period of time, which allows light to enter through the lens and expose the film. The film is then developed which leaves a pattern of particles on the film in proportion to the light they had been exposed to. The developed film can then be used to expose print paper to create photographs. The particles of the film can often be seen in blown up photographs or under magnification. The particles are called the *grain* of an image. In general, grain is to be avoided, as it lowers the ultimate resolution of the image. Underexposed photographs that are developed to attempt to compensate for the lack of light at exposure often have the worst grain. To make truly impressive, poster-sized prints, large-format cameras are often used. These cameras have a much larger film plane than a conventional 35mm camera. This reduces the effective grain by increasing the effective resolution of the resulting image. All film reacts differently to light. The particular chemicals used have formulations that vary from manufacturer to manufacturer, from batch to batch, and even from top to bottom of the film. Each film has a responsivity curve that is ideally similar to Figure 2-1. For color film, each of the three colors has it's own responsivity curve, which in turn yields a total

45

color response that is different than the human eye. This is why sometimes photographs can seem much more colorful than the original scene they were based on.

2.6.2   CCD Cameras

Digital CCD (charge-coupled device) cameras are in many ways similar to film cameras. Though they are completely electronic, requiring no chemicals or development, they are pixelated in much the same way the grain in film cameras. The CCD is an array of light-responsive pixels. It is placed at the focal plane of the camera's lens. An electronic shutter zeros the pixel levels and the CCD is "exposed" for a calculated time. Each pixel is sensitive to light striking it, and the total amount of light striking a pixel over the exposure period can be measured. By doing this for all pixels, an image may be produced proportional to the light intensity of the subject.

Raw CCDs have relatively flat response curves. That is to say, their response is proportionate to the radiative light striking them, regardless of wavelength. Using the total quantum response (effectively a measure of the percentage of photons striking the CCD sensor that are detected, which is analogous to the radiative response) Figure 2-8 compares some imaging sensors to Kodak's KAF-1400E CCD, which was designed to enhance overall and especially blue response. Figure 2-9 compares Kodak's newer 3.2 Megapixel KAF-3200E to an older KAF-1400 (non-E). Note that the range of response, while not flat, is certainly much more broad than that of the human eye (Figure 2-1 and the response for the LED frequencies of note, 450-550 nm, is only about 30% lower than that of the peak response at 600 nm.

Most color CCD cameras employ a color filter mask to enable color-specific light response. Pixels on the CCD array are exposed to light through alternating red, green, and blue filters. Each filter acts as a band-pass filter, allowing three narrow yet overlapping ranges of light wavelengths to strike the CCD. The three resulting sparse images are then interpolated to generate three separate images of the scene in blue, green, and red wavelengths.

CCD cameras have also been developed where a beam splitter is used to send the light to three red, green, and blue filtered CCD arrays. Not all digital cameras are CCD cameras, with inexpensive complementary metal oxide semiconductor (CMOS) sensor cameras also

100

90

80

Absolute Quantum Efficiency (%)

70

KAF-1400E (Blue Plus) ————

60

50

Traditional Full-Frame

40

Typical Interline
with microlenses ————

30

20

10

0

300   400   500   600   700   800   900   1000   1100

Wavelength (nm)
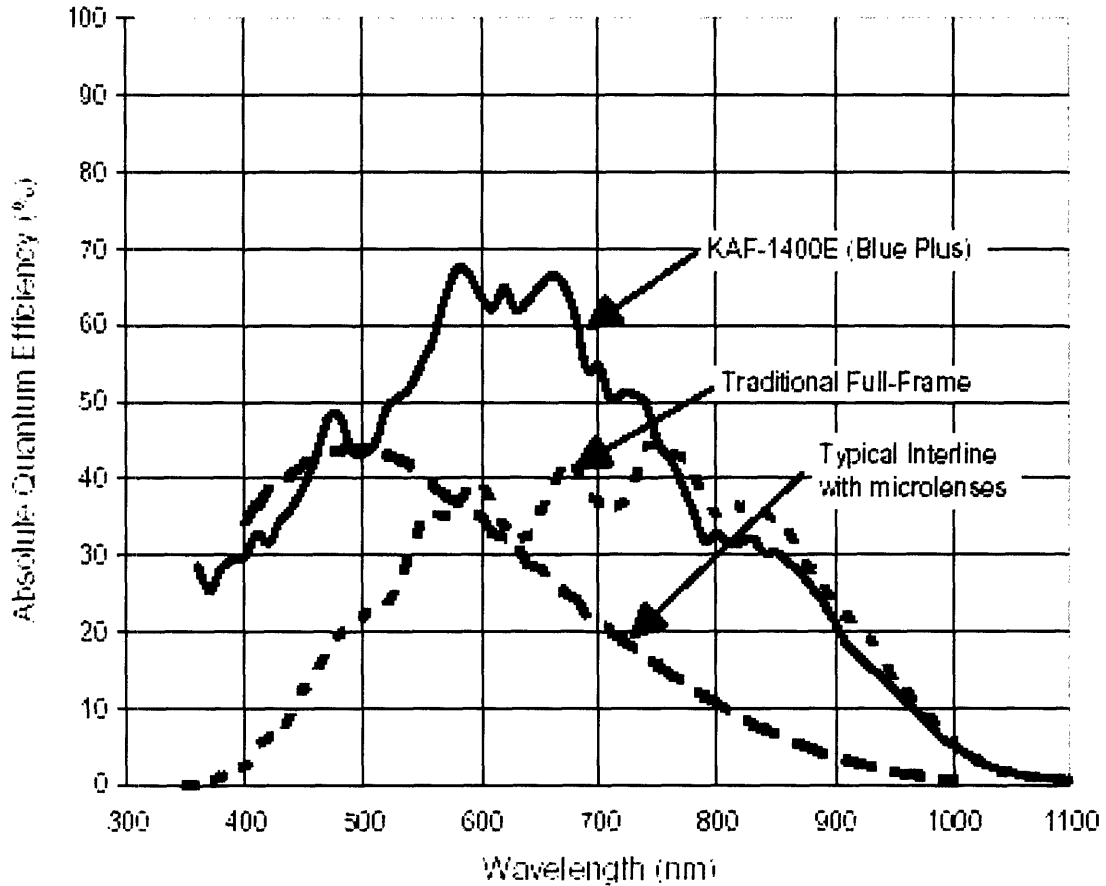
Figure 2-8: Spectral response of comparable image sensor technologies, from Kodak technical paper [10]

available. These CMOS cameras tend to have a lower light sensitivity, requiring longer exposure times, as additional transistors on the array take up usable pixel area. These extra transistors enable faster pixel read times and much lower power requirements, however.

Most digital cameras output an Red-Green-Blue (RGB) image. This is typically an array of data containing 24 bits of information for each pixel in the array. Each pixel has 8 bits of information to describe the intensity of each color *channel*, red green, and blue. That is to say that the absolute color of each pixel can be described as a combination of red, green, and blue. With 8 bits to describe each color intensity, the intensity can vary from 0 to 255, which is $2^8 - 1$. For example, black is RGB (0,0,0), white is RGB (255,255,255), and the bluest blue is RGB (0,0,255). This color intensity is proportional to the luminance of the corresponding region of the target.
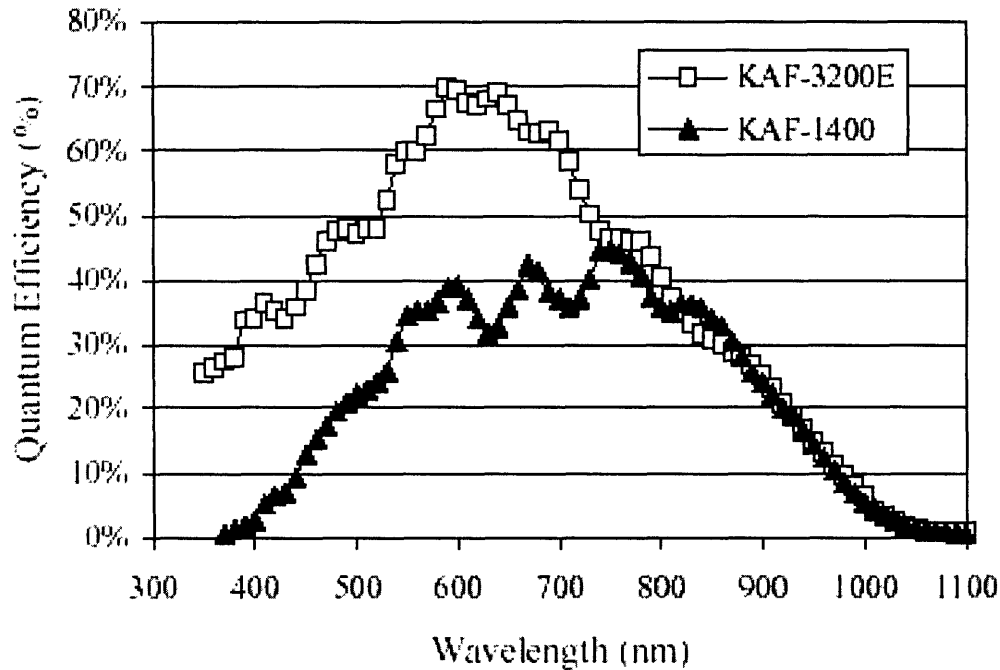
Figure 2-9: Spectral response of differently processed Kodak CCD sensors. KAF-3200E is a 3.2 Megapixel CCD. Plot adapted from [11]

In order for a CCD camera to generate a proper image, the exposure time of the camera must be correct. Photons from the target are counted during the exposure window. The resulting pixel value, 0 to 255, corresponds to the number of photons counted during that window. A simplification of the assignment of pixel values is shown in Figure 2-10. The normalized luminosity of a target and the resulting pixel values when that target is correctly, over, and underexposed, is displayed. Whereas the properly exposed image has the full range of pixel values, 0 to 255, the overexposed image is said to *saturate*, with any target regions with a luminosity higher than about 0.6 reading as 255 in the resulting image. Underexposed images also saturate, but in the other direction. Black, near-black, and dark gray, up to a luminosity of 0.4, all have a pixel value of zero.

To measure contrast in an image, or the difference in pixel values, regions of different luminosity are chosen. For example, if the target consists of black and white squares, for a correctly exposed image one would expect pixel values to be either 0 or 255. This would yield a contrast of 255, or a normalized contrast of 100%. Using the example of Figure 2-10, the maximum contrast would be 155 (the maximum pixel value minus the minimum pixel

value). This would yield a maximum normalized contrast of 60% due to saturation.
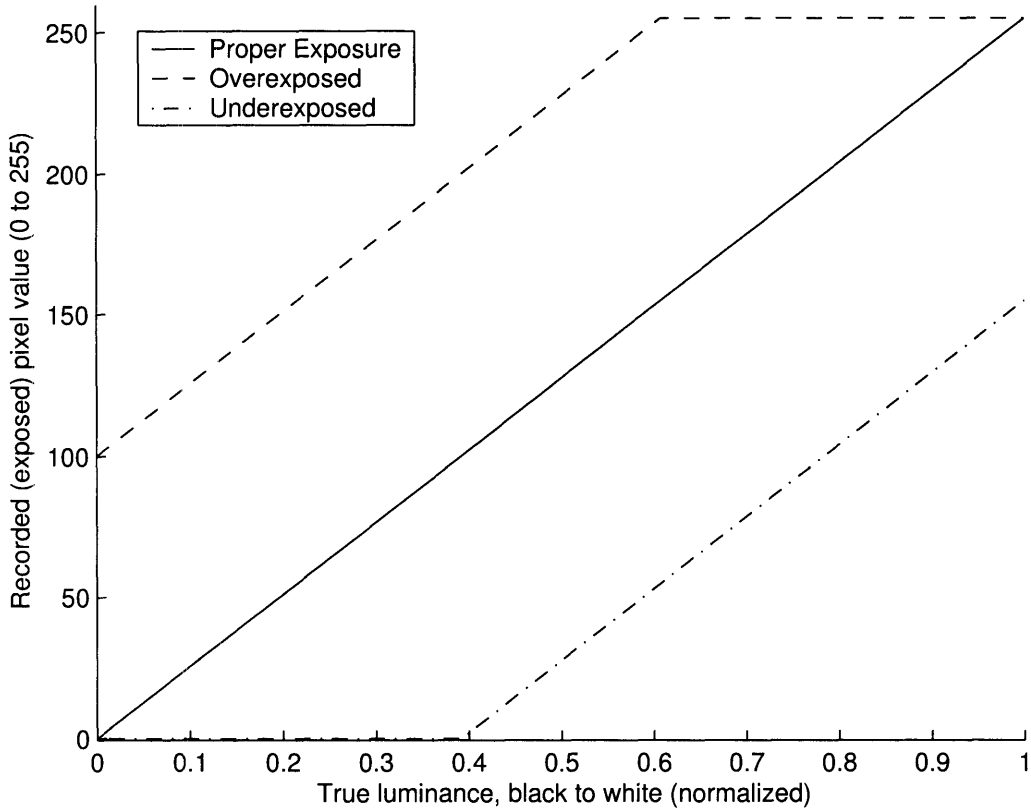
Figure 2-10: Pixel response to a given target ranging in relative luminosity from 0 (black) to 1 (bright white) for a correctly exposed, overexposed, and underexposed CCD sensor.

Figure 2-11 shows three versions of the same image exposed correctly, overexposed, and underexposed. This particular example is shown in black and white, but over and under-exposure saturation can occur for any one channel (or all channels) of a color image as well.

The most common output format for digital cameras is a JPEG image, which is a compression scheme used to decrease the total amount of data that must be stored. The JPEG format is universal, and images can be converted easily to true RGB images for analysis or display. Additionally, high-end cameras often allow output in TIFF or RAW format. Both of these formats offer true RGB zero-compression data storage, though the file sizes can be a factor of 10 to 30 times larger than a lightly compressed JPEG image.

Figure 2-11: Three different images of the same Kodak contrast target. The center image is correctly exposed (note that each step of the bar is visible. The top is overexposed (white and light gray saturate, so both appear white). The bottom is underexposed (black and dark gray do not register, so both appear black).

2.6.3 Exposure Value

Imaging is a function of more than just exposure time. In order to create a proper image, a certain relationship between the camera and the scene must be achieved. The measure each of these relationships is known as the Exposure Value, EV. On the scene side, the field luminance of the subject, B, and the film speed, S, are related to the exposure value by the following equation

$$2^{EV} = \frac{BS}{K} \tag{2.20}$$

where K is a non-dimensional constant that provides a conversion factor between the ISO film speed and the particular units of luminance. For B measured in cd/m^2, $K = 12.5$. On the camera side, the camera's aperture, A, and the exposure time, T are related to EV by

$$2^{EV} = \frac{A^2}{T} \tag{2.21}$$

The aperture, A, is defined as the f-stop or f-number of the lens. For example, the Canon S230 camera that provides the bulk of the images used in this project, has $f = 2.8$ at the wide-angle setting, and $f = 4.0$ at telephoto.

A better way to express both relationships is this

$$EV = log_2\left(\frac{A^2}{T}\right) = log_2\left(\frac{BS}{K}\right) \tag{2.22}$$

Typically, a photographer will have several variables to adjust. ISO film speed can be decreased for higher quality images with smaller grain (for example, ISO 100 film is commonly sold for outdoor photography, but ISO 25 is availible), or a faster (higher ISO) number film can be used for high-speed action photography or low light conditions (ISO 400 is common for color prints, and black & white film is often used up to ISO 1600). The f-stop may be adjusted to vary the depth-of-field (the range window over which things remain in focus), and the exposure may be set manually. Calculating the actual exposure value of the scene is useful in these situations when using tables to determine exposure times vs. f-stop, for example, when setting a manual camera.

For this project, and for any AUV project, the camera is assumed to be set "wide-open", that is the iris at its maximum opening, and the f-stop at the lens minimum value.

For the purpose of analysis, the actual exposure value is not needed, and the log_2 terms can be dropped. To replace B in terms of luminance with E in terms of illumination, Equation 2.4 is used. To make the conversion from units of luminance (cd/m^2) to illumination, (lm/m^2), and additional factor of π is required.

Using E as a measure of illumination, for $R = 1.0$ and $\alpha = 0$, this leaves

$$\frac{A^2}{T} = \frac{ES}{\pi K} \tag{2.23}$$

To account for lower values of R in water, and for off-axis illumination with angle of incidence α, Equation 2.8 is used to fully substitue E for B, leaving

$$\frac{A^2}{T} = \frac{ESR\cos\alpha}{\pi K} \tag{2.24}$$

Solving for exposure time T, this transorms to

$$T = \frac{A^2\pi K}{ESR\cos\alpha} \tag{2.25}$$

Once a camera's response or effective film speed is determined for a certain light source, it is a simple matter to predict exposure values based on illumination using Equation 2.25. Some implications of this equation are that as α increases, so does the required exposure time. As illumination E increases, exposure time drops.

2.7   Underwater Photography

Mertens [27] provides the following summary of the problems of some of the challenges of underwater photography.

> Photographs taken in water have significantly less contrast than similar pictures taken in air. Reduced contrast is caused by several important factors. First, natural light in water tends to be very diffuse and does not cast strong shadows. Second, light scattered from particles in the transmission path is superimposed on the desired image and reduces its contrast. Third, the image itself undergoes degradation in transmission due to refractive discontinuities. Image details are degraded or even obliterated as the image light rays propagate toward the camera.
>
> Several techniques are available to increase the apparent image contrast and offset the above-mentioned deteriorating effects. Unfortunately no perfect and universally applicable correction is presently available, and image contrast remains one of the most important problems of in-water photography. Supplemental light sources placed relatively close to the subject can provide illumination that is less diffuse and will increase the contrast at the subject. In clear water and at relatively short camera-to-subject distances this is often a very satisfactory

solution. However, in more turbid water strong backscatter of the suplemental
light from particles in the water will seriously degrade the image.

In this section, I will examine the challenges of generating underwater images and some
ways of analyzing them.

2.7.1 Underwater Imaging

Figure 2-12 shows the basic imaging situation in water. After light leaves the source (top
left), some attenuated through absorption and scattering, some is backscattered and reaches
the reciever (camera) without encountering the target, and some strikes the target (in this
case, a fish). On the return trip, light reflected from the target is subject to absorption
and scattering (attenuation), forward scattering (blurring), and some reaches the camera
unaltered.
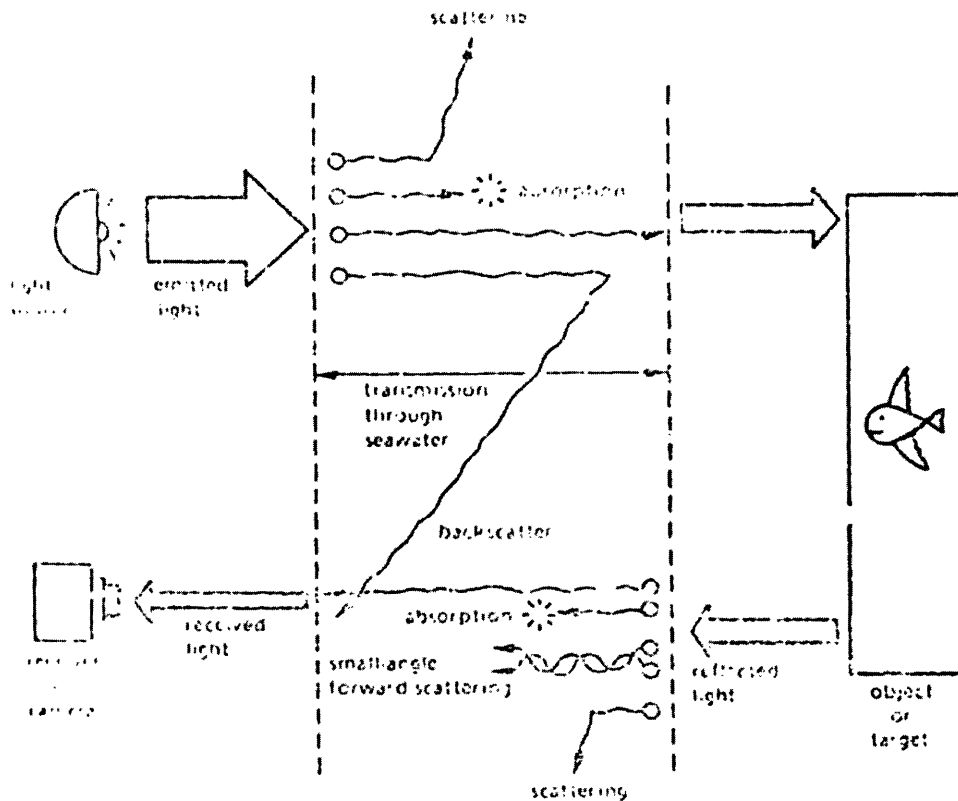
Figure 2-12: Block diagram of basic imaging situation, from [9]

Attenuation loss affects all lighting methods. Whether the light source is the sun, an incandescent light, or an LED, some radiative light energy is always absorbed and scattered away. This, however, affects only the exposure time of the camera and the resulting size of the light source for artificial lighting. In general, under the same geometric conditions for the light source, target, and receiver, only the exposure time will vary with the illumination level. The quality of the resulting image should be the same provided the exposure is correct.

Of greater interest to the underwater photographer is the quality of the image independent of exposure. Many things affect this. Mertens [27] shows that refractive gradients in the light path can bend the light, causing blurring of the image. Wells [28] points out that particles in the water can forward scatter the light, making it appear that light from a single object has come from multiple locations in the target area, and that this typically has a greater adverse effect on image quality.

For artificially illuminated scenes, poor image quality is most often a result of backscattered light. Light that is reflected off of particles in the water column between the target and the receiver tend to lower the contrast of the resulting image by creating a fog-like effect. This is shown by Jaffe [29] and is one of the primary motivations of this research. While there is little that can be done to prevent refractive gradients and forward scattered light, backscatter can be minimized by increasing the source/receiver separation distance and minimizing the total illuminated water volume. With a light source placed further away from the camera, and less of the suspended particles in front of the camera being illuminated, backscatter is minimized. This is, for example, why a SCUBA diver's camera rig often look like an enormous octopus, with the lights places far away from the camera, yet aimed at the camera's target.

Figure 2-13 shows a typical underwater lighting arrangement which illustrates some of the terms used in this project. The incident optical path (light traveling from the light source to the target), the reflected optical path (light reflected from the target to the camera), the angle of incidence α, the angle of reflection β, and the illuminated water volume are shown graphically for a simplified two-dimensional case.
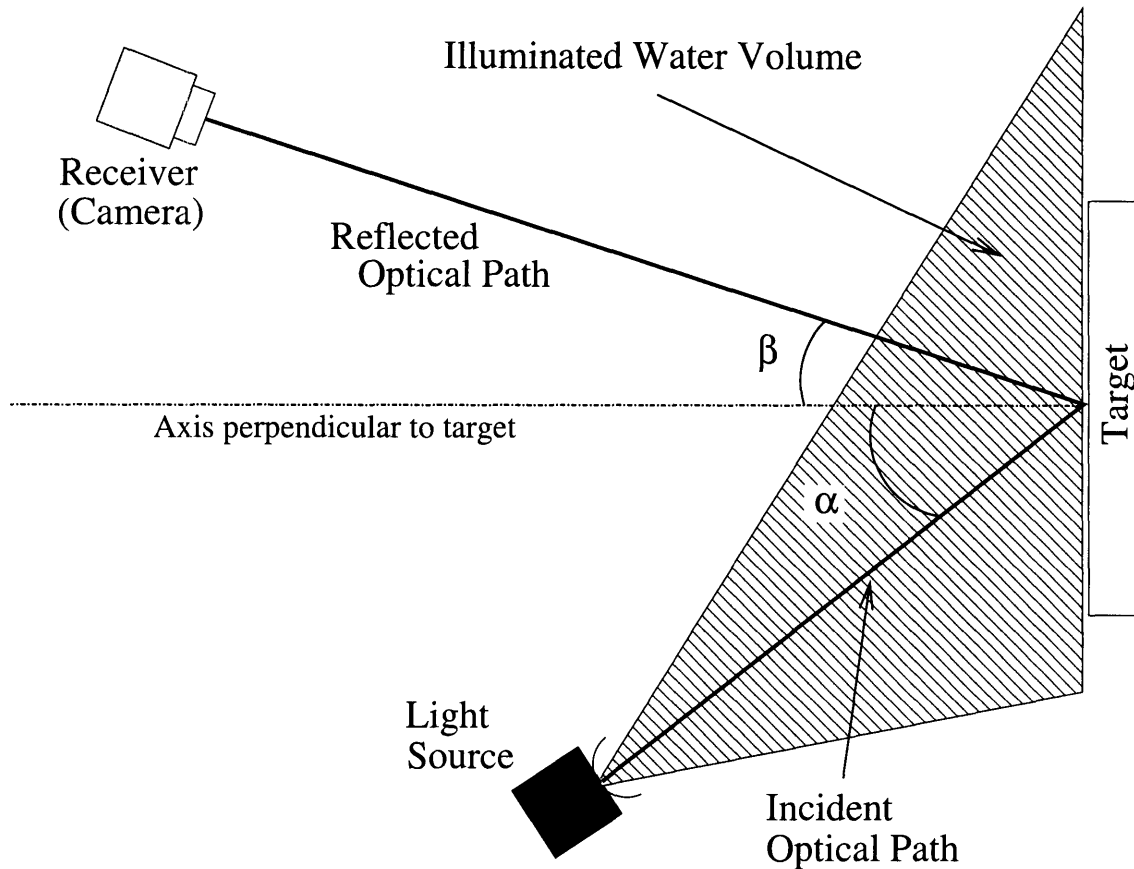
Figure 2-13: Diagram showing a typical underwater lighting and imaging arrangement. Light angle of incidence is shown as α. The reflected angle is shown as β. The incident optical path from the light source to the center of the target is labeled. The length of this path, the incident optical path length, is often abbreviated incident OPL. The reflected optical path from the target to the camera is also labeled. The length of this path is the reflected OPL. The total optical path length is the total OPL.

2.7.2 Image Quality

Blurred images due to forward scattered or refracted light tend to look fuzzy, as if out of focus. To judge the quality of these kinds of images, many image quality measures, or IQMs, exist. For example, the act of turning a sharp, black/white interface on a target image into a smoothed transition curve can be thought of being analogous to a system transfer function for an electric or mechanical system. A modulation transfer function (MTF) can be used to describe an optical system. An example of this method is shown in Mertens [27]

More advanced forms of IQMs using the MTF or the power spectrum of the image have

been generated to look at satellite images, for example. Some examples are the program developed by the MITRE corporation [30], and a more general application for compressed JPEG images [31]. A statistical review is given by Avcibaş [32].

2.7.3 Image Contrast

Image quality degradation due to forward scattered or reflected light is something that is not a function of the light source. Of greater importance to image quality is the effect of backscattered light, which is dependent on light position and type. An underwater image is said to be contrast-limited when backscatter is a factor. That is to say, backscattered light tends to add noise to the image such that the difference between light and dark subject areas is less distinct.

The effect of backscatter can be seen while driving on foggy days. The fog is a source of white noise that tends to obscure the details hidden in the fog. When using headlights, water droplets in the air (analogous to particles in the water column) reflect light back to the driver. Turning on the high-beams only makes visibility worse. When lights are required, fog lights are often the best option. These are located low to the ground, separating the source (the fog lights) from the reciever (the driver) as much as possible given the car's geometry.

To measure contrast, a contrast target is commonly used. This is a target containing black and white squares and a stepped grayscale band. Figure 3-7 shows several such targets intended for both black and white and color contrast response. By measuring the different values in the resulting image, and comparing them to what they "should" be had there been no contrast loss due to backscatter, a measure of the total contrast in the resulting image can be determined[3]. As focus, "correct" exposure time, forward scattered and refracted light, and other variables are assumed to be constant, the measured contrast of the image can be used as a metric to judge the resulting image quality. Section 4.4.1 discusses the image

---

[3]As an example, Garcia [33] shows a method of restoring lost contrast in an image. This method artificially enhances the separation between similarly hued regions of an image. For example, an image with two shades of gray could be made to display in stark black and white. This method is useful for enhancing the viewing of fine details in existing images, but does not address the fundamental source of the noise, which is the backscattered light. It also cannot change the total quantity or quality of data present in the original image, only display it differently. The contrast difference method using the original image as an input is still the best measure of image quality for contrast-limited scenes.

analysis used in this project and the particular method of extracting contrast data.

2.8   Modeling Light Behaviour in Water

Light behaviour in water can be simulated, as well as measured experimentally. Mobley [34] gives many examples of simulations of light propagating through water in his book.

If the relevant conditions are known for each wavelength (for example, the attenuation coefficient, absorption and scattering coefficients, and others), individual simulated photons can be followed from a light source to the target and back to the receiver. The effects of scattering and absorption can be simulated independently, and forward and backscattered light can be simulated. Jaffe [29] and Palowitch [35] show examples of *synthetic images* being generated in this manner, and give attenuation coefficients for simulations in light wavelengths of 400 to 600 nm. Tadamura [36] uses a single attenuation coefficient value, but adds complex reflections from multiple surfaces. Cerezo [37] shows a more recent method of generating synthetic images.

While beyond the scope of this thesis, the methods of generating synthetic images can be very useful for understanding light behaviour in water and for simulating the effect of illumination.

Chapter 3

Experiments

This chapter reviews the testing done to measure the effectiveness of LED illumination in sea-water. A series of in-air or dry experiments to characterize LED and camera performance were conducted at the MIT Strobe Lab. In-water or wet experiments were conducted in the MIT AUV Lab, at the MIT Towtank, and in the ocean at the Woods Hole Oceanographic Institute.

Though not necessarily presented in the order they were conducted, the experiments are presented grouped by location, following a section describing commonly used equipment, and a section describing the particular challenges involved in adapting that equipment to the ocean.

3.1 Equipment Used

3.1.1 Luxeon 5W LED Lights

Five watt LEDs manufactured by Lumileds were the primary light sources used during this project. Released under and referred to in this project by their product name "Luxeon", these high-output 5W LEDs are available in royal blue, blue, cyan, and green. Additionally, Lumiled's white LEDs are based on these emitters, with additional phosophors to produce a broader output spectrum.

Figure 3-1 shows an example of the Luxeon V Star, the 5W LED mounted on a small
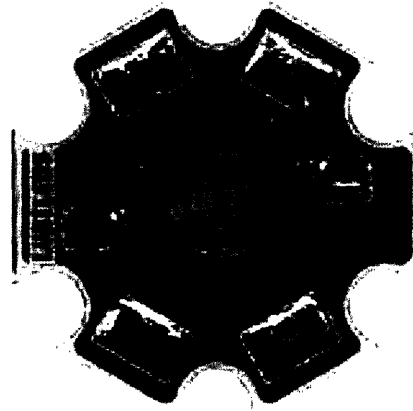
Figure 3-1: The Luxeon V Star, 5W LED light with hexagonal base, manufactured by Lumileds, San Jose, CA.

Luxeon LED	Color	Luminous Flux typical (lm)	Wavelength typical (nm)	Peak Operating Current (mA)	Voltage at peak current (V)
LXHL-LB5C	Blue	30	470	700	6.9
LXHL-LE5C	Cyan	120	505	700	6.9
LXHL-LM5C	Green	120	530	700	6.9

Table 3.1: Specifications of three Luxeon 5W LEDs

hexagonal piece of aluminum with solder contacts for power. The package is only 20 mm in diameter, or smaller than a quarter. The active part of the LED itself is a small square of aluminum indium gallium phosphide semiconductor material on a sapphire substrate measuring only 3 mm on a side. The LEDs used are encased in an acrylic dome lens which allows the LED output to be lambertian (falling off as $1/cos\alpha$, for the most part). Another option from Lumileds is a side-emitting acrylic lens, which internally reflects the light and sends much of it out to the side. The gap between the lens and the LED itself is filled with silicone, which matches the index of refraction of the lens and ensures that there is no air-gap in the LED light. The LED emitter itself (only the central black circle and LED lens in Figure 3-1) is available separately. The aluminum hex is not a sufficient heatsink for operation in air, but the slots in the base can be used to mount the LED on a larger heatsink, while the aluminum provides a good flat heat conducting surface. Relevant operating specifications of the Luxeon 5W LEDs are shown in Table 3.1.

Several Nichia LEDs had been used by the AUV lab in the past. Their specifications are included in Appendix section A.1 for comparison purposes.

3.1.2 Camera Systems

The principle vehicle of the MIT AUV Lab has for several years made use of an ROS Navigator video camera. The use of a better, CCD still camera had been planned for use in both the Odyssey IIc vehicle (to replace the ROS camera), and in the forthcoming hovering vehicle, the HAUV. We also tested the Elphel Model 313 camera and, most importantly, the Canon S230 Digital Elph, cameras we were considering for use in the Odyssey and HAUV respectively.

ROS Navigator

The ROS Navigator camera was specified and purchased by the MIT AUV Lab for the purpose of bottom surveying. It consists of a sensitive, unmasked (black and white only) CCD element with an NTSC video output. The Navigator has an external focus control (though the wide-angle version gives enough depth of field for this not to matter), and sets the exposure and gain automatically, attempting to maintain a good image for all light levels. Intended for use in an ROV, the camera was mounted in the nose of the Odyssey IIc "Xanthos". The video signal was recorded on a Super-8mm videotape, and the camera and VCR could be turned on and off remotely during the mission. The camera is waterproof to 3000 meters, and required only a lengthened cable to be made to work.

While the ROS Navigator presented some operational challenges, its most fundamental problem is a lack of resolution. Its output is a video signal, limited to 570 lines. As deployed on Xanthos, this signal was first stored on an analog videotape, and then video captured to make still images. Resolution was lost at each step.

For use during the WHOI experiments, the camera was connected to a small LCD monitor. An Imperx Inc. Video Capture Essentials model VCE-B5A01 PCMCIA video capture card was intended to record images directly, eliminating the need for a videotape. Unfortunately, a connector malfunction on the capture board prevented the taking of images on

the second night of testing at WHOI. Figure 3-14 shows the monitor as used. The ROS Navigator was not used during the Towtank experiments.

Elphel 313

An Elphel model 313 network camera was purchased by the AUV Lab and evaluated to determine its suitability in a vehicle application. The Elphel's primary advantage is its interface. The camera acts as a web server. Once it is properly set up and connected to a network with a Cat5e ethernet cable, it can be accessed and controlled through a webpage interface. With a human at the controls, the exposure and other camera controls can be set, the shutter triggered, and images taken.

Unfortunately for the AUV Lab, the Elphel proved too simple and required too much user input to be truly functional in an autonomous vehicle. When fitted with a lens, the CCD generated images of passable quality at 1280x1024 resolution, but the camera lacked an integral light meter. The user had to input an exposure value for the images being generated. This proved to be too much of a time commitment to consider using it for experiments. It also means that the Elphel will likely not ever see service in an autonomous vehicle.

Canon S230

Originally purchased for the HAUV because of its diminutive size, the Canon PowerShot S230 digital camera shown in Figure 3-2 proved to be the workhorse of the experiments.
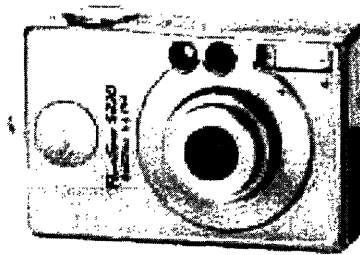
Figure 3-2: The Canon PowerShot S230 digital camera.

The Canon S230 camera has a 3.2 megapixel CCD capable of producing images of up to 2048x1536 pixel resolution. It has a 5.4 to 10.8mm zoom lens (equivalent to a 35-70mm

Effective pixels	≈ 3.2 million
Lens	5.4(W) - 10.8(T)
	(35mm equiv: 35-70mm)
	$f2.8$(W) - $f4.0$(T)
Autofocus	TTL 9-point AiAF/TTL 1-point center AF
Focus range	47cm to infinity
Shutter	Mechanical and electronic
Shutter speed	15 - 1/1500 sec
	1 - 1/1500 sec in standard operation
Light metering system	Evaluative metering/
	Spot metering
Exposure compensation	+/- 2 stops in 1/3-stop increments
Continuous shooting	2 images/second
Interface	USB

Table 3.2: Specifications of Canon S230 Digital Elph camera

lens on a traditional 35mm camera), with an f-stop of 2.8 (wide) to 4 (telephoto). Exposure is determined by either evaluative metering (linked to the focusing point) or spot metering. Exposure compensation, useful for bracketing during experiments, is limited to +/- 2 stops, in 1/3-stop increments. In standard mode, the exposure time is limited to 1 second, though up to 15 seconds is possible. 1/1500th of a second is the minimum exposure time. The CCD has an effective sensitivity equivalent to that of ISO 50, 100, 200, or 400 film, and was set to ISO 400 for all tests (i.e. the most sensitive). Of greatest interest to AUV operators is the camera's size. It is only 3.4 x 2.2 x 1.1 inches and weighs a third of a pound.

The camera communicates through a USB port. This can be used to download images, or to operate the camera remotely. The camera can store up to 154 full-resolution/highest quality images on it's memory card. However, when being triggered remotely over the USB using the manufacturer supplied Windows software, the camera defaults to uploading images as they are being taken. This takes several seconds for full-quality images, whereas the camera can otherwise run at up to two frames per second. Using a different software interface should allow the maximum frame rate.

Figure 2-9 shows the spectral response of a Kodak CCD available at the time of the Canon S230's release with the same dimensions as that in the S230. While no source could be found stating which CCD sensor Canon uses in its S230 camera, it is entirely possible it

Sensor	Silicon Photo-diode
Ranges	20, 200, 2000, and 20,000 Fc and Lux
Resolution	0.1 Fc and Lux
Accuracy	± 3% of reading
Repeatability	± 2%
PC Interface	RS232C at 9600 bps
Sampling Time	2.5 readings/sec.

Table 3.3: Specifications of Extech Model 401036 Datalogging Light Meter

is the Kodak KAF-3200E. Whatever CCD sensor it contains almost certainly has a similar spectral response.

3.1.3 Test Equipment

Extech Light Meter

The Extech model 401036 datalogging light meter was used extensively for testing both in and out of water. It consisted of a base unit which gives a digital readout of illumination in either footcandles (Fc) or lux and a remote head unit which contained the photodiode. The head contained a 1/4"-20 hex nut molded into the back that could enable the head to be mounted on a tripod. The remote head also allowed for easy measurement of the illumination level at the face of the target on a wall. The base unit allowed for serial communications with a laptop computer via a supplied serial tether. This came in very handy when taking readings in a dark room when the display on the Extech could not be read. Some specifications of the Extech light meter are shown in Table 3.3

Sea Tech OBS

The Sea Tech Light Scattering Sensor was used to indirectly measure particulate matter in the water during the Towtank and WHOI tests. It is referred to in the MIT AUV Lab as an optical backscatter sensor, and is abbreviated OBS throughout this work.

The OBS projects light into the sample volume using two modulated 880 nm infrared LEDs, which are outside the human visible range. Light scattered from suspended particles

Range	33 mg/l (high-gain)
Resolution	0.01% of full scale, ≈ 3 $\mu g/l$
Sensor Output	0 to 5 VDC
Depth Rating	6000 m
Length	5.0 in
Diameter	1.25 in
Weight	0.26 kg

Table 3.4: Specifications of Sea Tech Light Scattering Sensor (OBS)

in the sample volume is measured with a solar-blind silicon detector. A light stop between the light source and light detector prevents the measurement of direct transmitted light so that only scattered light is measured.

By operating at infrared wavelengths, the OBS limits the amount of ambient light entering the detector, as light at that wavelength does not propagate for very long due to absorption. Table 3.4 shows some of the relevant specifications of the OBS.

3.2 Waterproofing Equipment

In order to conduct experiments underwater, some existing equipment had to be modified or adapted to be made waterproof. In some cases, this meant a special housing needed to be made or adapted. For equipment originally intended for underwater use in an AUV, all that was needed was a lengthened cable. Rather than describe the equipment repeatedly as it is used, this section summarizes the waterproofing process for the various experimental equipment. This includes the changes made to the equipment and descriptions of housings what were constructed and modified.

3.2.1 Waterproofing Luxeon 5W LED Lights

The need for waterproofing the 5W Luxeon LEDs was evident after the experiment described in Section 3.4. Potting with epoxy is described in Rosser [13], and has been used for many other pieces of equipment in the MIT AUV Lab in the past.

Initial LED Potting Experiment

The effectiveness of potting with clear epoxy was proven using a single LED on a foam float. The LED was held on the flat face of the foam, and a mold was formed with a ring of cardboard just larger than the LED. 2-part epoxy was mixed and poured into the mold. It covered the face of the LED up to the level of the lens, which was left bare. By covering the solder contacts, corrosion would be kept to a minimum. As long as Luxeon has manufactured its lenses correctly, there should be no problems with using this arrangement bare in seawater. Additional good news is that even with the thin (approximately 2 mm) layer of epoxy, the Luxeon V Star by itself (only the LED emitter and the hexagonal aluminum base) appeared to provide sufficient cooling when submerged in water. An additional small piece of aluminum may be desired, but the LED could be run indefinitely while submerged attached to the foam float.

Potted LED Blocks

In order to conduct the experiments at WHOI efficiently, four LED "Blocks" were constructed. Each block had three 5W Luxeon LEDs, one blue, one cyan, and one green. Each LED had it's positive terminal wired to two conductors of a Cat5e ethernet cable, and the three LEDs shared a two conductor ground (the brown and white/brown wires). The LEDs were arranged in a row on a piece of angled aluminum. They were held on with nylon screws, with thermal compound between the back of the LED star and the aluminum which acted as a heat sink. The aluminum block was drilled for a 3/8" hole and bolted to a plastic dowel that happened to exactly fit 3/4" PVC unions. This enabled the block to be rotated for aiming, and to be mounted easily to PVC structures.

To waterproof these blocks, Scotchcast^{TM} compound was used. This is a two-part flexible epoxy that hardens into a black rubber-like compound. No mold was used, rather the epoxy was poured and brushed onto the contacts of the LEDs, completely covering the faces up to the lenses. The wires of the ethernet cable were also covered with epoxy up to where they entered the sheathing. At the sheathing junction, self-vulcanizing rubber was used to ensure a good seal.

These LED blocks were used for many Strobe Lab experiments, and all experiments at WHOI and in the MIT Towtank. Out of the four blocks and a total of 12 LEDs, only two LEDs failed, one each of blue and green. Additional pressure testing would be required to verify this, but it has been the experience of the MIT AUV Lab that solid-state components can tolerate water pressure up to 6000 meters when encased in oil or otherwise separated from the corrosive seawater. The Luxeon 5W LEDs, with a silicone filled space between the diode and an acrylic lens, should be no different.

Reflectors
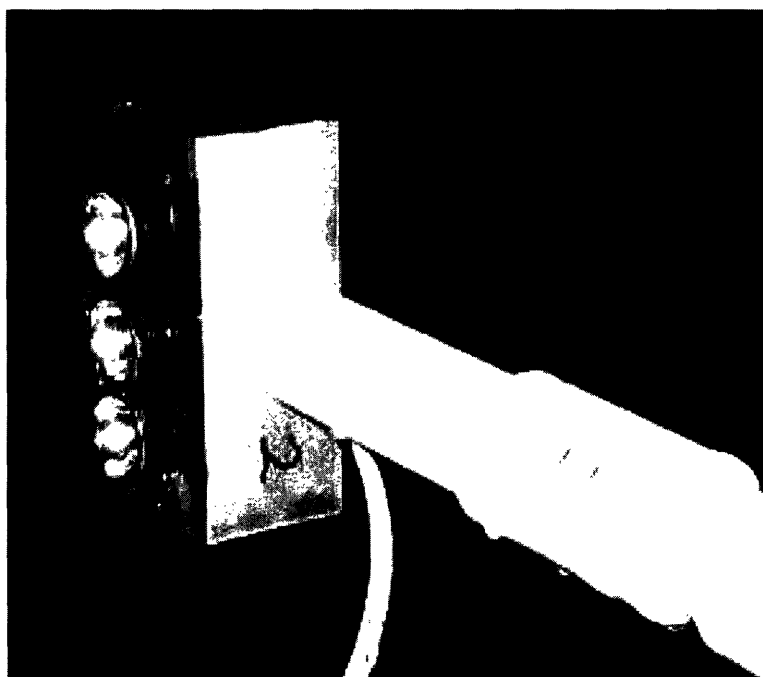
Figure 3-3: LED block with reflectors attached

For the Towtank experiment, reflectors were attached to the LED block to narrow the total angle range of emitted light. This was accomplished by adapting off-the-shelf reflectors from a AA MAG-LITE^R flashlight. The flashlight they are from has a narrower diameter bulb than the lens of the LED. To make them work, I drilled out the hole to the appropriate size, and then ground the back flat with a bench grinder. The reflector then sits on the black ring surrounding the LED, with the back of the reflector even with the base of the lens. For the tests, the reflector was held onto the block using a ring of butyl rubber. While not a

production ready solution, it worked fine for testing. Figure 3-3 shows an LED block with reflectors mounted, ready to be tested in the MIT Towtank.

3.2.2 Waterproofing Camera Systems

ROS Navigator

The camera is waterproof to 3000 meters, and required only a lengthened cable to be made to work. Cat5 ethernet cable was spliced into a pigtail and waterproofed with splicing tape. The twisted pair ethernet cable prevented signal degradation. By supplying power at the shore end, the camera's signal could be viewed remotely during underwater testing.

Elphel 313

A camera housing recycled from a much older, non-functioning camera was found that would accept the Elphel. A matching connector was located, and a Cat5 ethernet cable was used to extend the length of the shore cable. However, due to the operational challenge of using the Elphel discussed in Section 3.1.2, it was never tested in the water in the Towtank or at WHOI.

Canon S230

While the camera itself is very small, the required USB connector effectively lengthened the body. Also, a USB booster needed to be placed inside the housing to amplify the signal beyond the several feet allowed with standard USB. In order to waterproof the camera for remote operation, a Ikelite camera housing used by SCUBA divers was purchased. The housing was intended for a larger digital camera, but the Canon, the USB booster, and cables were a perfect fit. A sphere penetrator from the Odyssey vehicle was used to run the USB signal (now on 8 conductors) out of the housing. 100 feet of Cat5 cable ran to the shore side reciever of the USB booster system, and a USB cable connected to that reciever enabled remote picture taking underwater using a laptop computer.

Figure 3-4 shows the Ikelite camera housing used for the Canon S230
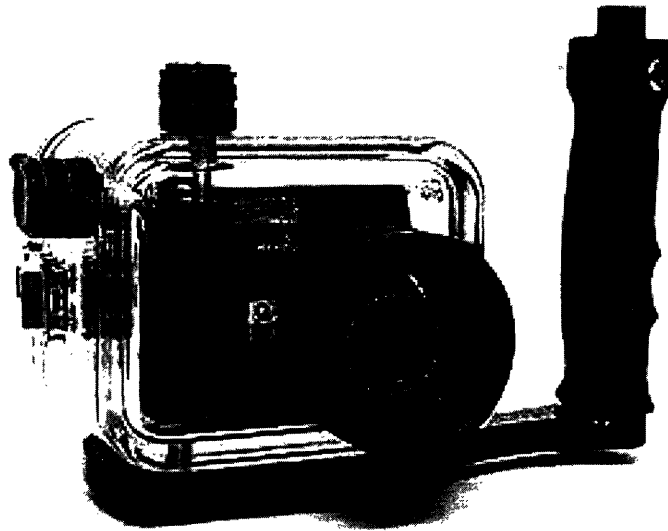
Figure 3-4: The Ikelite 6130 camera housing, intended for use with an Olympus 3030 digital camera

3.2.3 Waterproofing Test Equipment

Extech Light Meter

While it may have been possible to waterproof only the head unit, there was less than a meter of cable between it and the base unit. Extending that cable may have altered the calibration of the meter, so it was decided to waterproof the entire system.

An "Otter Box" was borrowed from Dr. Tom Consi of the MIT Ocean Engineering Teaching Lab (OETL). This box is an off-the-shelf housing usually meant to keep electronics or other objects dry when taking them on a boat or for a shallow scuba dive. It has a clear top cover which has a gasket that seals with the bottom half. The OETL as well as the AUV Lab have made use of Otter Boxes as waterproof housings in the past. As it turned out, the OETL had in stock an Otter Box that was the perfect size to accept the Extech.

To adapt the housing for the Extech, a hole was drilled in the side of the box that lined up with the serial port connector on the Extech. This hole was lined with butyl rubber (a.k.a. "monkey dung" in the AUV Lab, it is used to seal the glass spheres in the Odyssey class vehicles). The connector for the serial interface passed through the hole, and the butyl rubber made a watertight seal. The cord for the head unit was curled up, and the photodiode

68

side was placed on the top of the base unit, facing out through the clear cover.

Figure 3-5: The Extech light meter inside its waterproof Otter Box housing. The exposed photodiode (under the white diffuser dome), the penetration for the serial cable, and the serial cable splice are visible. The Extech sits on the target used during the WHOI experiments.

To use the light meter in water, the serial cable was extended to 33 meters by splicing it into a Cat5e ethernet cable. This had been determined to be a good working distance at for the experiment at WHOI during a preview visit to the site. The wet junction was waterproofed with self-vulcanizing splicing tape. The dry end of the tether cable had a standard DB-9 connector soldered at the end which was plugged into a laptop during testing. The only trick was to remember to turn the light meter on at the beginning of testing, and to turn it off at the end, as the Extech had no auto-off capability and replacing the 9V battery required unscrewing the Extech case in addition to breaking the waterproof serial cable seal on the Otter Box. Software installed on the laptop enabled remote readouts of the light meter, and the range could be changed to get better resolution in changing light conditions. See Figure 3-5 for an image of the Extech as it was deployed.

International Light Photodiode

A light detecting photodiode manufactured by International Light was also experimented with. Though waterproof from the factory, the photodiode was without its expensive reader unit. The cables to this sensor needed to be lengthened in order to work at WHOI. Readings taken in the lab with the longer cable seemed to show that current proportional to incident light could be detected with a simple circuit and a voltmeter. In practice, however, this proved not to be the case. The experiment of October 28 was scrubbed partly due to an inability to detect anything more than noise using this sensor in the ocean at WHOI. No useful experimental data was ever taken with this device.

Sea Tech OBS

The optical backscatter (OBS) device used was the Sea Tech Light Scattering Sensor. The device used was recycled from the Odyssey AUV program and had spent much time at sea. As such, it was already waterproof and depth rated to 6000 meters. All that needed to be done was to extend the cable so that it could be controlled remotely from a decent working distance.

The matching Odyssey connector was found and its pigtail was cut for splicing. This kept the connector molded to the device intact, rather than splice from its built in pigtail. Again, Cat5e ethernet cable was used to initially extend the cable to 33 meters. This was shortened to 17 meters, and again to 3 meters for the second WHOI and Towtank experiments respectively. The shore end of the cable was left bare to enable remote powering and signal output. As the OBS signal is simply a voltage that needs to be interpreted, changing the cable lengths, and therefore changing the output voltage for the same input signal, meant that direct comparison between different tests was impossible. The OBS was used simply to ensure that the conditions of the test remained constant during the test.

3.3   Strobe Lab

A number of dry experiments were conducted at the MIT Edgerton Center Strobe Lab. These included tests to characterize the LEDs themselves, to characterize the digital camera

used for most tests, and to examine the interactions between the LED illumination and that camera.

The Strobe Lab has black painted walls, blocked windows, and with the door closed and the lights out has virtually no ambient light. Though there are often other experiments set up or being prepared, there is a large open space that can be used for quick experiments. The space I used for the experiments is approximately 15 × 20 feet, with a blackboard backstop that was useful for both recording exposure data and as an illumination target. The space also has black curtains that may be drawn to divide the space or to partially block additional ambient light.

3.3.1 LED Characterization

LED Beam Pattern

One of the first tests conducted was to determine the beam pattern (in air) of the LEDs in question. This involved taking precise light meter readings of the LED from different angles relative to the "straight-ahead" position of the LED.

I mounted the photodiode receiver head of the Extech light meter (see Section 3.1.3) on top of a tripod. The Extech base unit was connected via a serial cable to a laptop for data recording. On top of another tripod, I mounted the LED in question. Tests were conducted for both the Luxeon 5W LED and the Nichia LEDs described in A.1. Using tripods enabled the LED and light meter heads to be accurately aligned at the same height. The LED tripod was located behind partially closed curtains to block reflected light from the LED illuminated room behind. This tripod had angle measurements which enabled light meter readings to be taken at multiple LED angles at a fixed distance, rather than having to move either the LED or light meter. The LEDs were powered remotely with an adjustable HP power supply with digital readouts of voltage and current, enabling precise control and measurement of power usage.

The results of this and all subsequent experiments are listed in Chapter 4.

LED Illumination

To test the usefulness of the LED for photographic illumination, images were taken of a target illuminated by a 5W Luxeon LED. By varying the LED and camera position, many effects of lighting could be examined.

A target was set up on the blackboard in the Strobe Lab. A newspaper was used for the center of the target. This was chosen due to its contrast (black and white text is easy to read, and comes in several sizes on the same page which enables one to gauge resolution) and diffuse reflectivity (the newspaper has a matte finish, so incident light is scattered in all directions, minimizing bright spots when the camera and light source are aligned in a certain way). Surrounding the newspaper, the various details of the experiment were recorded in chalk, which were recorded as part of the camera's image. This turned out not to be the easiest way to keep track of the image details, but it was worth a try.

The 5W Luxeon LED was placed on a tripod and powered remotely. Three different color LEDs were used for this test: Blue, Cyan, and Green. The LED's straight-on distance and horizontal offset from the target center were recorded, and adjusted repeatedly during the course of the test by moving the tripod.

For this test only, the Canon S230 was unavailible. Instead, a Sony Mavic digital camera was borrowed. The camera settings (f-stop, for example) were set to mimic the Canon S230. It was set on a tripod at the same height off the ground as the LED and the center of the target. It, too, was moved to different locations and aimed at the target from different directions. Images were captured using a timed release shutter (to ensure that camera movement was minimized), stored on the camera during the duration of the test, and downloaded at the test's conclusion for analysis. A sample shot of the complete setup is shown in Figure 3-6.

From the different LED position combinations, and the resulting camera images, it was possible to develop a very basic model of LED performance for photographic illumination. The results of this preliminary test are not discussed in Chapter 4, but were used as a baseline comparison to help design subsequent experiments.
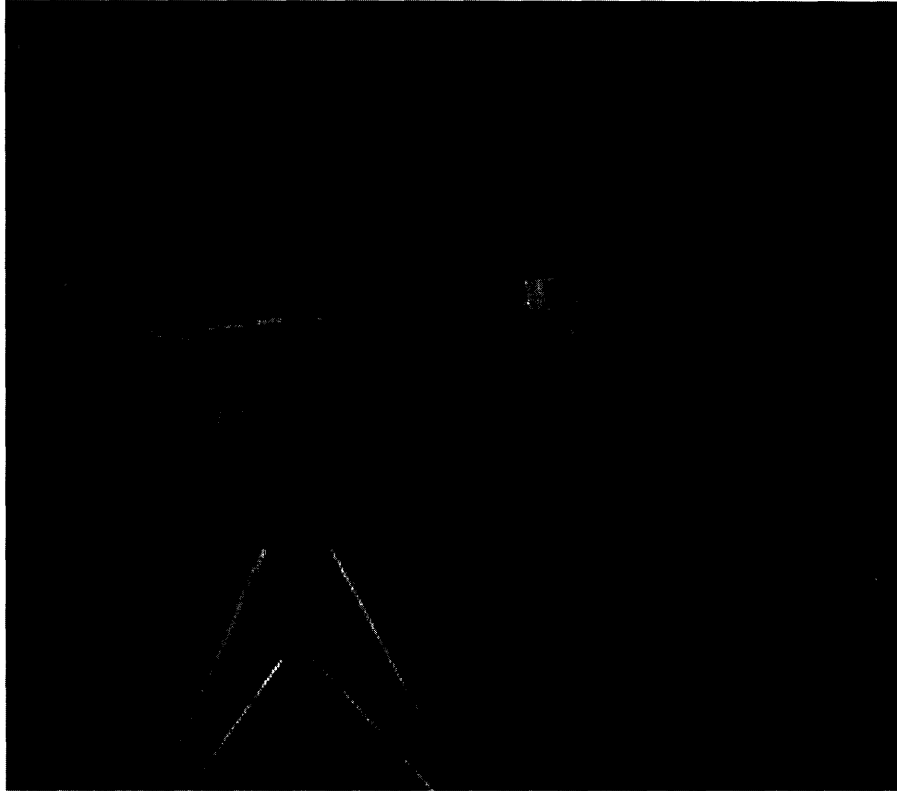
Figure 3-6: The setup of the preliminary LED and camera characterization experiment in the MIT Strobe Lab. The empty tripod in the center of the image holds the camera (when not being used to take this image). The image was taken using ambient fluorescent light in addition to a blue 5W LED to better show the true colors of the target and to allow a hand-held image to be taken.

3.3.2 Camera Characterization

In addition to the LEDs, the response of the digital camera had to be quantified.

Camera Exposure vs. Illumination

The experiment described in Section 3.3.1 was also used to predict the camera's response. Specifically, the incident light level at the target was measured using the Extech light meter. Images were bracketed in exposure at each LED and camera position combination. This would later enable the "best" exposure to be determined, and the corresponding exposure time for a given illumination level and LED color.

Verification of the Linearity of Contrast Response

A followup experiment conducted in the Strobe Lab used a different digital camera and more thoroughly explored its response.

For this experiment, the Canon S230 Digital Elph camera was used. This camera is the one that is used for all in-water experiments as well. The camera was set to mimic a film speed of ISO 400, it's highest sensitivity. In a setup similar to that shown in Figure 3-6, the camera was placed on a tripod, and controlled remotely via a USB cable connected to a laptop. The program interfacing the laptop to the camera enabled remote control of the exposure time compensation and also stored resulting images directly on the laptop's hard drive.

A block of potted, 5W LEDs was used as the light source. This block contained one each of the blue, cyan, and green LEDs, each powered individually. Four LED blocks in total were constructed for the WHOI experiments and are described in Section 3.2.1. The LEDs were mounted on a tripod and, like the camera, kept in a fixed position for the duration of the test. The power supply controlling the LEDs was adjusted to vary the luminous flux output of the LEDs.

The incident light at the target was measured and recorded using the Extech light meter, again connected via a serial cable to the laptop. The readings, in lux, were recorded for each of 5 locations marked on the target. The target consisted of several Kodak grayscale and color contrast checking standard cards taped to the blackboard in the Strobe Lab. An example image, shot under fluorescent light, is shown in Figure 3-7.

By varying the incident light intensity without changing anything about the geometry of the imaging system (i.e. without changing the location of the LED or target or the location or settings of the camera), it was possible to determine whether the length of exposure had any effect on image quality as judged by contrast in the image. Exposures were carefully bracketed at each of three illumination levels for each of the three LED colors. The results of this critical experiment are presented in Appendix section B.1.

Figure 3-7: The target used for the verification of contrast response linearity experiments in the MIT Strobe Lab.

3.4 MIT AUV Lab

Preliminary characterization tests of the Luxeon 5W LEDs were conducted in the MIT AUV Lab. These tests included the construction of simple power circuit prototypes and the first test of the LED's effectiveness in water.

3.4.1 Power Circuit

To verify the 5 watt claim listed in Luxeon's literature, LEDs were individually hooked up to an adjustable HP DC power supply with digital readings of voltage and current. Using these readings, it was easy to see that when the cable lengths were kept short, the LEDs did require 5 watts of power to run at maximum output (700 mA at $\approx$ 6.5V). For the longer cable runs necessary for wet testing, voltage loss over the cable required additional voltage and power. However, the total current could be kept the same and the voltage drop across

the LED would be known to be consistent. It was also possible to test the efficiency of various simple current regulator circuits that were constructed or purchased for the project.

3.4.2 Initial Wet Potting

Some very basic wet tests of a prototype LED candle were conducted in a 5 gallon bucket filled with water in the MIT AUV Lab. In addition to some preliminary battery-life estimates, the most critical result of these simple tests was the observation of the LED behavior in water.

For this test, an LED was attached to a piece of foam (the 150m rated brown foam used in the Odyssey AUV for shallow missions). A weight was placed in the bottom of the bucket, and the LED was strung above, held in the middle of the water by the float's buoyancy and the LED's two lead wires. The lead wires were led out of the bucket and powered the LED remotely.

The most relevant observation is that the LED had a visible plume of particles trailing off the anode side of the LED. It resembled a faint wisp of smoke. When removed from the bucket, the solder at that contact was visibly deteriorated. This corrosion observation, though no great surprise, lead to the immediate conclusion that the contact surfaces must be protected from the water. The test was conducted in Cambridge city water. While not pure, it was far freer of impurities and salt than seawater would be.

To avoid the corrosion problem, the LED was potted in epoxy. A two part epoxy (resin and hardener) was mixed, and poured over the LED up to the level of base of the lens. When hardened, the epoxy covered the contacts, but left the LED's lens bare. The test was repeated, and no plume of particles was noted. Protecting the solder contacts with epoxy became the standard for all subsequent testing, as previously described in section 3.2.1.

3.5 MIT Towtank

A series of photographic tests were conducted at the MIT Towtank to better quantify image quality's dependence on source/receiver geometry. Geometries that could not easily be tested in ocean water at WHOI were tested at the Towtank, as well as a number of other geometries to enable a good comparison between the two tests.

The MIT Towtank is roughly 36 m long by 2.6 m wide by 1.5 m deep. At the time of the tests, the water level was a little low at 1.04 m depth. The Towtank has a wavemaker (a piston actuated hinged plate) at one end, and a wave absorbing "beach" made of plastic mesh at the other. The tests were conducted near the wavemaker end, making use of a platform strung across the tank to hang a target from. One of the experimental carriages was left approximately 6 meters from the target platform, leaving a volume of $6 \times 2.6 \times 1\,m$ in which to work. A tape measure varnished into the edge of the Towtank provided X-axis measurements along the length of the tank. The Y-axis, measured out from the side of the tank, could be easily measured with a stiff tape measure. The Z-axis, measured down from the side of the tank, was used to ensure that all experiments took place at the same level, in the midpoint of the water.

Most of the lights in the Towtank lab could be turned off on the main switch panel, or via the fuse box. The only exceptions were two fluorescent emergency lights at either ends of the tank. By conducting experiments near the center of the tank, and by blocking the lights with plastic sheets, ambient light in the tank could be kept to a minimum. The emergency lights also made it possible to conduct the experiment and record data without needing a flashlight.

Many of the results of this experiment are shown in Section 4.4.3.

3.5.1 Measurement of the Optical Properties of Water

First, the water itself was tested. Visually, the water in the tank was very clear. The water in the tank had likely been left standing for several months. When this happens, the sediment usually present in Cambridge city water and the old pipes in the building settles out. A layer of sediment at the bottom of the tank is clearly visible in some images. A filter also turns on during the night, removing additional particulate matter.

As a result of this, the water was visually much clearer than would be expected in most coastal oceans. To quantify this properly, optical properties of water were measured.

77

Attenuation

A block of three LEDs were attached to a PVC pipe rig and suspended in the water. A measured distance away, the Extech light meter was suspended at the same height as the LED block. The Extech was in its waterproof Otter Box housing and was read remotely via a serial cable. A piece of PVC pipe was taped to the face to minimize reflected light to ensure that all light striking the Extech's photodiode came directly from the LED. Light meter readings were taken at various distances for each of the three LEDs. The results of these measurements are presented in Section 4.3.1.

Backscatter

The Sea Tech OBS was used. It was powered remotely, and suspended in the water at the end of a stick. Its output voltage was measured remotely with a digital test meter (see Figure 3-8). Backscatter was measured at the start of the tank experiment and checked again during the run. Most importantly, measurements were made both before and after a water filter pump activated in the Towtank. The outlet of the pump stirred the surface of the water during the test. The OBS readings presented in Chapter 4 show the result of this.

The OBS was on a shortened tether; 7 meters compared to 33 for the ocean tests at WHOI. This tether would have a decreased voltage drop, so readings would seem abnormally high compared to those at WHOI. The OBS was only used to check consistency during the course of the tests. Results are shown in Section 4.3.2.

3.5.2   LED Characterization in Water

A preliminary test conducted in the Towtank implied that the LED's lens had little effect in water. The LED's emission pattern remained similar what it was in air. The LED was fairly uniformly bright for all angles $\pm 75°$. With an accurate method of measuring angles, this test was repeated in the Towtank.

To generate a plot of the LED output as a function of angle, a test was conducted similar to the Strobe Lab test. The LED block was suspended in the water, and the Extech light meter was suspended at the same level, 1.22 meters away. The Extech was in the same
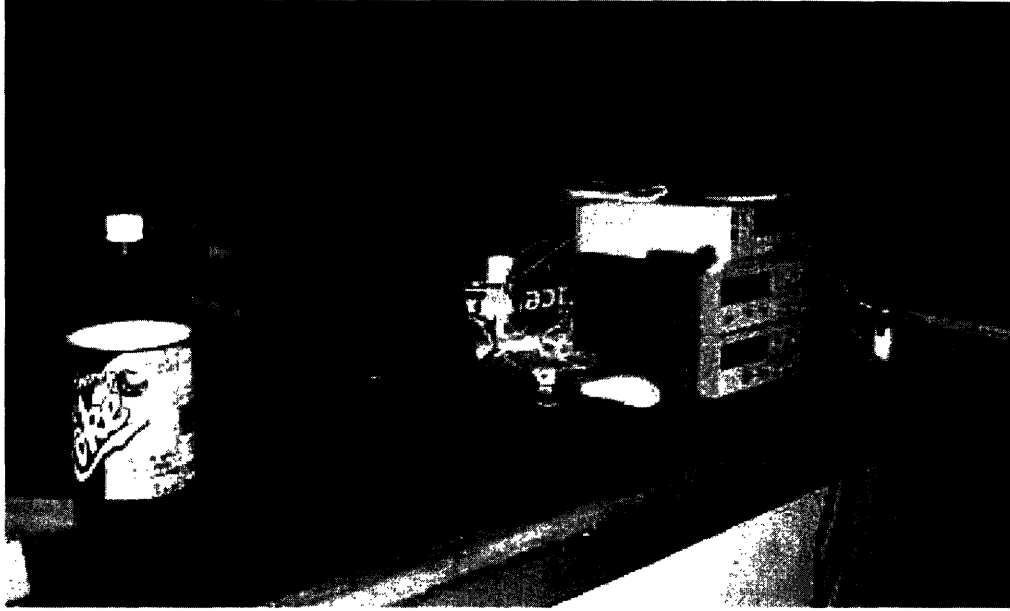
Figure 3-8: The lab bench setup for the Towtank experiment.

configuration as for the attenuation measurement. The LED block head could be rotated on its PVC mount to any arbitrary angle. Light meter measurements at every 10° increment were taken for each of the three LEDs. The test was conducted for bare LED bulbs, and then repeated for the LEDs with reflectors attached. The results of this test are shown in Section 4.1.

3.5.3 LED Illumination Effectiveness

After determining the conditions of the test, the next step was to take a large series of images to establish the effectiveness of underwater illumination using LEDs. Over five-hundred images were collected in this series, with a wide array of different geometries imaged. The target remained in one place, but by varying the location of the LEDs and camera independently, a large number of different configurations were possible. Many were tested, and the location and results of those test are presented in Section 4.4.3.

Imaging Target

Figure 3-9 shows the imaging target that was hung in the tank. The target consisted of a gray plastic sheet with several Kodak contrast targets taped to it. The Extech light meter in its waterproof housing was tie-wrapped to the face of the target to provide a rough measure of the incident light, as well as ambient light when the LEDs were turned off. The target was attached to two L-shaped PVC pipes, and hung from the platform in front of the wavemaker. The face of the wavemaker ended up about two meters behind the target, and the target's center was in the horizontal and vertical center of the towtank, facing the long axis of the tank. The five pound weight was attached to counteract the buoyancy of the Extech's housing.
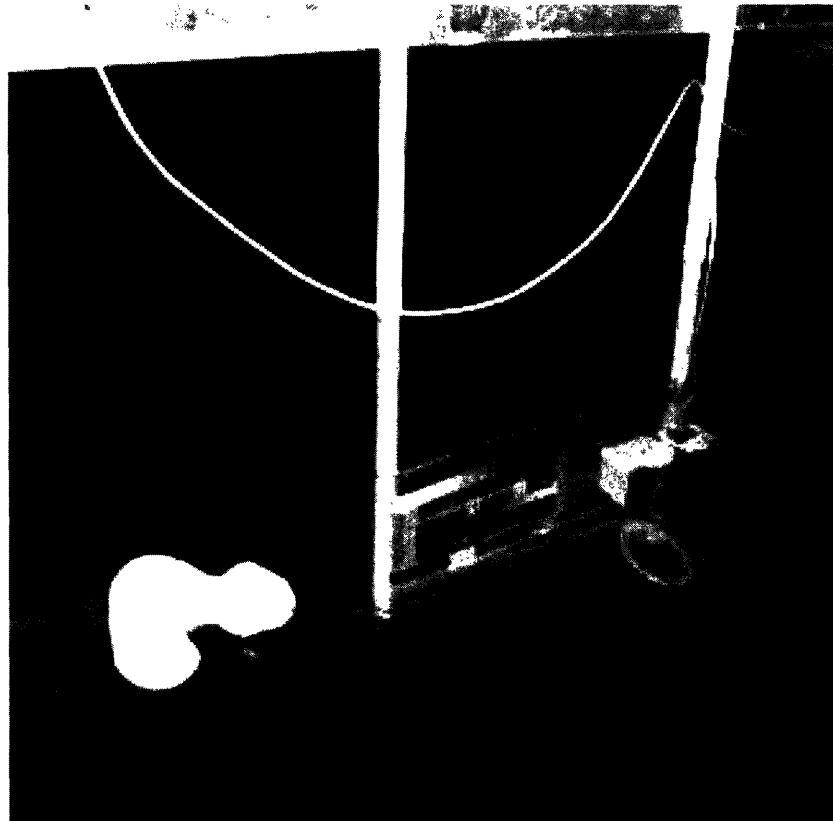
Figure 3-9: The target used for the LED illumination tests in the MIT Towtank. The rubber ducky is a long-time resident of the tank and is not involved in the experiment.

LED mount

The LED block was mounted on an adjustable PVC rig. The rig held the LEDs in the middle of the water vertically. It could be lengthened or shortened to slide the LEDs in or out in the Y-axis, and it could be moved along the side of the tank to any position in the X-axis. The LED block could be rotated into any position by adjusting the vertical PVC pipe in its fitting. This ensured that the LED block could always be aimed directly at the target. All experiments were conducted such that the "center" of the LED was aimed at the center of the target (another way to think of this is that the face of the LED was perpendicular to the center of the target). Both bare LEDs and LEDs with directional parabolic reflectors were used for the test. This difference allowed for testing of the effect of the illuminated water volume.

Camera mount

A PVC pipe was strung above the tank. It rested on the rail of the experiment cart on the far side, and sat elevated on the wooden tank rail on the near side. A number of fittings on the pipe enabled a vertical pipe to be suspended down into the water (see Figure 3-10). In the midpoint of the water, the Canon S230 digital camera was suspended in its waterproof housing. The camera was powered by an internal battery, and controlled remotely via a USB connection to a laptop. The camera could be rotated around its mount and was always aimed directly at the target.

3.5.4   Camera Characterization

In addition to different geometries, at certain LED/camera location combinations the exposure of the camera was bracketed. By bracketing for specific conditions, and recording exposure data and incident light measurements for all images, it is hoped that the conditions required for the "best" image may be discovered.
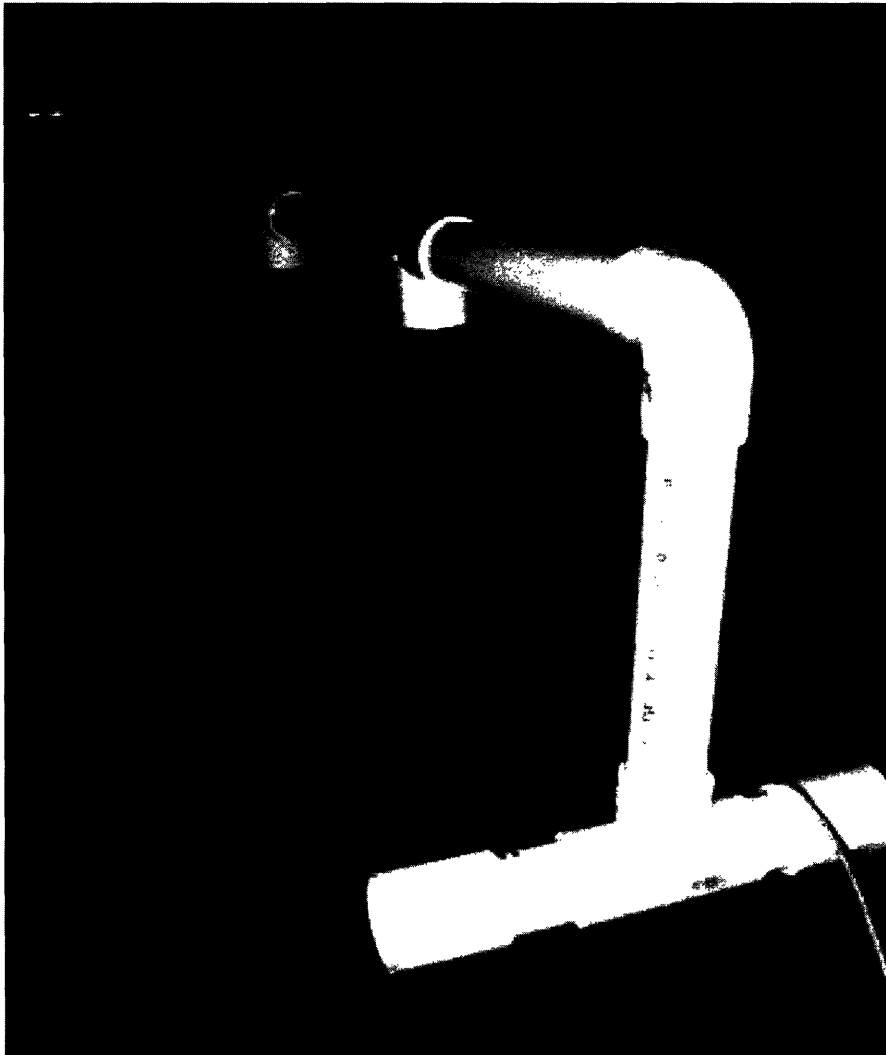
Figure 3-10: The dry portion of the camera mount. The camera is suspended from the vertical pipe.

3.6 WHOI Well

Two major experiments were conducted in ocean water at the Woods Hole Oceanographic Institute (WHOI). Access to the water was through a hole in the dock called the "well". The water below the dock in the vicinity of the well is up to twenty meters deep. The dock sits in a partially sheltered bay open to the ocean. A more sheltered harbor and bay behind provide a body of water for tidal action such that a strong current was periodically witnessed in the well.

Experimental test rigs were lowered into the well with a crane, and data was recorded from within a laboratory equipped shipping container called a "van". The experiments resulted in over 200 LED illuminated images in real-world conditions testing a wide variety of source/receiver geometries.

Figures 3-11 and 3-12 show the WHOI dock in the vicinity of the well. Figure 3-13 shows the camera rig for the experiment.
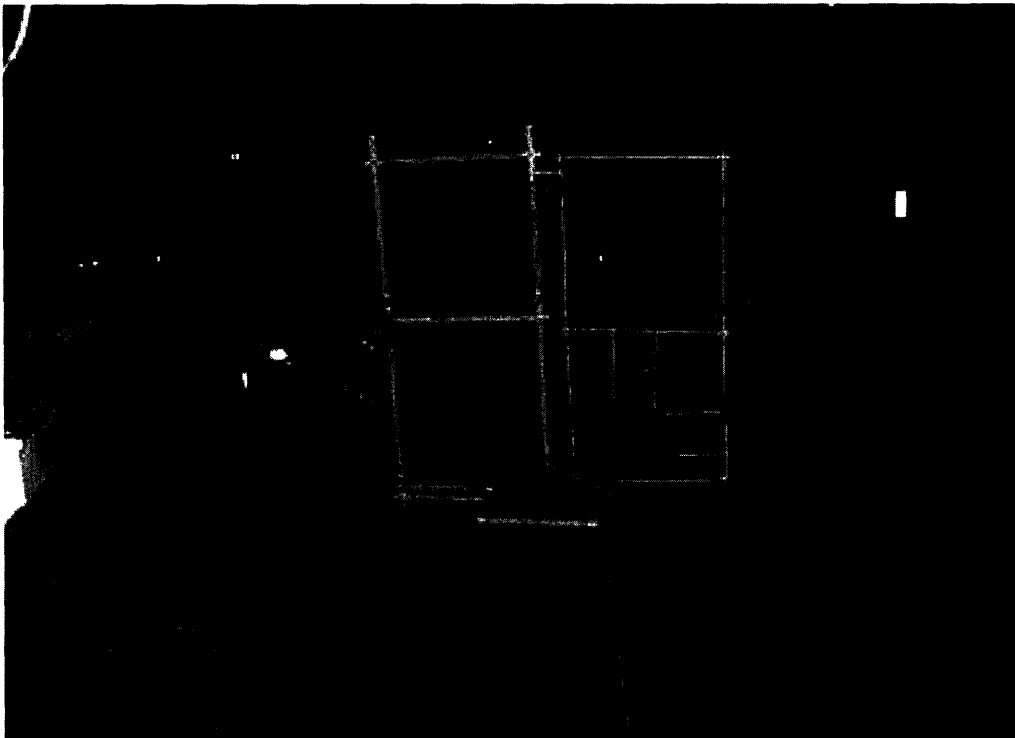
Figure 3-11: The author's father stands by the experiment rig, ready to drop it in the well

The first experiment, conducted on October 28, 2003, ended prematurely after repeated
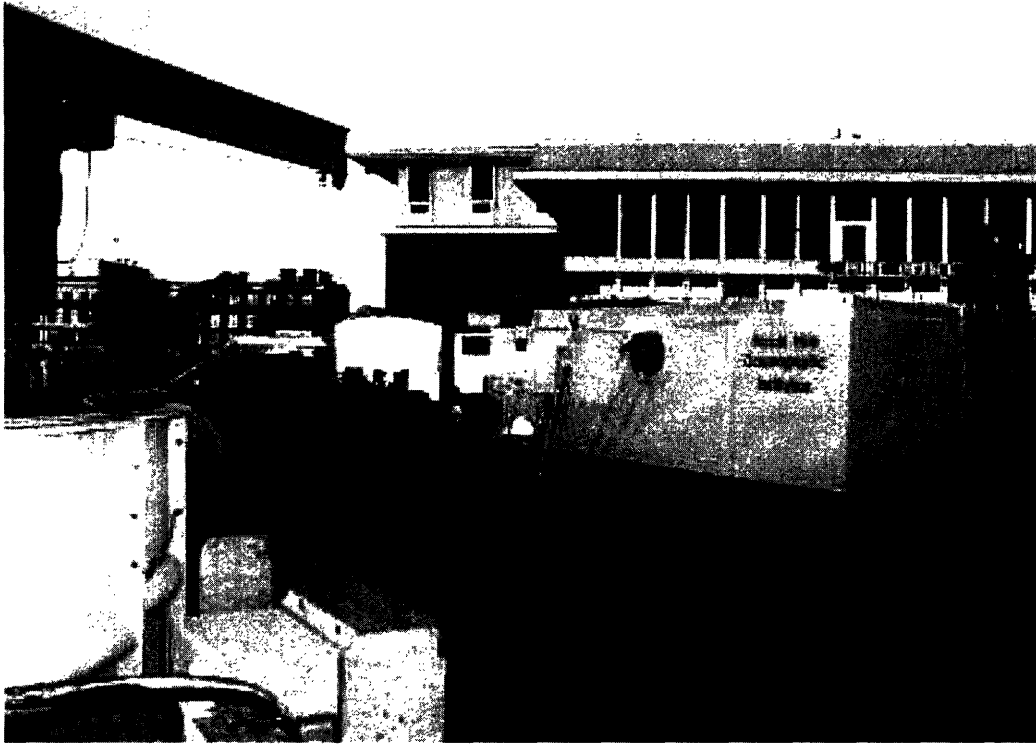
Figure 3-12: A daytime shot of the WHOI well shows the crane and van used in the experiment. The author prepares the attenuation rig.

equipment failures. Some data was collected, but not used. The problems were corrected, and a better prepared experiment was conducted on October 30, 2003. The second experiment went off almost without a hitch. The remainder of this section describes only that second experiment.

Figure 3-14 shows the experimental setup inside the van. The scene is monitored with the ROS Navigator camera and the LEDs are controlled with the power supply. The laptop computer records information, monitors the light meter, and controls the Canon digital camera remotely.

Many of the results of this experiment are shown in Section 4.4.2.

3.6.1 Measurement of the Optical Properties of Water

As before, the water was tested to quantify the conditions of the test.
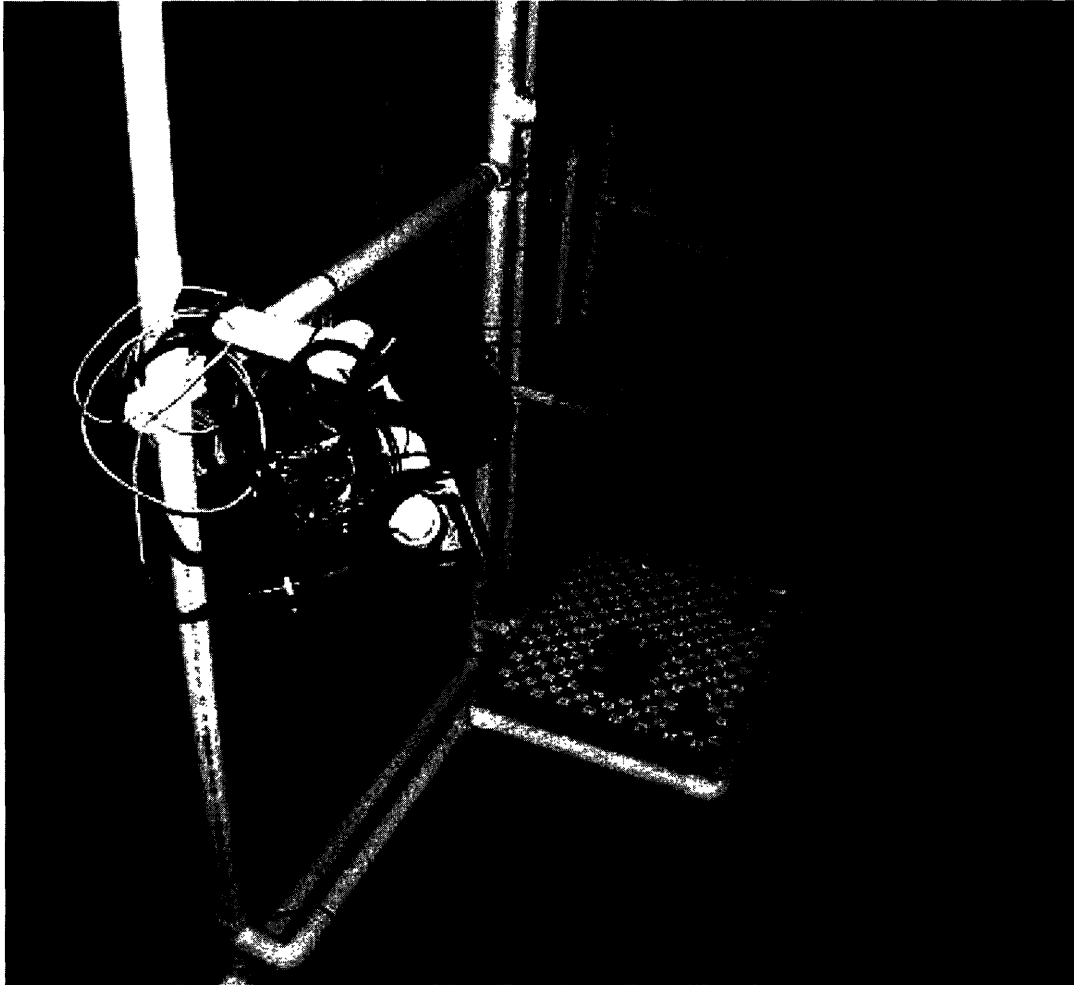
Figure 3-13: A closeup of the camera mount and target on the experimental rig used in the WHOI well.

Attenuation

A long PVC pipe was used to measure attenuation. An LED block was attached at a marked point from which a good distance measurement could be made. The Extech light meter was waterproofed and hung at the end of the pipe. The rig was lowered into the water and a light meter measurement for each of the LEDs was taken remotely. For each distance, the rig was removed from the water, the LED block moved, and the rig was then placed back in. This yielded data that is analyzed in Section 4.3.1.
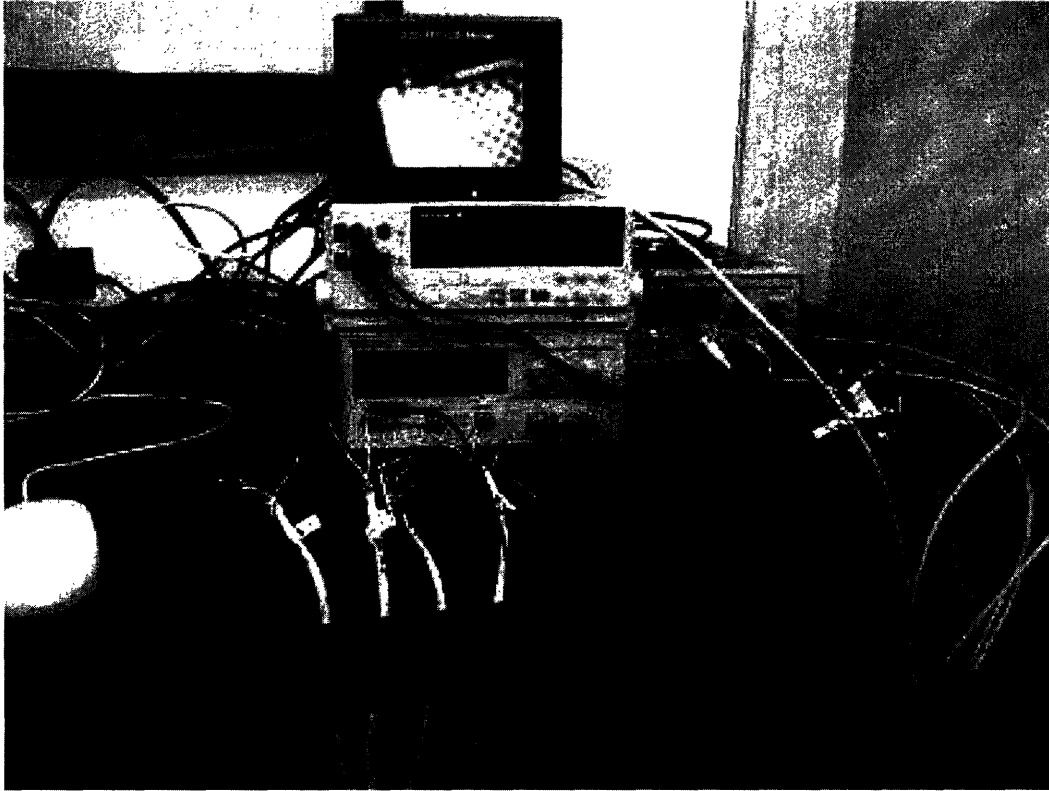
Figure 3-14: The bench setup inside the van on the WHOI dock.

Backscatter

The Sea Tech OBS was used throughout the experiment. It was attached to the camera mount directly and aimed into empty water. It was powered remotely and its voltage output was read on a digital test meter. It was operated through 33 meters of cable, the voltage drop over which would tend to make the readings lower than reality (i.e. the OBS would show less scattering than it observed). The OBS functioned to monitor the changing conditions of the test, ensuring that the water remained relatively consistent. Results are shown in Section 4.3.2.

3.6.2 Camera Effectiveness

Two cameras were used during these tests. The Canon S230 provided the bulk of the experimental images. The ROS Navigator 3.8mm digital video camera provided additional images on the first night, and real-time scene monitoring throughout.

The results of this experiment are presented in Chapter 4. Specific to the camera itself, four camera positions were tested, and several bracketed exposures were taken. This provided a good number of data points with which to evaluate the camera's function, and compare it to what was predicted in previous experiments and simulations. Though not a completely thorough evaluation of the camera's wet performance, the testing was intended to confirm that the camera performed consistently.

3.6.3 LED Illumination Effectiveness

The focus of this experiment was to determine the effectiveness of different LED illumination geometries that may be experienced by an AUV. Eight mounting locations were selected on the test rig, along with four camera positions. This enabled 32 different geometries to be tested with three different colors of LEDs.

For this experiment, only bare LEDs were used (LEDs without a reflector). Though not intended, this meant that source/receiver separation as measured by the optical path length was for many geometries coupled with the illuminated water volume. In other words, as the LED was moved further from the target, more of the water column in front of the camera was illuminated. Results from this experiment are shown in Section 4.4.2.

3.7 Simulation and Modeling

In addition to both wet and dry testing, several models were created to simulate illumination underwater. These models were used to predict the performance of an eventual system resulting from this work, as well as to better understand the experimental data. The inner workings of some of the models and simulations are presented here, with analysis of the results in Section 4.5.

All mathematical modeling was done with the help of MATLAB, a product of Math-Works, Inc.

3.7.1 Required Illumination

After the results of the first camera and LED characterization experiments in the Strobe Lab were analyzed, a model could be developed of an LED lighting system. A "best case" simulation was developed modeling the light available from LEDs illuminating a flat target area.

The Strobe Lab experiments enabled a first cut estimate at the light required to generate an image at a given exposure. To get the best case estimate, the overarching assumption was made that all LED light would be uniformly spread out on the target area, with no overlaps, hot-spots, or unlit regions. This, of course, is not the case in real life, but provided a best case LED performance estimate from which inferences could be drawn about the ultimate performance of an LED candle or other LED illumination system.

Using the exposure value equations, and experimental data to quantify the Canon S230 camera's response, a model was developed showing the relationship between the size of a patch of ocean bottom illuminated by a single LED and the required exposure of the Canon S230 imaging the scene. The diameter of this patch is referred to as the *footprint diameter*.

The results of this simulation, including estimated footprint diameters, are shown in Section 4.5.1.

3.7.2 Light Efficiency

By knowing the wavelength dependent light energy input to the system, and the approximate dimensions of the target area and imaging system (which yield the total optical path length), the total illumination effectiveness can be estimated.

Using radiative output curves based on the three Luxeon LEDs tested, as well as on three comparative halogen lamps, the radiative loss due to attenuation could be simulated for any optical path length (OPL). Doing this for a number of OPLs, and integrating to find the total radiative and luminous outputs, the effective efficiency of the light sources could be simulated.

The results of this are shown in Section 4.5.2

Chapter 4

Results

In this chapter, the results of the experiments described in Chapter 3 that directly pertain to the project are presented. Supporting experimental data (such as comparison LEDs and Camera justification experiments) are saved for the appendices.

4.1   LED Characterization

The Luxeon 5W LEDs were tested experimentally and compared to the specified values (see Table 3.1) given by the manufacturer. They were tested both in air and in water and their output radiation patterns were measured. The total luminous flux was calculated based on an integral of their outputs. Finally, their outputs were compared to existing Nichia LEDs that had been used in the past to create LED illumination arrays [13].

By using a lightmeter to measure the incident illumination at a fixed distance from the source at various angles, a radiation pattern can be determined. Figure 4-1 shows the polar radiation pattern of the Blue Luxeon LXHL-LB5C 5W lambertian LED. This process was repeated for the same LED in water. By normalizing the radiation patterns by their maximum values, the two patterns are compared in Figure 4-2. This pattern agrees very well with the typical patterns given by Luxeon, shown in Figure 4-3

Three Luxeon 5W LEDs (blue, cyan, and green, shown in Table 3.1) were examined in water. Their polar radiation patterns, which clearly display their relative brightness, is shown in Figure 4-4. Their normalized radiation patterns are shown in Figure 4-5. Additionally,
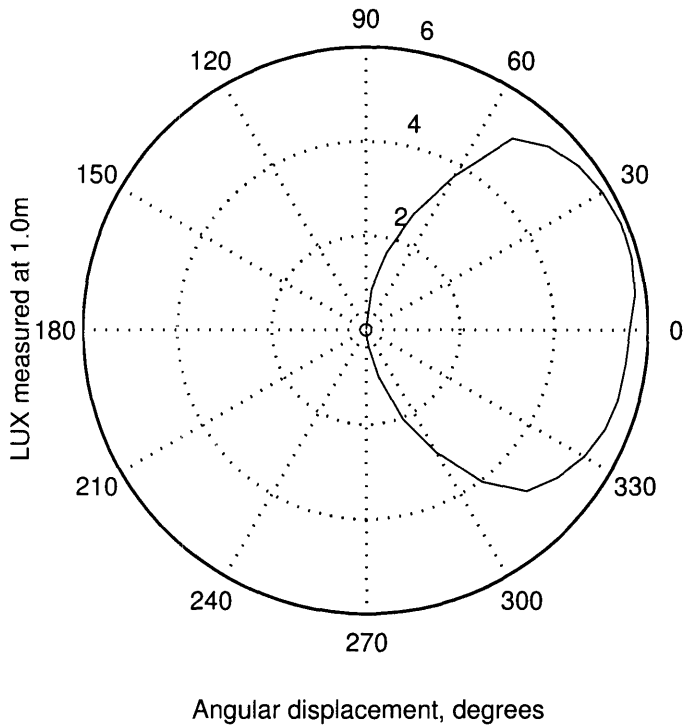
Figure 4-1: Radiation pattern of Blue 5W Luxeon LED, LXHL-LB5C, in air, in polar coordinates. Incident illumination measured in lux at a range of 1.0 meters.

the normalized radiation patterns of the three LEDs in water with parabolic reflectors is shown in Figure 4-6.

Using the data from these radiation patterns, it is possible to calculate the total luminous flux of the LEDs. This is done via piecewise integration using Equation 2.2. As is shown in Table 4.1, with the exception of the blue LED, the integrated luminous flux measurements agreed well with the specified values from Luxeon. It is possible that the Extech light meter does not adequately detect blue light, as the measured flux is lower than the Luxeon specification. However, Luxeon specifies a minimum output of 18.1 lm for the Blue 5W LED, so it is entirely possible that the particular LED used in the test was simply at the lower bound of acceptable performance. Additionally, similar experiments with small Nichia LEDs provided similar results (see Appendix section A.1 for more on the Nichia specifications and calculations), with the results likely limited by the resolution of the input data.

Because the peak output wavelengths for the Nichia LEDs correspond to the peak output wavelengths for the cyan and green Luxeon 5W LEDs, (see Tables 3.1 and A.1), it is possible
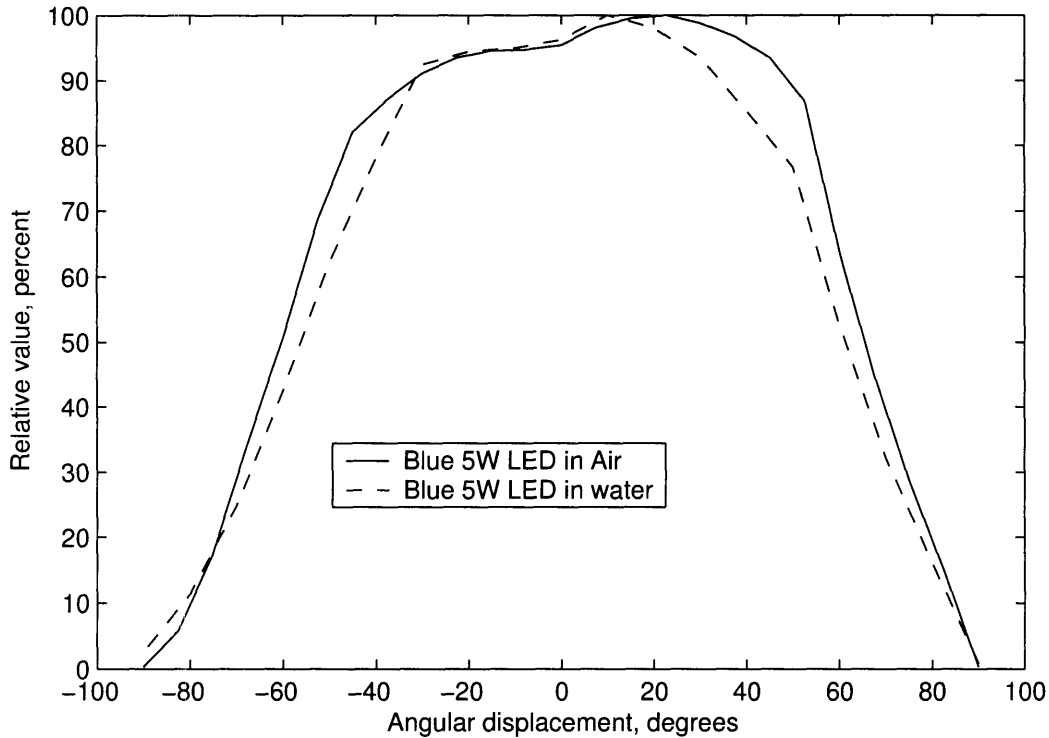
Figure 4-2: Normalized radiation pattern of Blue 5W Luxeon LED in air and in water

to directly compare the LEDs using only their specified luminous output. Using the luminous outputs given in Table A.1 (see Appendix section A.1 for a derivation), and a 120 lm output for both cyan and green Luxeon LEDs, Table 4.2 shows the number of Nichia LEDs required to have a total luminous output equal to a single Luxeon 5W cyan or green LED and the minimum diameter of the equivalent LED array.

For comparison, a Luxeon V Star, which was used in this project, has a diameter of 20 mm, most of which is the aluminum base it sits on and its solder contacts. A Luxeon emitter, which includes only leads, has a diameter of 7 mm, but would require an additional heat sink. The Luxeon 5W LEDs, of course, draw 5 watts of power.

The Array dimensions listed in Table 4.2 are the best case, assuming the LEDs are packed as tightly as possible. In actual practice, Rosser [13] developed an array of 60 Nichia LEDs that was at best 80 × 45 mm, and with the extra potting compound was 110 × 90 mm and 50 mm tall. This could be replaced by a single Luxeon 5W LED which, with a reflector and mount, could be smaller than a stack of 20 quarters.

LED	Luminous Flux, (lm)		
	Measured	Specified	Minimum Spec.
5W Blue *in air*	20.43	30.00	18.1
5W Blue *wet*	16.86	30.00	18.1
5W Cyan *wet*	118.35	120.00	67.2
5W Green *wet*	116.92	120.00	67.2
5W Blue *reflector*	26.99	30.00	18.1
5W Cyan *reflector*	94.90	120.00	67.2
5W Green *reflector*	103.30	120.00	67.2
Nichia E500	0.78	0.50	none
Nichia E510	1.53	0.84	none
Nichia G500	1.04	0.62	none
Nichia G520	2.09	1.32	none

Table 4.1: Total luminous flux output, in lumens, of the various LEDs tested. "Wet" refers to measured output of the bare LED bulbs in water. "Reflector" refers to bulbs in water with a parabolic reflector attached. Measured values are calculated based on experimental data. Specified values are either provided by Luxeon, or in the case of the Nichia LEDs, calculated based on other specifications

Nichia LED	Nichia LEDs Required	Array Diameter (mm)	Factor of Area Increase	Power (Watts)
NSPE500S	243	83	17.0	25.5
NSPE510S	143	63	10.0	15.0
NSPG500S	192	74	13.5	20.2
NSPG520S	91	51	6.4	9.5

Table 4.2: Size and power consumption of an array of Nichia LEDs equivalent to a single Luxeon V star 5W cyan or green LED. Both Luxeon LEDs are 20 mm in diameter and output 120 lumens at wavelengths comparable to the Nichia LEDs.
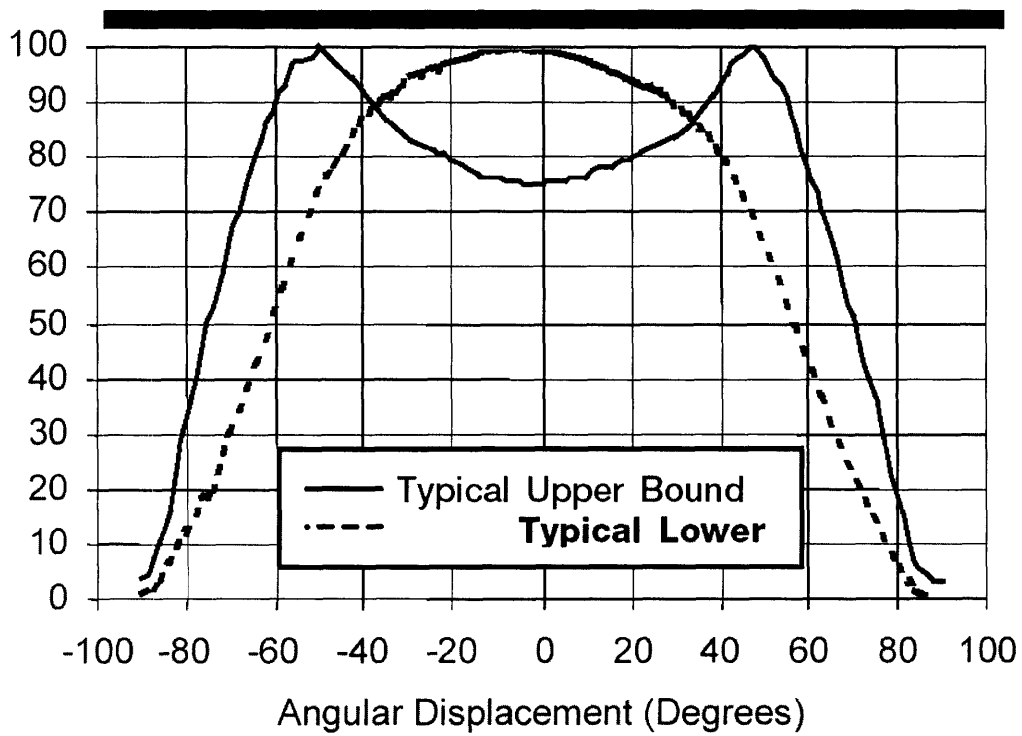
Figure 4-3: Representative typical spatial radiation pattern for Luxeon V Star (5W Luxeon LED). Reproduced from Luxeon technical datasheet DS30.
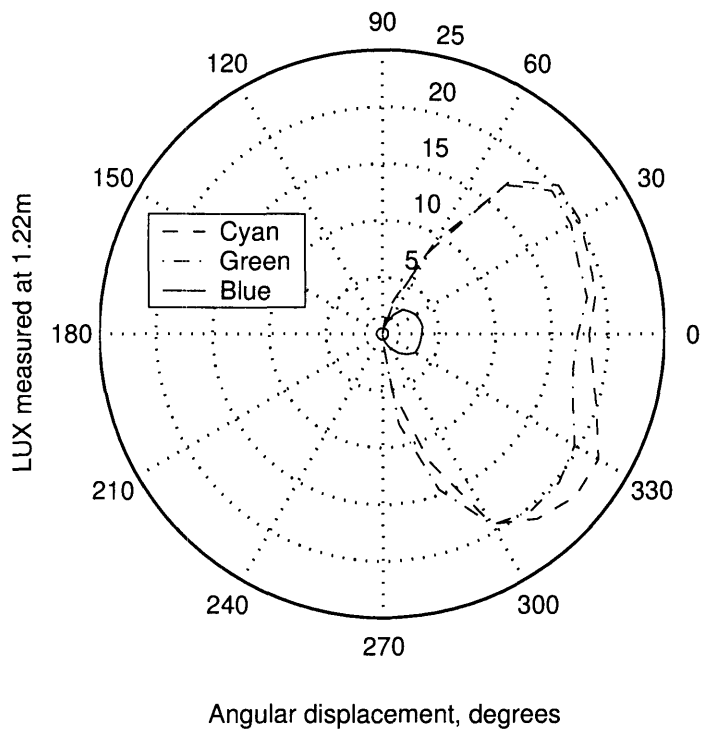
Figure 4-4: Polar radiation pattern of the three 5W Luxeon LEDs in water. Illumination, measured in lux, at a range of 1.22 meters is shown.
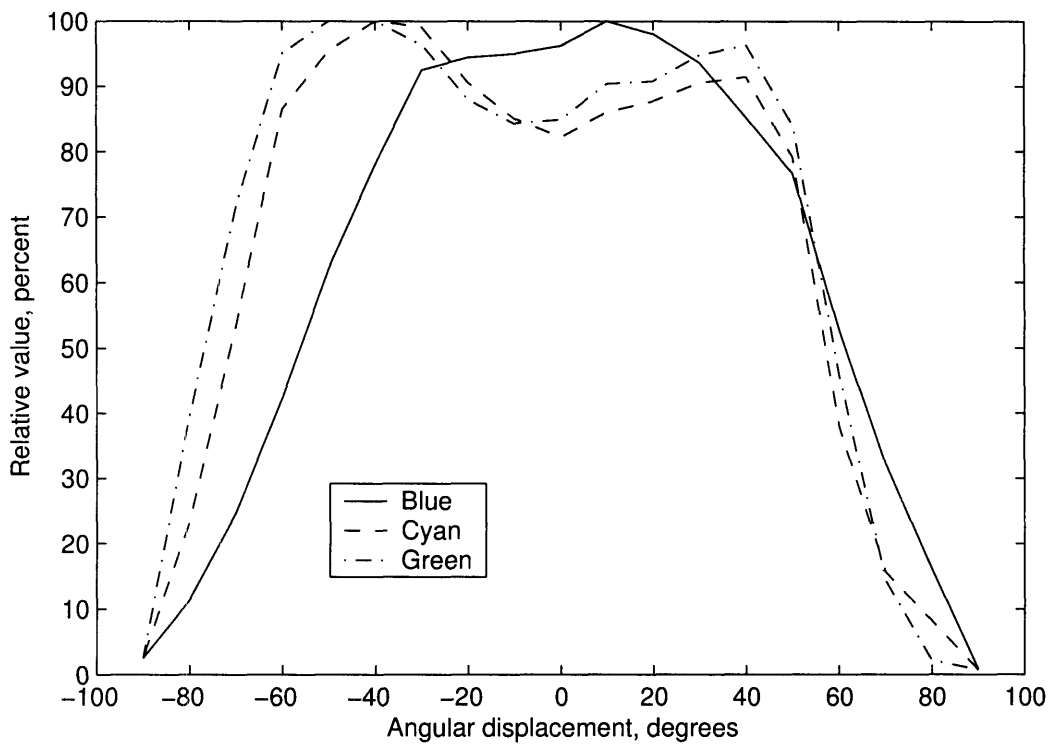
Figure 4-5: Normalized radiation pattern of the three 5W Luxeon LEDs in water.
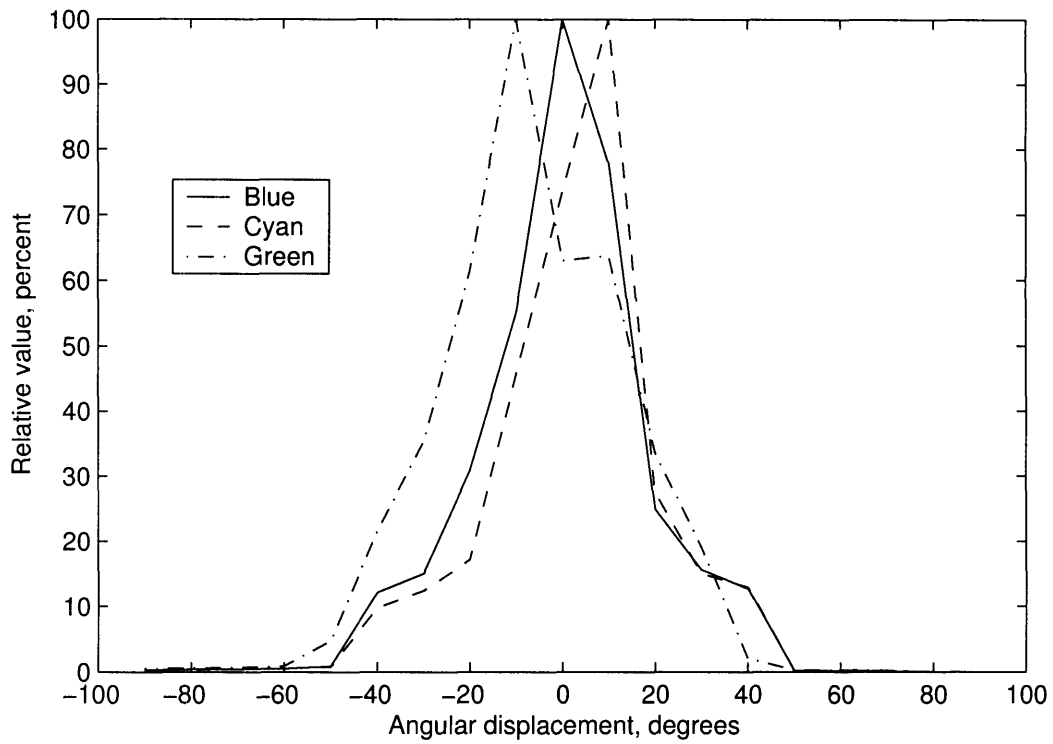
Figure 4-6: Normalized radiation pattern of the three 5W Luxeon LEDs in water with parabolic reflectors.

4.2 Camera Characterization

4.2.1 ROS Navigator

The ROS Navigator was primarily used to monitor ongoing experiments. Even before passing through the additional layers of abstraction (video capture board to compressed JPEG image to post-script image reproduced in this document), the quality of the output image from the ROS is very low. The CCD chip is of a much lower resolution than is now available, and the internal conversion from CCD to output video yields a great loss in quality. An example image of the target used on the first night of the WHOI experiment (different than the subsequent night) is shown in Figure 4-7.

Figure 4-7: ROS Navigator image, captured at WHOI using an Imperx Inc. model VCE-B5A01 PCMCIA capture card. Inset shows a much reduced image of the same scene imaged by the Canon S230.

No further characterization of this camera was deemed necessary, as the initial impres-

sion of the Canon digital still camera made the ROS Navigator seem woefully inadequate. Combined with its large size and operational overhead, it is unlikely that it will see use in an MIT AUV in the future.

4.2.2 Canon S230

The Canon S230 digital camera exhibited exemplary performance throughout testing. A sample image, slightly cropped and displayed at one quarter native resolution, is shown in Figure 4-8. The camera provided consistent images, and even auto-focused accurately underwater.

Two qualities of the camera are of critical importance to this project, and to future application in AUVs. The camera must accurately expose images, and it must have a linear contrast response.

The first camera characteristic tested was its exposure response and accuracy of light metering. In other words, does the camera consistently capture images using the correct exposure? Using the bracketed exposure time[1] data shown in Appendix section B.1, it can be seen that the camera is quite consistent for cyan and green illumination, but overexposes scenes lit with the blue LED.

The camera must also maintain a linear contrast response. That is to say, for multiple light levels (and therefore for multiple exposure times), the contrast between light and dark sections in the resulting image must be the same. Appendix section B.1 shows the data and analysis that proves the camera is linear in contrast response.

The linearity in contrast response is especially important. One of the assumptions used in the simulations is that, all else being equal, doubling the amount of light at the target (in other words, doubling the illumination or lux reading at the face of the target), will halve the exposure time, but not change the contrast of the resulting images. During in-water testing, illumination changes due to differently placed LED light sources and a correspond-

---

[1] A so-called bracketed exposure is one where the same image is exposed with multiple exposure times. The Canon S230 can be made to expose for times up to two stops above and below what it calculates as the "correct" exposure time in 1/3 stop increments. That is to say, based around what the camera determines the correct exposure time to be, exposures up to four times longer or four times shorter can be dictated by having the camera compensate. For the bracketed data in B.1, up to 13 exposure times are used for each scene.
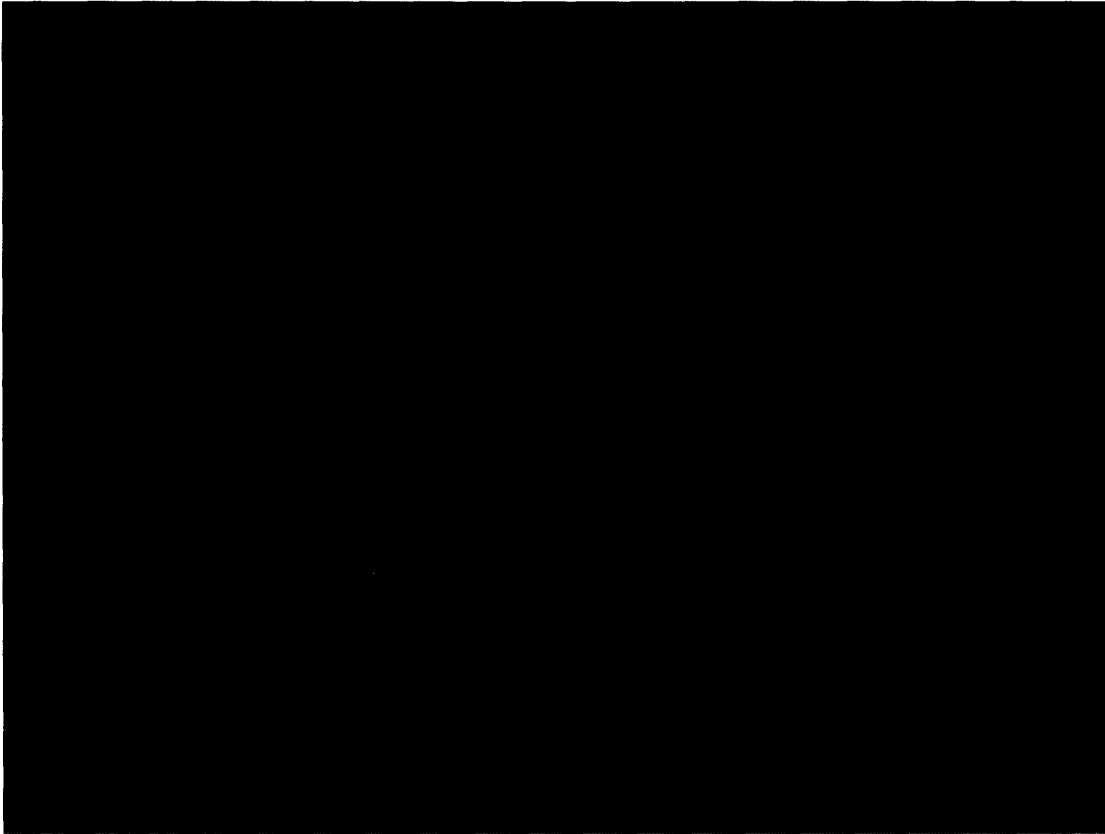
Figure 4-8: A sample image captured by the Canon S230. This is an image of the target used at WHOI. Illumination was with the Cyan 5W LED from 0.5 meters away. The camera was at a range of 2.44 m. Exposure was 0.077 seconds.

ingly different illumination measurement for each LED position. In order to compare the contrast of images exposed for different lengths of time, contrast linearity is critical. The results shown in B.1 show that this assumption is valid, which justifies assumptions used in imaging system tests and simulations.

4.3 Optical Properties of Water

The optical properties measured in the two main bodies of water studied are presented in this section.

4.3.1 Attenuation Coefficient

The data collected in the Towtank and at WHOI presented an interesting problem. The Extech light meter returned values in lux, measured at various ranges from the bare LEDs in water. In order to extract the attenuation coefficient, α, from a given dataset, several steps were required.

First, the ambient light was subtracted out. Then, the $\frac{1}{r^2}$ effect of range[2] was accounted for by multiplying the readings by r^2, where r is the distance from the LED to the Extech light meter. The resulting values now appeared to lay on a straight, downward sloped line. The values were normalized by the highest value, and MATLAB was used to calculate a linear fit using the least squares method in the form $y = p_1 x + p_2$, where p_1 is given as the slope of the line. For the wavelength of light corresponding to the LED used for that particular data, the attenuation coefficient α is then given by

$$\alpha(\lambda) = -\ln(1 + p_1) \tag{4.1}$$

Note that p_1 is negative, as the normalized illumination decreases with range independent of $\frac{1}{r^2}$ according to Equation 2.18.

The attenuation coefficients of the water in the MIT Towtank and in the well at WHOI are given in Table 4.3.

To allow for a comparison, the values of the attenuation coefficient α generated during the experiments are plotted in Figure 4-9 along with other data. Though only three wavelengths were examined, the α of the WHOI water correlates well with the "coastal" water from [9], while the Towtank water is optically similar to clean deep ocean water. The relative

---

[2]Illumination falls of as as $\frac{1}{r^2}$, where r is distance (radius) from the source. This is the rate that the surface area of a sphere grows. If, at $r = 1$ meter, a certain illumination is measured, at $r = 2$, the same light will now be spread over four times the area, so the measured illumination will be one fourth as much.

Location	Wavelength λ		
	470	505	530
Towtank	0.049	0.037	0.037
WHOI	0.292	0.275	0.297

Table 4.3: Values of the attenuation coefficient α for three wavelengths, as measured in the MIT Towtank and the ocean water in the WHOI well.

values of α is most interesting, with both showing a local minimum near 505 nm[3], the peak wavelength of the cyan LED.

---

[3]For the Towtank experiment, the measured α for cyan (505 nm) is only less than that of green at the fourth decimal place (530 nm). Fitting a curve to the three points, the minimum would be somewhere around 517 nm.
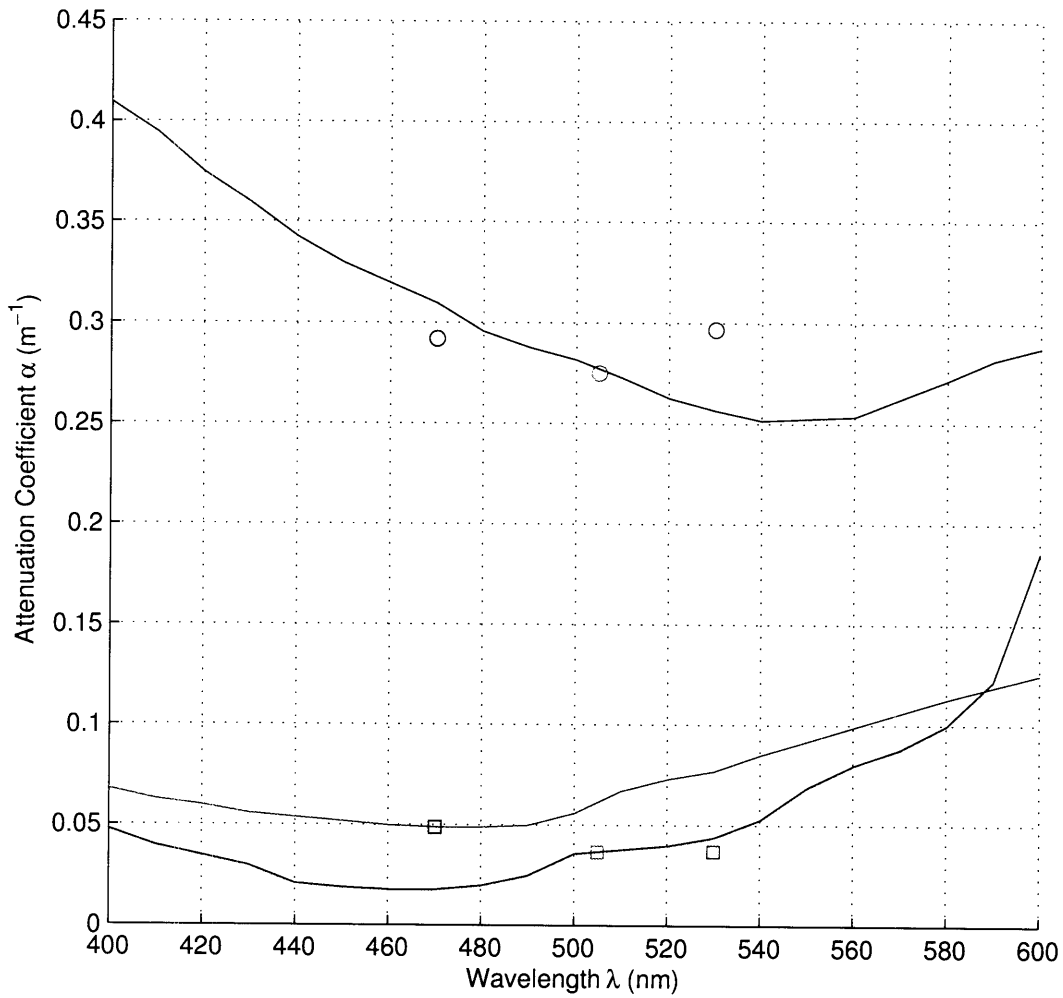
Figure 4-9: The attenuation coefficient measured in the MIT Towtank (squares) and at WHOI (circles) for three wavelengths. The data is presented with the distilled, deep ocean, and coastal water attenuation coefficient data from Figure 2-6. The wavelengths (470, 505, and 530 nm) correspond to the peak wavelengths of the Luxeon LEDs (blue, cyan, and green).

4.3.2　Optical Backscatter

The Sea Tech optical backscatter sensor (OBS) was most useful in ensuring that the conditions of the test remained the same during the duration of testing.

Towtank OBS Results

During the Towtank tests, the OBS cable had a length of 3 meters. The raw voltage output from the OBS was ≈ 62 mV whenever it was measured. This was at the start of the test, during the test, and at the end, including both before and after a pump turned on in the tank. Given the invariance of the OBS readings, it is doubtful that the water conditions changed during the test. The attenuation coefficient was only measured at the start of the experiment, but is assumed to have remained constant.

WHOI OBS Results

The experiment at WHOI lasted long enough for the tides to change direction. They were coming in at the start of the experiment, still during the middle, and going out near the end. Therefore, it is likely that the particulate content of the water changed during the experiment. The attenuation coefficient was only measured only once at the start of the experiment. The OBS data, however, noted a change.

At each new camera position during the imaging portion of the experiment (four positions, repeated twice for two banks of LED positions yielding eight total measurements), an OBS reading was taken. These readings ranged from 260 mV to 340 mV, a thirty percent swing. Additionally, the readings fluctuated slightly from moment to moment by 10%. Visible particles could be seen in the monitor passing in front of the ROS camera. It is possible that the time-variant nature of these particles created the noise in the OBS readings. If a direct correlation between the backscatter seen by the OBS sensor and the attenuation coefficient of the water is assumed, the calculated values of α may be off by 30%, or more. The OBS works at a wavelength of 880 nm, so it may be seeing changes in the water that are not seen at the LED wavelengths (470, 505, and 530 nm). Without additional attenuation data, it is hard to say what the relationship is.

103

4.4   Underwater Imaging

The results of the WHOI experiment and the Towtank experiment are presented in this section. As it pertains to the methods used to extract contrast information from the resulting images, I will first discuss image analysis.

4.4.1   Image Analysis

Both the WHOI and Towtank experiments produced a large number of image files which had to be analyzed systematically in order to be compared intelligently. Sections 2.7.2 and 2.7.3 describe the background of this comparison. Short of polling a large sample of people to yield a comparative, and subjective, quality analysis, established quality measures and image contrast comparisons were the only viable options.

Several image quality measures (IQMs, Section 2.7.2) were tried. Using a single color channel as an input, effectively generating a grayscale image, images were processed using several methods. Unfortunately, no correlation could be found between the results of the modulation transfer function or power spectrum based IQMs and what was percieved as the best image from visual inspection. That isn't to say that these types of IQM are fundamentally flawed, only that they didn't work for me in this application.

As the attempted IQMs did not work, Image contrast was used exclusively in order to determine the "best" image. To do this, light and dark regions of the target images were chosen and the values differenced to generate a contrast measurement. The targets had been chosen specifically to make this easy, by placing Kodak contrast target standards in their centers. This contrast measurement made it easy to determine the best lit images (correct exposure) and to witness the effect of backscatter on image contrast.

Figure 4-10 shows an example image from the WHOI experiment illuminated by a cyan LED. The image is cropped displayed in grayscale for clarity and is cropped such that only the target region is seen (Figure 4-8 shows the full image in color). In the center of each numbered square, the average value of 25 (5×5) pixels was determined for each of the three color channels (red, green, and blue), and for the MATLAB determined grayscale channel (a weighted combination of the three, favoring the green channel). By differencing the pairs of

104

values of black and white squares, (1 − 2, 3 − 4, 5 − 6, etc. and the dotted pairs), and then averaging these differences, a fair measure of the contrast of each channel of the image could be determined. The compared squares are focused around the center of the target, and for each camera position, the same squares are used.

For the Towtank experiment images (see Figure 4-19 for an example), black and white regions near the center of the Kodak contrast targets (and therefore near the aiming center of the target) were chosen. These differences were normalized the same as the WHOI contrast results, with contrast percentages ranging from 0 to 100%.
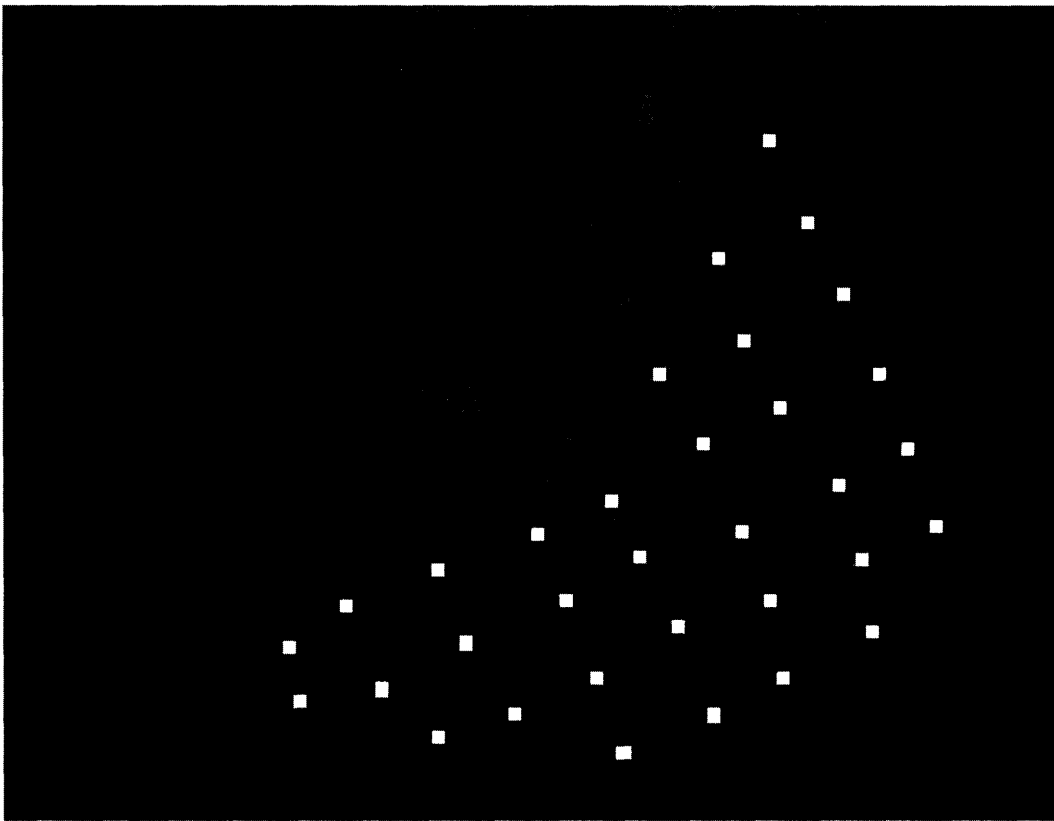
Figure 4-10: Contrast difference example, detail of an image from WHOI. Light and dark number pairs are differenced (1 and 2, 3 and 4, 5 and 6, and the dotted squares) around the target center (the large black dot) which is the corner of a Kodak contrast card and served as the aim point of the camera and LEDs.

4.4.2 WHOI Experiment

At WHOI, 48 different Camera/LED position combinations were tested for each of the three LEDs. The resulting images (for example, Figure 4-8) were analyzed for contrast by differencing a particular pattern of neighboring white and black squares on the target (see Section 4.4.1). The average of these contrast measurements was then normalized by the theoretical maximum contrast (255) for each of the color channels in the resulting images. This number was multiplied by 100% to yield the contrast percentage, or the % of the measured contrast compared to the maximum.

The results of this for the most distant camera position[4] tested are shown in Figures 4-11 and 4-12. These show the normalized contrast vs. the incident optical path length[5] (incident OPL), which measures the range of the LED to the target, for both the blue and green channels for all three LEDs. The red channel is ignored. Images for which the calculated contrast is zero correspond to images for which either the blue or green LED failed. This occurred at incident OPL = 0.97 and 1.01 m for the blue LED, and at OPL = 1.86 and 2.17 m for green.

Note that the first reading of the blue LED's blue channel response (Figure 4-12) is very low. This is due to overexposure saturation of the blue channel for much of that image meaning that light patches as well as actual white sections of the target read at the maximum value of 255 for that channel. Additionally, several images with differing contrast were exposed with LEDs at a range clustered near 1.0 to 1.2 meters. This is explained shortly.

The contrast of the two channels is averaged and presented in Figure 4-13. This measure best describes the total amount of data present in a given image. While the LEDs can never be used to generate a true color image, more image data, or additional properly exposed channels of data, is usually a good thing. If nothing else, it ensures that if one channel fails for some reason (usually due to saturation, either from overexposure or under), the other may still have useful data.

However, true color data will never be an option for a single color LED light source. The

---

[4]The reflected optical path, from which the camera range is determined, is illustrated in Figure 2-13

[5]The incident optical path is illustrated in Figure 2-13

Figure 4-11: Green channel contrast response vs. incident optical path length of Canon S230 camera for three Luxeon 5W LEDs, blue (diamonds), cyan (stars) and green (circles), in ocean water at WHOI. Camera is located 2.44 m from the target at an angle $\beta = 26.0°$ from perpendicular. The four zero contrast values are due to failed LEDs at those positions.

Figure 4-12: Blue channel contrast response vs. incident optical path length of Canon S230 camera for three Luxeon 5W LEDs, blue (diamonds), cyan (stars) and green (circles), in ocean water at WHOI. Camera is located 2.44 m from the target at an angle $\beta = 26.0°$ from perpendicular.

color digital camera used effectively splits the incoming light into three channels, interpolating to fill in the holes (only one third of the CCD pixels are exposed by each color filtered channel). So while the average contrast of the two channels is a fair metric to describe the total image data collected by this camera, an unfiltered black and white CCD would be a far better choice, as splitting the light between two channels actually represents a loss of image data.
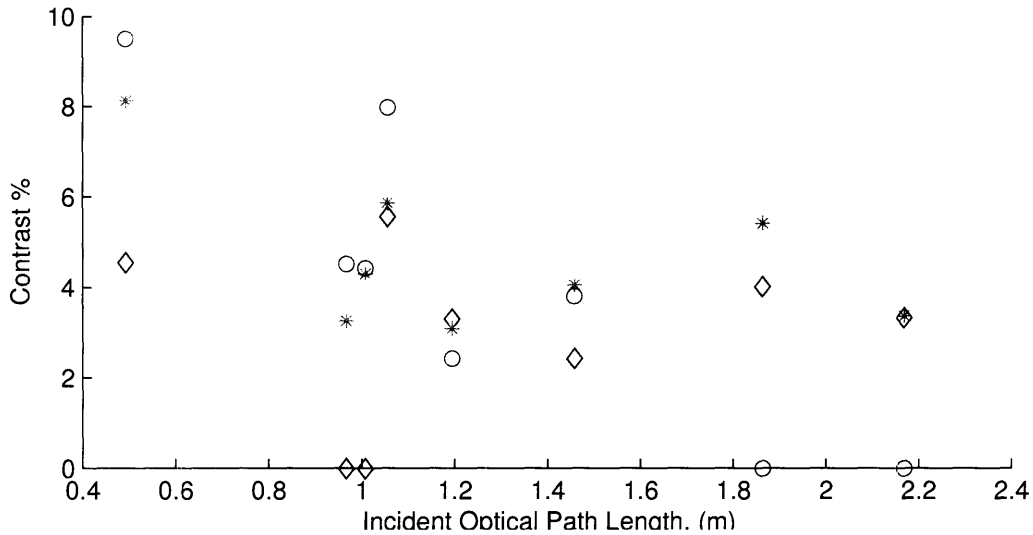
Figure 4-13: Combined blue and green channel contrast response vs. incident optical path length of Canon S230 camera for three Luxeon 5W LEDs, blue (diamonds), cyan (stars) and green (circles), in ocean water at WHOI. Camera is located 2.44 m from the target at an angle $\beta = 26.0°$ from perpendicular.

A slight trend favoring minimizing the incident optical path length is visible in these figures. The cyan and green illuminated LED images appear to have roughly equivalent contrast, beating the blue LEDs (the blue LED illuminated scenes suffered from the camera mismatch, as explained in Section 4.5.2).

Figure 4-14 shows the normalized contrast vs. the incident light angle, α, for combined blue and green color channels at the most distant camera position. It appears here that the camera adjusts to different illumination levels and resulting target luminosity by altering its exposure time. A false contrast peak peak at $\alpha = 13°$ is due primarily to the proximity of the light to the target, not to some target specific preferred α. However, a slight secondary trend showing a slight contrast improvement for α closer to perpendicular can be seen. Figure 4-15
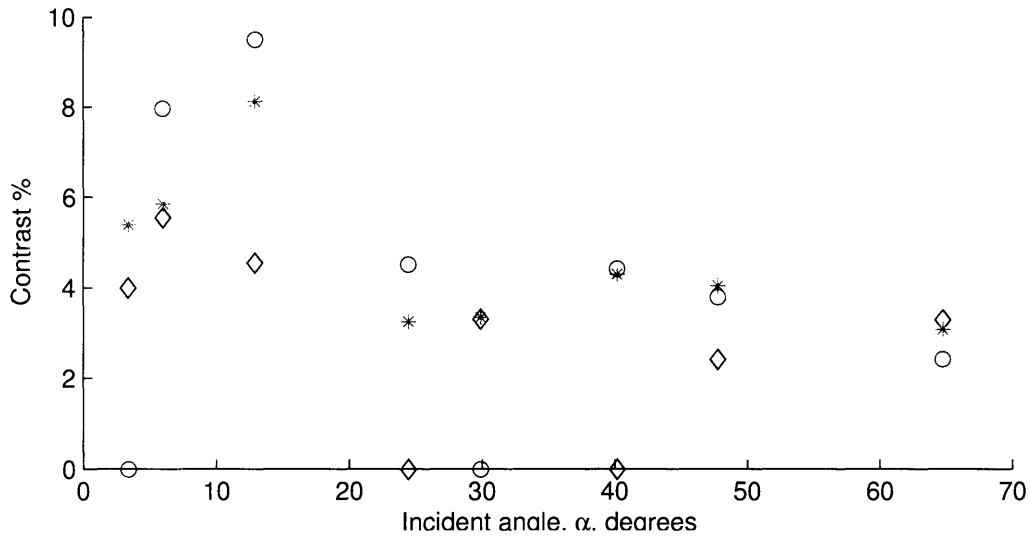
Figure 4-14: Combined blue and green channel contrast response vs. incident angle of illumination, α, of Canon S230 camera for three Luxeon 5W LEDs, blue (diamonds), cyan (stars) and green (circles), in ocean water at WHOI. Camera is located 2.44 m from the target at an angle $\beta = 26.0°$ from perpendicular.

shows this more clearly, using only the four LED positions clustered around 1.0 to 1.2 meters OPL. The effect may be more dramatic for a 3D target, where much of the contrast from a directional light source is due to shadows.
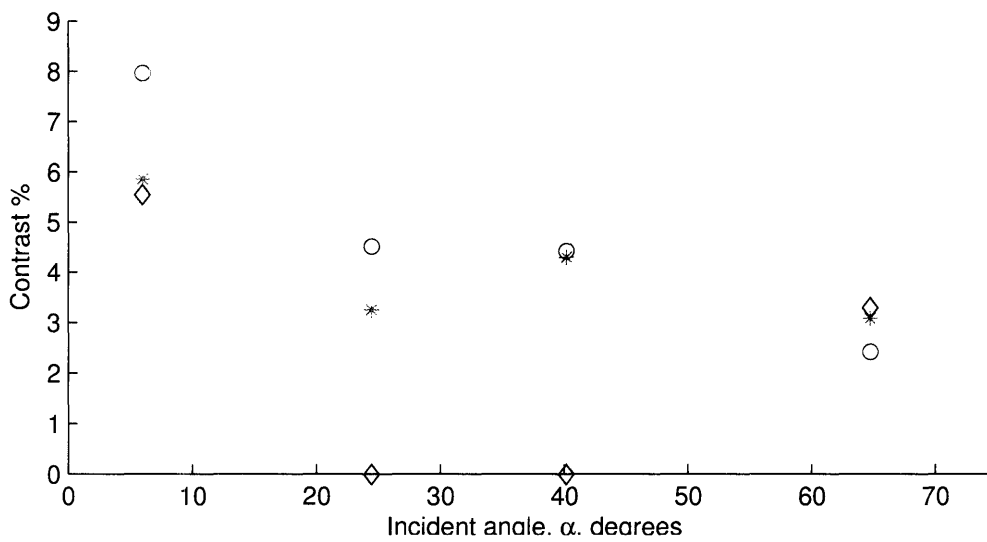
Figure 4-15: Combined blue and green channel contrast response vs. incident angle of illumination, α, of Canon S230 camera for three Luxeon 5W LEDs, blue (diamonds), cyan (stars) and green (circles), in ocean water at WHOI. Only four LED positions are displayed, clustered from 1.0 to 1.2 meters OPL. Camera is located 2.44 m from the target at an angle $\beta = 26.0°$ from perpendicular.

Figures 4-11 through 4-14 show the worst case scenario camera position, with the camera located the furthest distance from the target (within the bounds of the test rig, which is still less than a typical survey vehicle altitude). Figures 4-16 and 4-17 show the best case (tested), similar to what may be expected of a more precise HAUV survey, for example. Only the combined blue and green channel normalized contrast averages are shown, vs. the incident OPL and α.

For the closest camera position, the relation between contrast and incident OPL is less distinct. It seems to matter very little where the LED is placed. However, this may be due to a variable not tested directly. For this camera position, all but the closest LED illuminates the entire water volume between the camera and the target. This illuminated water volume is the source of all backscattered light. It has been shown that source-receiver separation is important to reduce this backscatter, and the experiment at WHOI tested many different source receiver geometries. The WHOI experiment failed, however, to fully account for or quantify the illuminated water volume effect.

Figure 4-17 shows an almost flat response for different α values. The flatness is more dramatic for Figure 4-18, which shows only the four LED positions clustered around 1.0 to 1.2 meters OPL. This is a promising result for a 2D target as it shows that target contrast can be maintained independent of target illumination angle (this was not entirely the case for the more distant camera location, perhaps as a result of differing illuminated water volumes in that case, whereas nearly all cases for the closest camera position had the entire imaged water volume illuminated). However, though contrast may be independent of α, it will be shown that as α increases, total illumination efficiency is lost, resulting in longer required exposure times.
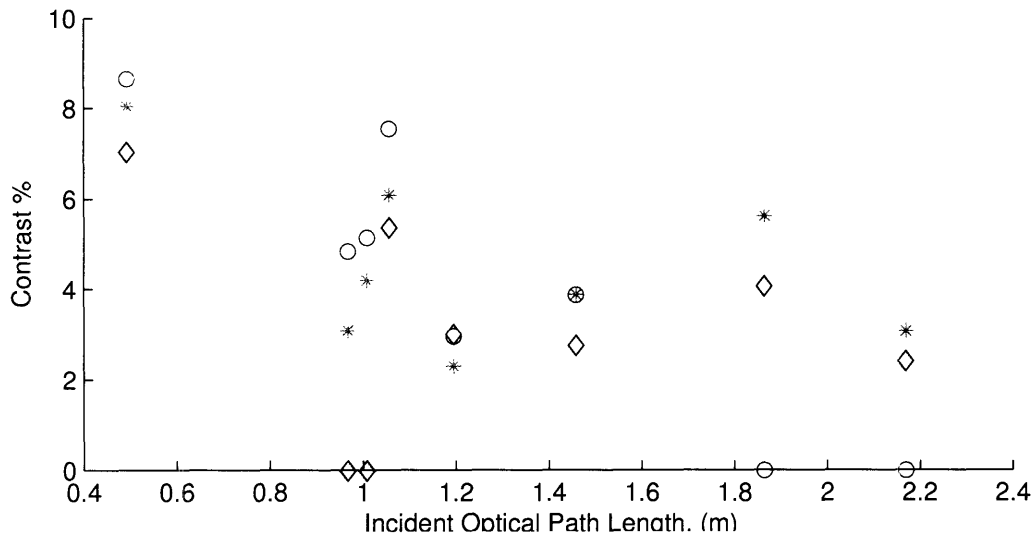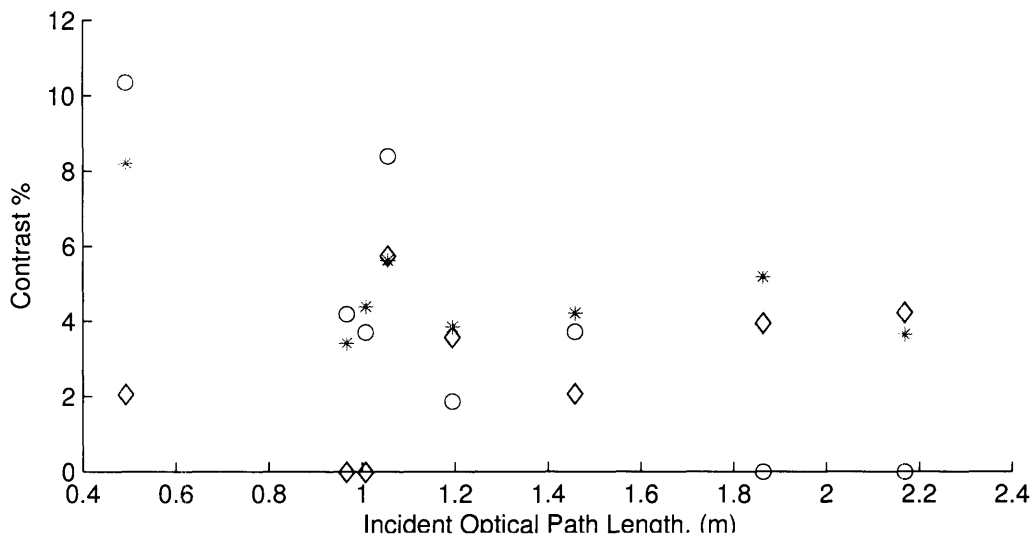
111

Figure 4-16: Combined blue and green channel contrast response vs. incident optical path length of Canon S230 camera for three Luxeon 5W LEDs, blue (diamonds), cyan (stars) and green (circles), in ocean water at WHOI. Camera is located 1.18 m from the target at an angle $\beta = 3.4°$ from perpendicular.

Figure 4-17: Combined blue and green channel contrast response vs. incident angle of illumination, α, of Canon S230 camera for three Luxeon 5W LEDs, blue (diamonds), cyan (stars) and green (circles), in ocean water at WHOI. Camera is located 1.18 m from the target at an angle $\beta = 3.4°$ from perpendicular.

Figure 4-18: Combined blue and green channel contrast response vs. incident angle of illumination, α, of Canon S230 camera for three Luxeon 5W LEDs, blue (diamonds), cyan (stars) and green (circles), in ocean water at WHOI. Only four LED positions are displayed, clustered from 1.0 to 1.2 meters OPL. Camera is located 1.18 m from the target at an angle $\beta = 26.0°$ from perpendicular.

4.4.3 Towtank Experiment

Due to the relative sparsity of the WHOI data, the limited maximum LED and camera range available, and the inability to predict and control the illuminated water volume effect, a followup test at the MIT Towtank was conducted. In this test, LEDs were tested both bare and with reflectors, which were added to direct the light and minimize the illuminated water volume (for example, an LED laterally separated from the camera would illuminate only the target, and a conical patch of water in front of the camera, rather than all of the water).

Unfortunately, the water in the Towtank had been sitting undisturbed for many weeks, leading to very low attenuation coefficients at the wavelengths of the LEDs (see Table 4.3). This meant that backscatter was minimal at best and the resulting images were abnormally clear. Figure 4-19 shows an example of the images used for contrast analysis.

Figure 4-19: Image of the target used in the Towtank tests illuminated by a Luxeon 5W cyan LED. Four Kodak contrast cards are used, with the Extech light meter attached to the side.

Due to previous experiments that showed the Luxeon 5W LED in cyan to be preferable

114

to blue and green for the Canon S230 camera, the cyan LED was tested most extensively in the Towtank. Blue and green LEDs were used only for the most distant camera position. Figures 4-20 and 4-21 show the normalized average green and blue channel contrast results for the three LEDs for that camera position for both bare LEDs and LEDs with reflectors.

A slight correlation between incident OPL[6] and contrast may be seen. More dramatic is the superiority of the green and cyan LEDs over the blue for this camera. In fact, the blue LED appears to show contrast increasing with increased OPL, though this is in fact due to saturation of the blue channel for images exposed with blue LED light. With the correct exposure for blue light, the blue LED would come out well ahead, at least for the blue channel contrast response, and especially considering the much lower required exposure. Additional contrast plots are presented in Appendix section B.2.2.

Reflectance, R, which is discussed in Section 4.5.1, is known not to be uniform. For a lambertian surface, R is angle independent, with the resulting luminance of the target constant in all directions. For off-angle illumination, where the angle of incidence $\alpha > 0$, the resulting luminance of the target is governed by Equation 2.7. Therefore, for a light source at the same distance from the target (incident OPL), the required exposure time for an image of a target will be inversely proportional to the luminance, B, and therefore proportional to $\cos \alpha$.

However, for real world targets, such as the ocean floor, the assumption of a fully lambertian surface is invalid. In these cases, Equation 2.8 must be used. Figure 4-22 shows normalized Towtank data plotted against $1/\cos \alpha$. In this plot, the exposure time (seconds) and illuminance (lux) calculated at the target are multiplied together to yield a measure of the total exposure in lux-seconds. All things being equal, this should be a constant value except for the effect of α. The values are normalized by the lowest value in order to compare them to a plot of $1/\cos \alpha$.

As can be seen in Figure 4-22, the total exposure (normalized lux-seconds, or illumination $\times$ exposure time) increases much faster than $1/\cos \alpha$. One possible explanation [12] is that as the incident angle becomes more oblique, the horizontal component of the light is reflected

---

[6]The incident optical path is illustrated in Figure 2-13
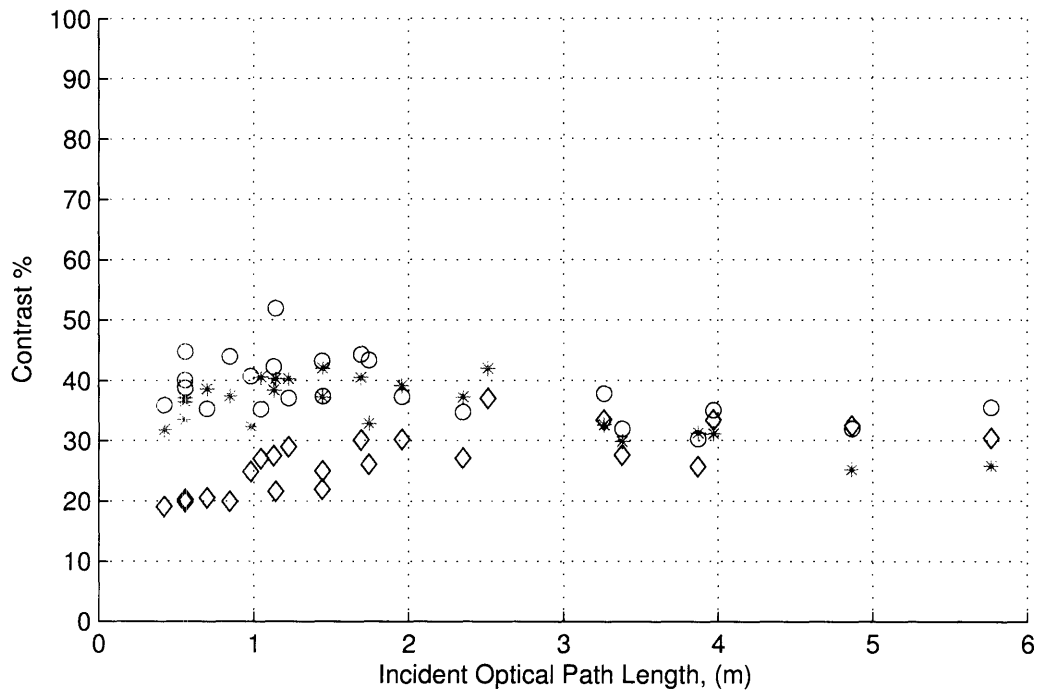
Figure 4-20: Combined blue and green channel contrast response vs. incident optical path length of Canon S230 camera for three *bare* Luxeon 5W LEDs, blue (diamonds), cyan (stars) and green (circles), in the MIT Towtank. Camera is located 5.69 m from the target at an angle $\beta = 2.0°$ from perpendicular.
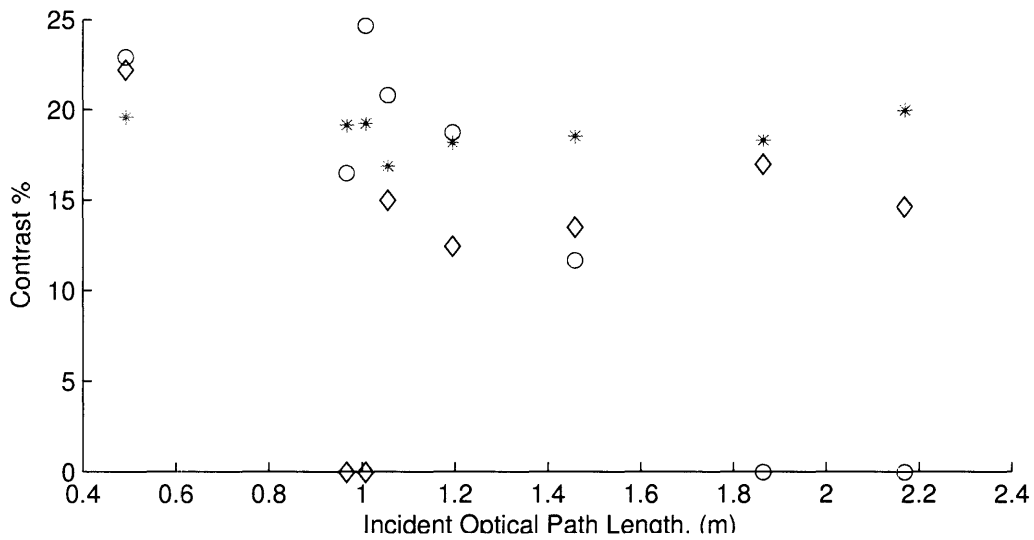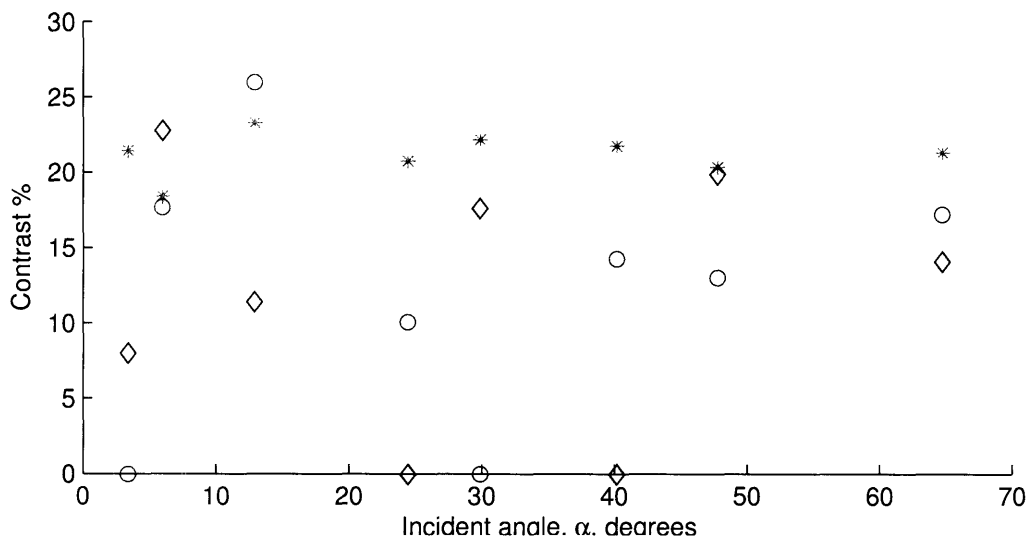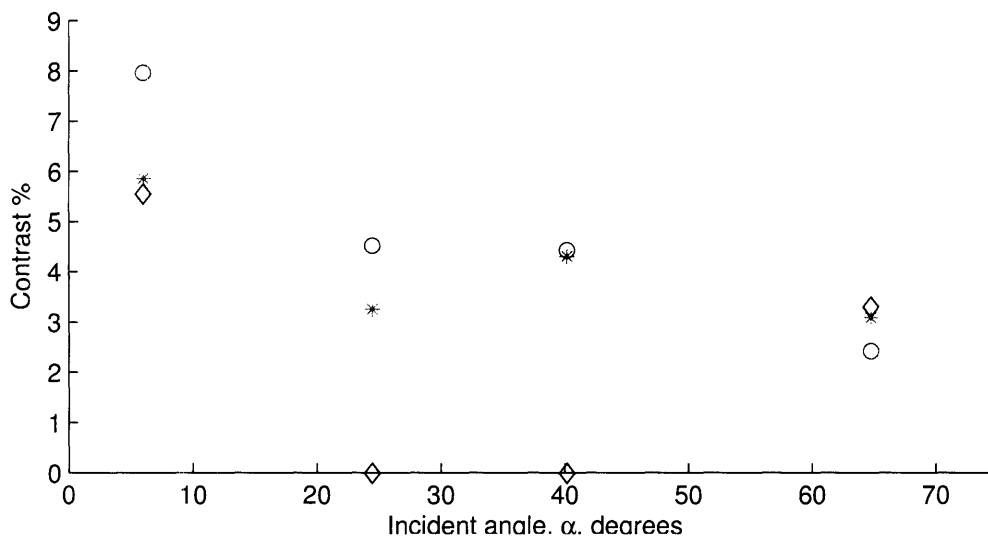
116
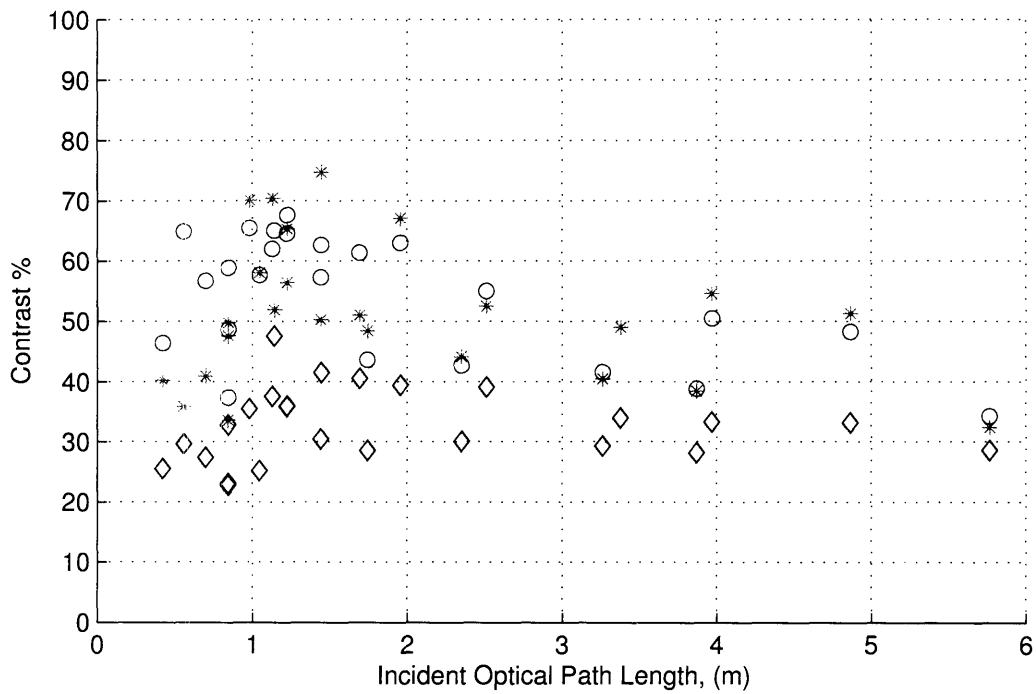
Figure 4-21: Combined blue and green channel contrast response vs. incident optical path length of Canon S230 camera for three Luxeon 5W LEDs, blue (diamonds), cyan (stars) and green (circles), with *reflectors*, in the MIT Towtank. Camera is located 5.69 m from the target at an angle $\beta = 2.0°$ from perpendicular.
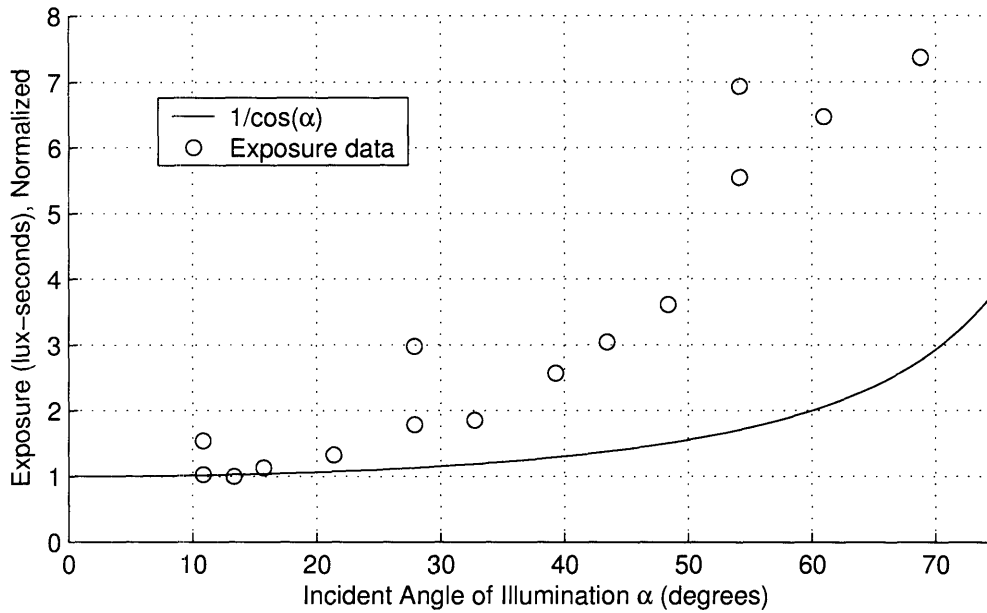
Figure 4-22: Normalized exposure vs. light angle of incidence, α, for one series of cyan reflector LED illuminated images in the MIT Towtank, compared to $1/cos\alpha$.

off in a more specular manner[7]. Whatever the reason, the result is that there is an angle dependence on the reflectance such that $R = R(\alpha)$. In other words, Equation 2.8 must be used.

Additional discussion of the implications of R is at the end of Section 4.5.1. The main implication of this incident angle dependence on R is that, for the target investigated, illumination becomes less effective as α increases. In order to make the most use of LED illumination, α should be kept to a minimum, with the light source nearly perpendicular to the target.

The reflectors used in the Towtank test were chosen due to their availability and low cost. They worked well to narrow the beam, reducing stray light and unwanted illuminated water volume, but the beam patterns were not completely uniform[8]. The purpose of the reflectors

---

[7]Polarized light is not considered in this project. In order to make use of it, both the light source and the receiver must be carfully aligned. As this project is more concerned with a general application of LEDs, which includes off-the-vehicle lighting systems where it would be impossible to properly align a bottom mounted system with an independent observer, polarized light is not examined, although one of its effects may be seen

[8]Dr. Hanumant Singh at WHOI has found an alternate source for his reflectors which may offer an improvement. For a high volume application, such as disposable LED candles, designing and manufacturing an optimal reflector based on the wet beam pattern of the LED, the distance from the LED to the target,

Camera range (meters)	Average Contrast (normalized)		Standard Deviation σ	
	bare LED	reflector	bare LED	reflector
1.74	56.3	61.2	4.95	6.93
2.35	N/A	56.8	N/A	6.21
3.87	44.7	48.0	4.88	7.51
5.69	35.6	51.1	4.83	11.74

Table 4.4: The average normalized contrast and standard deviation for all images illuminated with a cyan LED at each camera position in the MIT Towtank. No data was collected from the bare LED with the camera at 2.35 meters.

was to witness the effect of the illuminated water volume on contrast. Unfortunately, the water was too clear to see much difference. Backscattered light was of little concern in the Towtank.

Taking the average contrast of all images taken with cyan LEDs at a camera position compared the range of the camera to the target (This data is displayed in Figures B-7 through B-13 in Appendix section B.2.2), a statistical comparison between bare LEDs and LEDs with reflectors is shown in Table 4.4. This data is shown graphically in Figure4-23. In general, the contrast is slightly higher in images where the LED is used with a reflector, though the standard deviation was higher as well, owing to the non-uniform illumination. A better designed reflector would make the contrast readings much more consistent. The contrast advantage of using an aimed LED with a reflector is expected to be much more dramatic for coastal water with more particulate matter.

The points to take away from the results of the Towtank experiment are that the light incident angle, α should be kept to a minimum, if possible. As α increases, the effective value of R of the target decreases, making the illumination less efficient. Also, even with very clear water, minimizing the illuminated water volume appears to have a positive effect on image contrast. Using reflectors to direct the light only at the target is the best way to accomplish this. While it is clear that light not striking the target is wasted light, and detrimental to the illumination efficiency, reflector directed light has the added advantage of minimizing backscatter by reducing the volume of water in which it can occur.

---

and the size of the target (or footprint diameter) should be a fairly simple matter.
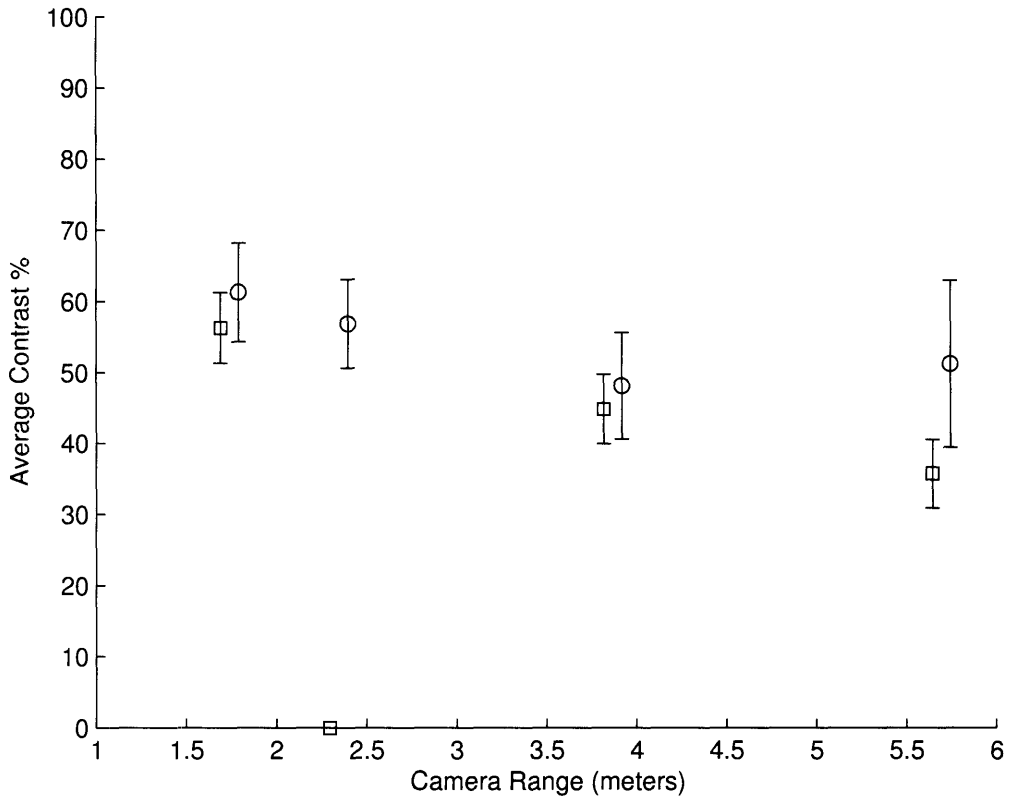
Figure 4-23: The average normalized contrast, with standard deviation $\pm\sigma$, for all images illuminated with a cyan LED at each camera position, plotted against the Canon S230's range to the target, in the MIT Towtank. The squares represent the bare LEDs, the circles represent the LEDs with reflectors. Only four camera positions are tested, the data is split slightly at each position to allow the reader to see σ. No data was collected using bare LEDs with the camera 2.35 meters from the target.

Luxeon 5W LED Color	Film Speed ASA/ISO Equivalent
Blue	1543
Cyan	202
Green	129

Table 4.5: The ASA/ISO film speed equivalents used to simulate the response of the Canon S230 digital camera. For the blue LED, this corresponds to the camera's blue channel response. For the cyan and green LEDs, this correponds to the camera's autoexposure setting. Taken from Table B.2.

4.5 Underwater Illumination Simulation

Based on both previous experimental results and theory, simulations were run of LED performance in water. This section shows the results for the LED footprint simulation and for the comparative efficiencies of LEDs and halogen lights after propagation in seawater.

4.5.1 Required Illumination

The exposure value method can be used to predict camera exposure for various lighting conditions. To predict the exposure time to illumination level for the Canon S230 and the Luxeon LEDs, the ISO film speed equivalent values presented in B.2 (see Appendix secton B.1 for an explanation) were used with Equation 2.24. For the camera's film speed equivalent for the blue LED, it's blue channel response was used. For the cyan and green LEDs, the camera's auto-exposure values were used. These are displayed in Table 4.5

These values were based on the camera's response to a fairly reflective target in air. In water, the value of R is expected to be much lower. Using exposure and illumination data from the Towtank experiment, Figure 4-24 shows the predicted camera response to the Cyan LED at a reflectance value of $R = 0.3$ along with experimental data from the Towtank. This R is not absolute, but merely the scaled R from the Strobe Lab experiment that generated the ISO film speeds. As can be seen in this figure, this value of R actually overestimates the exposure time for some of the experimental data, and underestimates for others.

Only fairly shallow angles, $\alpha < 25°$ are used as the reflectance is also angle dependent. Highly oblique angles have a much lower effective R, as the target is not lambertian. This

121

Luxeon 5W	Footprint Diameter (m)	
LED Color	1/60 sec exposure	1/10 sec exposure
Blue	0.97	2.40
Cyan	0.70	1.73
Green	0.56	1.39

Table 4.6: The maximum footprint diameter for a single Luxeon 5W LED for exposure times of 1/60 and 1/10 with a Canon S230 digital camera. R is assumed to be 0.3.

is shown in Figure 4-22. However, assuming non-oblique illumination, where $R = 0.3$, it is possible to predict the LED illumination effectiveness for the Luxeon 5W LED lights when used with the Canon S230 camera.

To measure the effectiveness of the Luxeon 5W LEDs, it is useful to determine the dimensions of a patch of ocean floor that could be illuminated using a single LED. Figure 4-25 shows the situation. With an arbitrary light source (in this case a single Luxeon 5W LED), whose total luminous output is uniformly distributed on the ocean bottom, the patch or *footprint* of the light source is a circle of diameter D. This diameter is the *footprint diameter*, and assumes a perfectly uniform distribution of light on the bottom, with no hot spots or shadows.

Figure 4-26 shows the footprint diameter of the potential patch of ocean floor that could be illuminated using a single Luxeon 5W LED as a function of the exposure time of the Canon S230 camera. The standard guideline for hand-held photography is a maximum of a 1/60th of a second exposure. Anything more than that and body movement will blur the image. Not knowing the ultimate application or imaging platform, 1/60 sec is a good starting point. A very steady imaging platform, which the HAUV may be, could perhaps support up to a 1/10 sec exposure, or longer. The footprint diameters for these exposure times are shown in Table 4.6.

Unfortunately, as can be seen in Figure 4-22, R is not constant, or else the experimental data would line up with the $1/\cos\alpha$ curve. Therefore, while $R = 0.3$ may be a valid approximation for small values of α, and may in fact be an underestimate, as the illumination angle becomes steeper, the effective illumination becomes less.

To attempt account for the $R(\alpha)$ effect, without directly calculating R for each angle

Luxeon 5W	Footprint Diameter (m)	
LED Color	1/60 sec exposure	1/10 sec exposure
Blue	0.56	1.38
Cyan	0.41	1.00
Green	0.32	0.80

Table 4.7: The maximum footprint diameter for a single Luxeon LED for exposure times of 1/60 and 1/10 with a Canon S230 digital camera. R is set at 0.1 to account for non-optimum conditions.

(ocean bottoms may have a different R, and the geometry of the source is still a variable), Figure 4-27 plots footprint diameter vs. exposure time for illumination by a single Luxeon 5W LED for $R = 0.1$. Table 4.7 shows the resulting footprint diameters for two exposure times. This additional compensation may also make up for imperfect reflectors, as it would be nearly impossible to have perfectly uniform illumination of any target using a single LED.
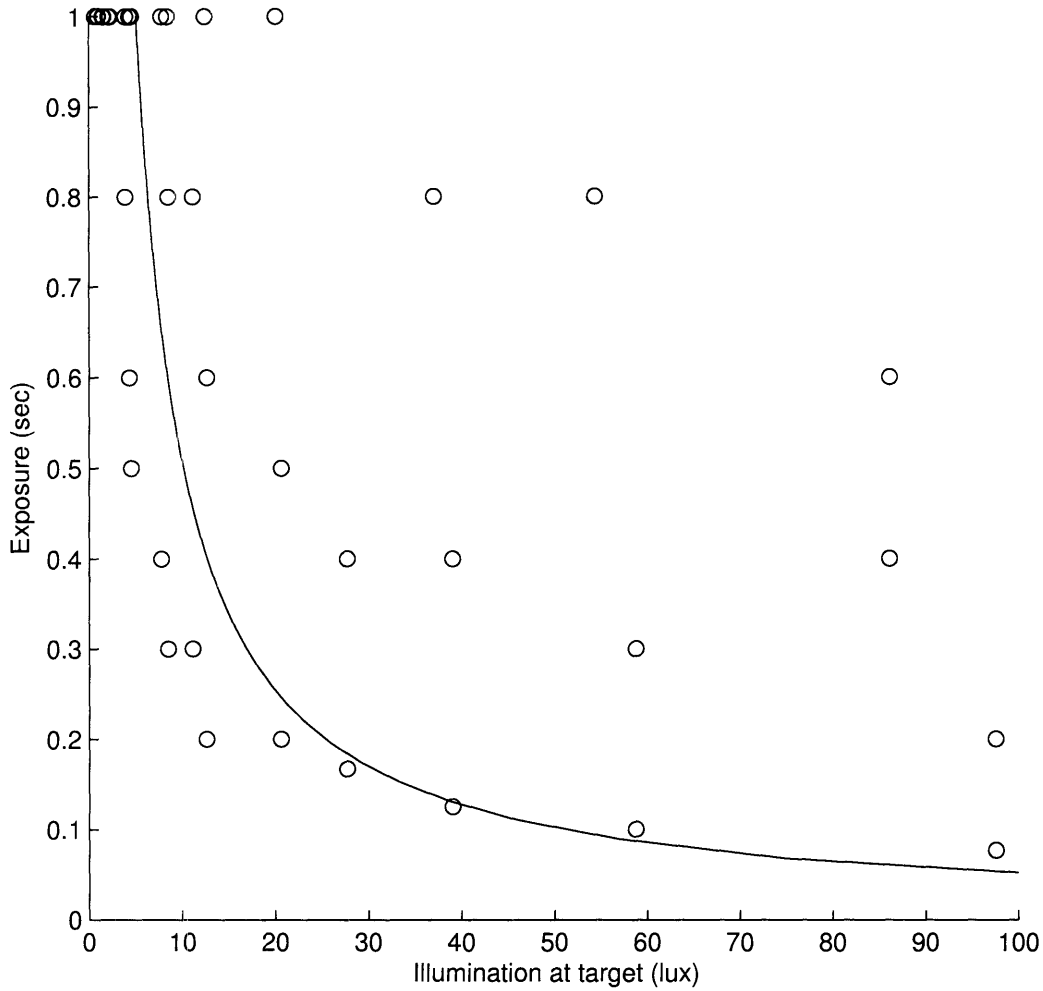
Figure 4-24: Predicted (solid line) and experimental (circles) exposure vs. illumination levels. The predicted value is based on a reflectance $R = 0.3$ and an equivalent film speed of ISO 202 for the Canon S230 exposed to cyan light. Experimental values are from the MIT Towtank experiment, and represent all Luxeon 5W cyan LEDs illuminated images where the incident angle of illumination, α, is less than 25°. Illumination levels for experimental data are predicted based on LED range to the target, accounting for the LED's beam pattern in water and the attenuation seen in the Towtank.
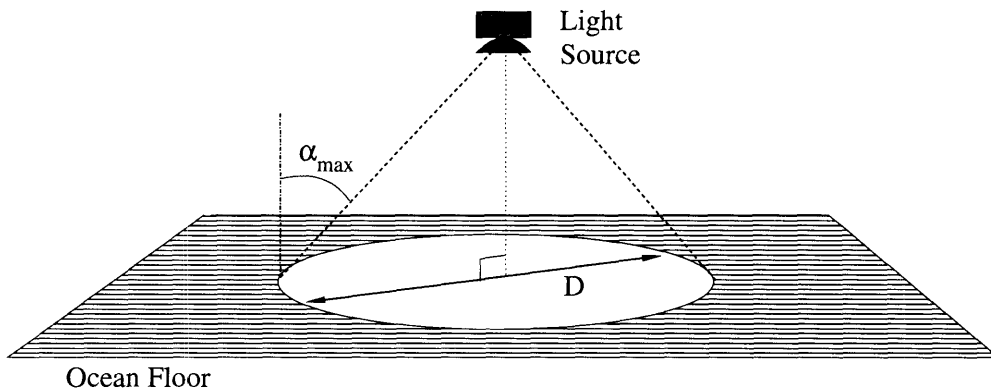
Figure 4-25: The dimension D refers to the *footprint diameter* of a patch of flat ocean floor illuminated by the light source. By employing different reflectors, the height of the light source above the bottom can be adjusted to keep the maximum light incident angle, α_{max}, to a minimum, avoiding partial specular reflection and a loss of illumination efficiency. This must be balanced with the image contrast advantage witnessed by placing the light source nearer the target.
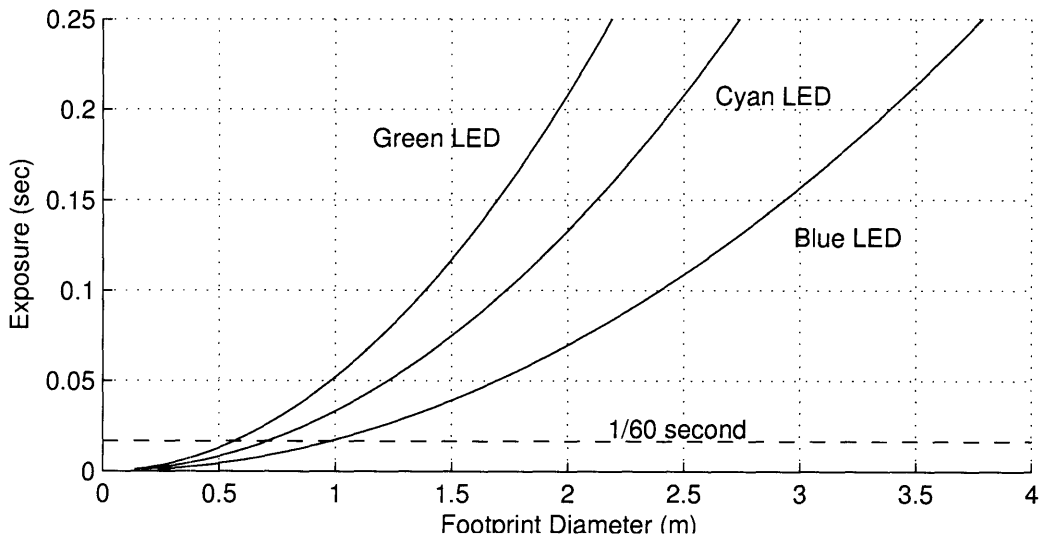
Figure 4-26: Predicted coverage of a single Luxeon 5W LED and the resulting required exposure of a Canon S230 digital camera for $R = 0.3$. The *footprint diameter* refers to diameter of a circular patch of ocean bottom a single LED could illuminate assuming a perfect distribution of its flux.

125
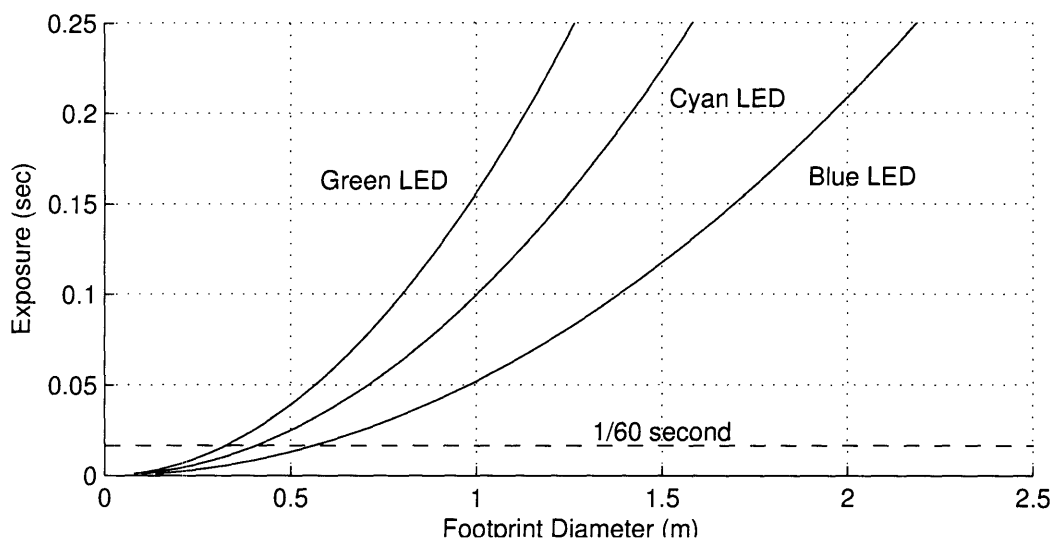
Figure 4-27: Predicted coverage of a single Luxeon 5W LED and the resulting required exposure of a Canon S230 digital camera for $R = 0.1$. This represents a more reasonable estimate of an actual illuminated footprint. $R = 0.1$ was chosen to take into account off-axis illumination at the fringe and uneven illumination rather than a perfect distribution of flux.

126

Source	Power (W)	Flux (lm)	Radiative Power W_r	lm/W	mW_r/W
Luxeon blue	5	30	0.76	6	152
Luxeon cyan	5	120	0.44	24	87
Luxeon green	5	120	0.24	24	48
Halogen 3000K	50	950	3.91	19	78
Halogen 3100K	100	2200	8.99	22	90
Halogen 3300K	100	3600	14.5	36	146

Table 4.8: Total luminous and radiative outputs of the LEDs and Halogen lights, with their photopic, lm/W, and radiative, mW_r/W, efficiencies.

4.5.2 Light Efficiency

Using the radiative power distributions of the light simulations defined in Appendix section C.1, initial radiative and photopic light efficiencies can be calculated by integrating the distributions shown in Figures C-2 and C-4. The flux (luminous output measured in lumens) of the respective lights are given in the specifications. Table 4.8 shows the initial light photopic and radiative efficiencies with no loss.

In water, radiative power is absorbed and scattered. Using the attenuation constant curves shown in Figure C-5 in Appendix section C.2, the radiative power distributions of the LED and simulated halogen lights were acted on as if passing through one of two types of water. At each wavelength and for each total optical path length (OPL)[9] simulated, Equation 2.18 was applied, generating new radiative power distributions for each OPL. For example, Figure 4-28 shows the initial and resulting radiative power distributions of the 3300 K halogen light after passing through up to 10 meters of simulated deep ocean water. Figure 4-29 shows the same light passing through simulated water similar to what was encountered during the WHOI experiment.

By re-integrating the resulting distributions, the total radiative power remaining after propagation of a certain distance may be determined. By first normalizing by the initial radiative power, Figures 4-30 and 4-31 show the relationship between OPL and the percentage of the initial radiative power, W_r, remaining. These figures show that LEDs retain more of

---

[9]See Figure 2-13. The total optical path length is the total distance light travels from the source to the target and back to the receiver. It is the sum of both the incident OPL and the reflected OPL

their radiative power after propagating through water. Cyan LEDs have a slight advantage in WHOI water, and blue has a more signifigant advantage in deep ocean water, but all of the LEDs have a substantial advantage over all of the Halogen lights in this respect.

Of equal interest is the resulting efficiency of the light sources, measured in mW_r/W, after a propagating over a given OPL. Figures 4-32 and 4-33 show this relationship. Note that after propagating for 5 meters in deep ocean water and for 3.5 meters in WHOI water, the cyan LED becomes more efficient than even 3300 K halogen light. The blue LED is far ahead of the other light sources examined in terms of total radiative efficiency in both types of water. Due to these results, it is quite clear that the Luxeon 5W blue LED is the preferred source of persistent light, not only compared to the other LEDs, but compared to the halogen lights as well.
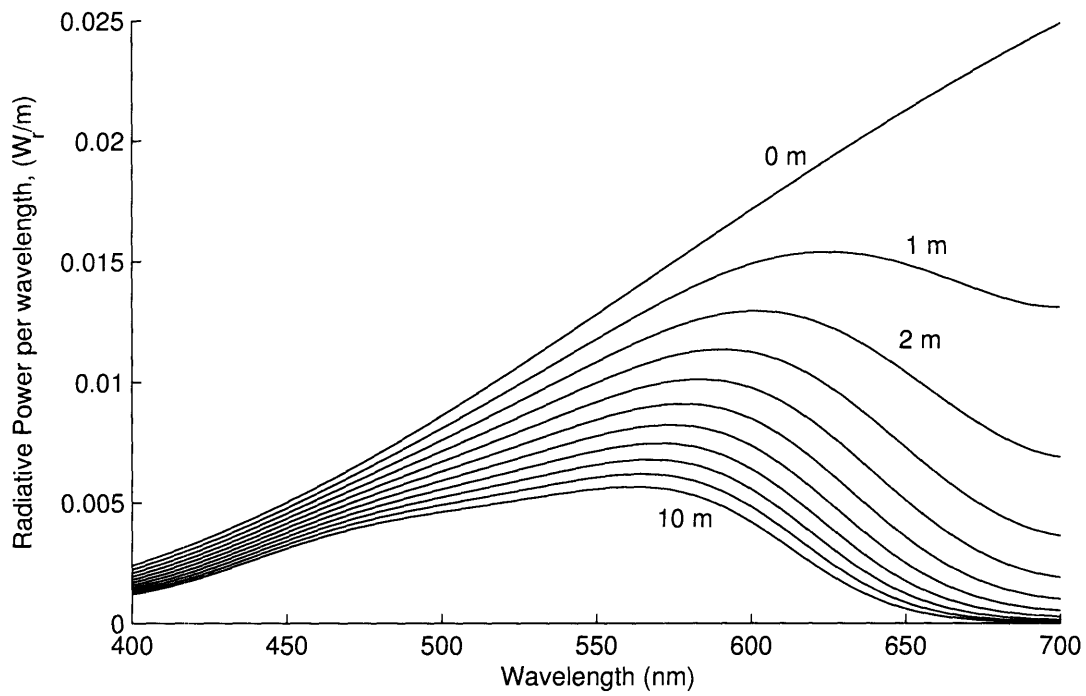
Figure 4-28: The initial (0 m) and resulting radiative power distributions of the 3300 K halogen light after passing through 1 to 10 meters of deep ocean water.
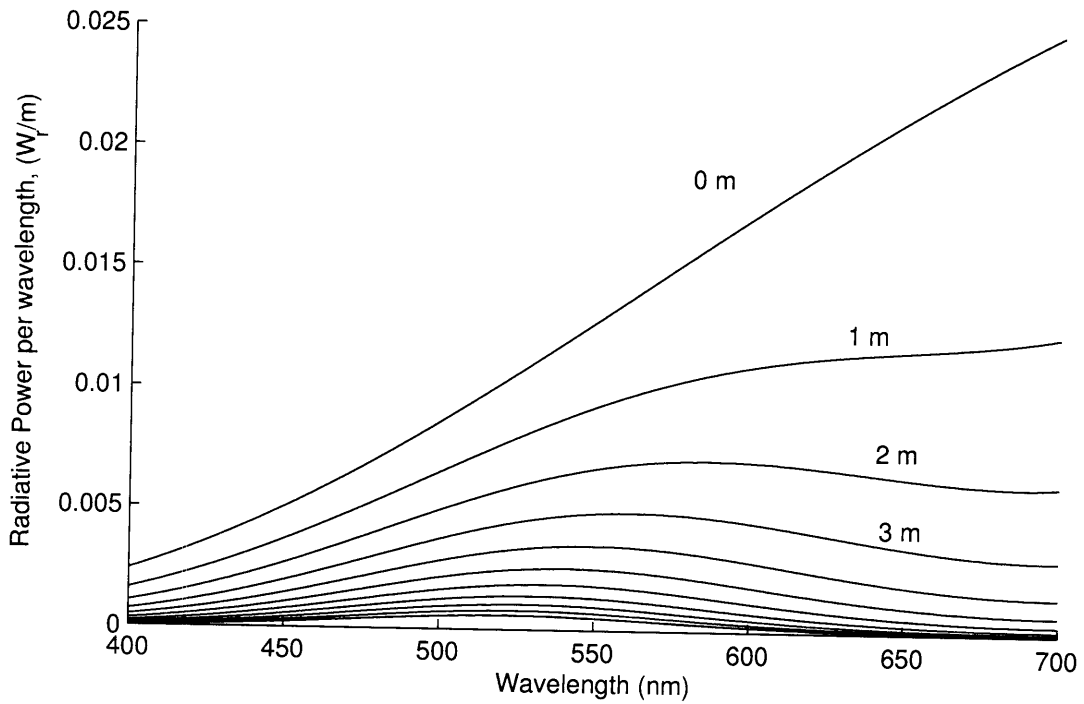
Figure 4-29: The initial (0 m) and resulting radiative power distributions of the 3300 K halogen light after passing through 1 to 10 meters of water similar to what was encountered in the WHOI well.
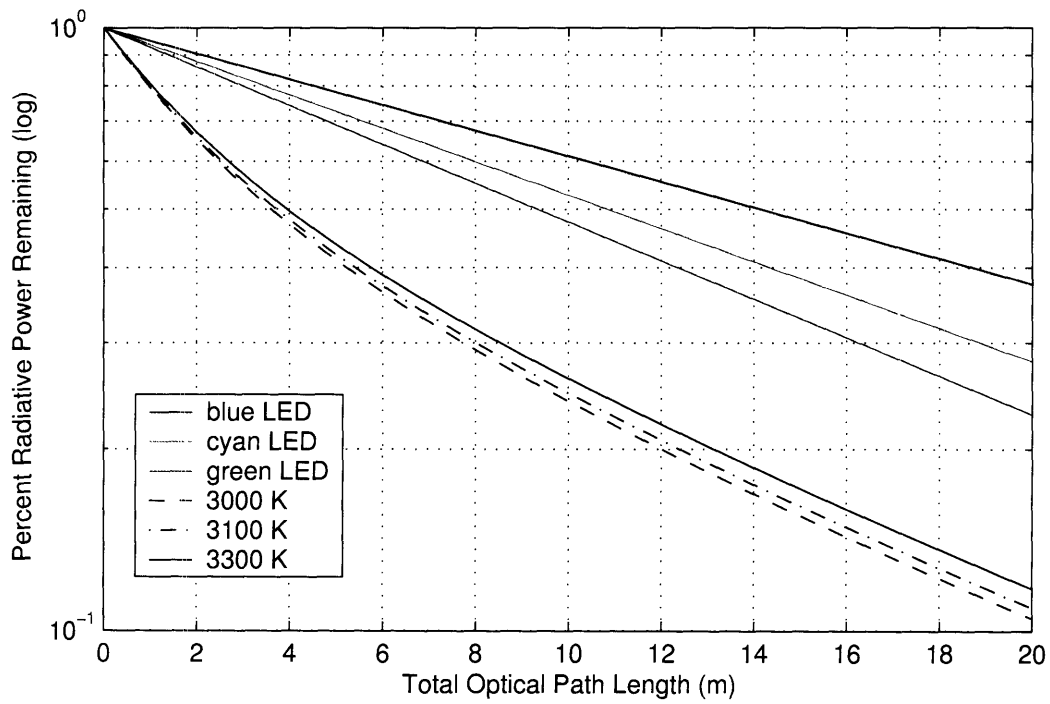
Figure 4-30: Percent of initial total (integrated) radiative power over all visible light wavelengths for Luxeon 5W LEDs and simulated Halogen lights after propagating through simulated deep ocean water.
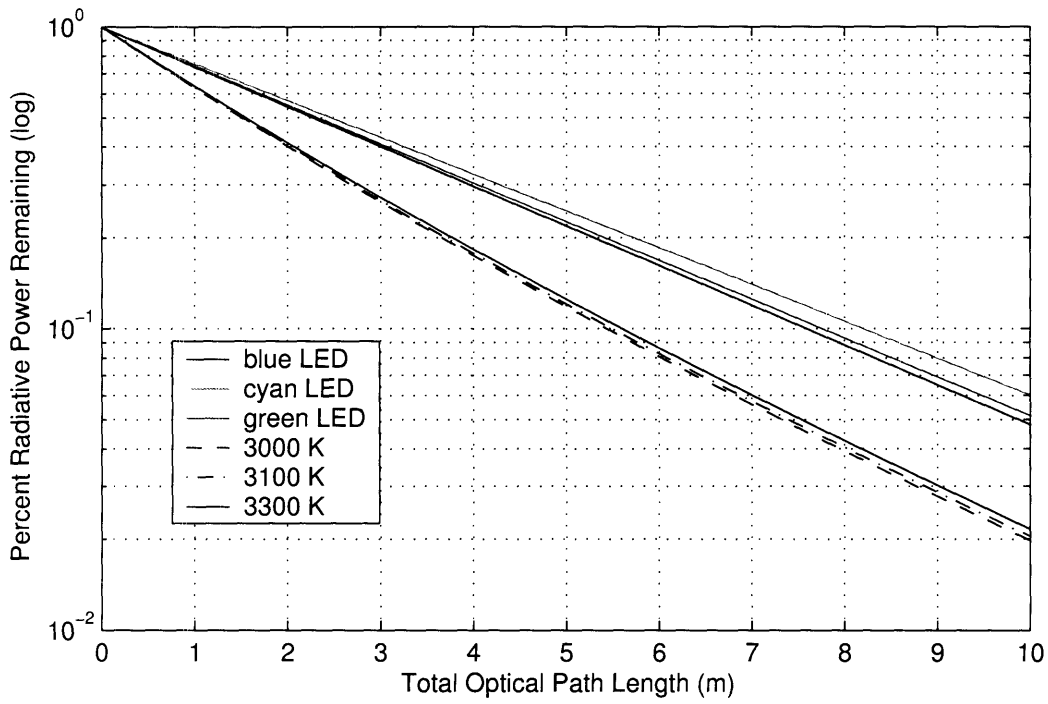
Figure 4-31: Percent of initial total (integrated) radiative power over all visible light wavelengths for Luxeon 5W LEDs and simulated Halogen lights after propagating through simulated coastal ocean water similar to that seen at Woods Hole, MA.
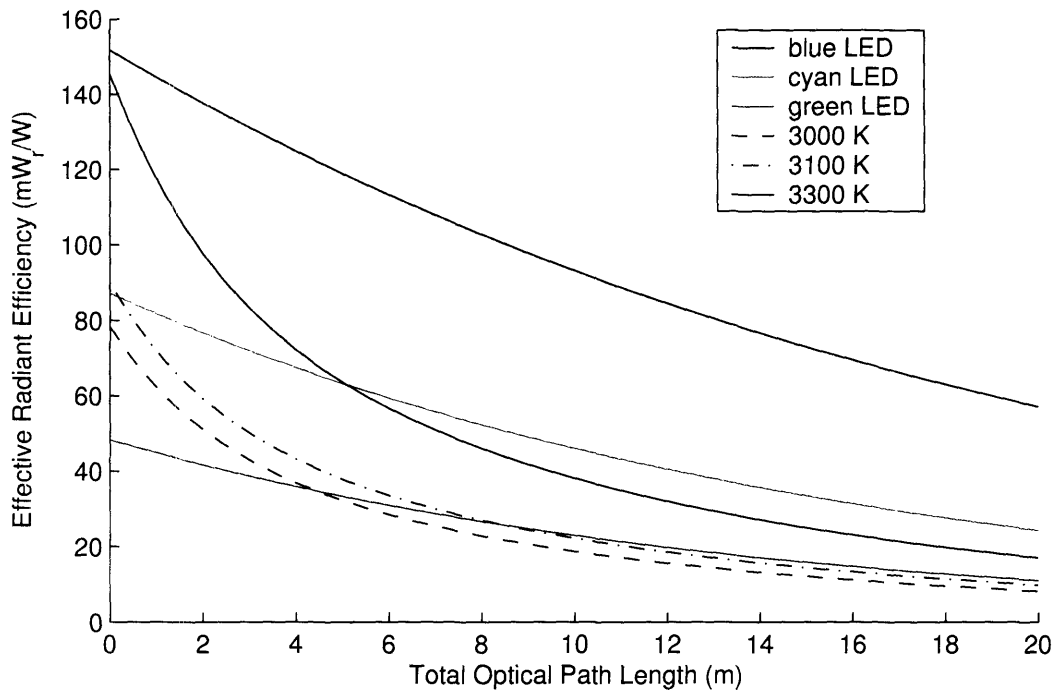
Figure 4-32: Total radiative efficiency of Luxeon 5W LEDs and simulated Halogen lights after propagating through simulated deep ocean water
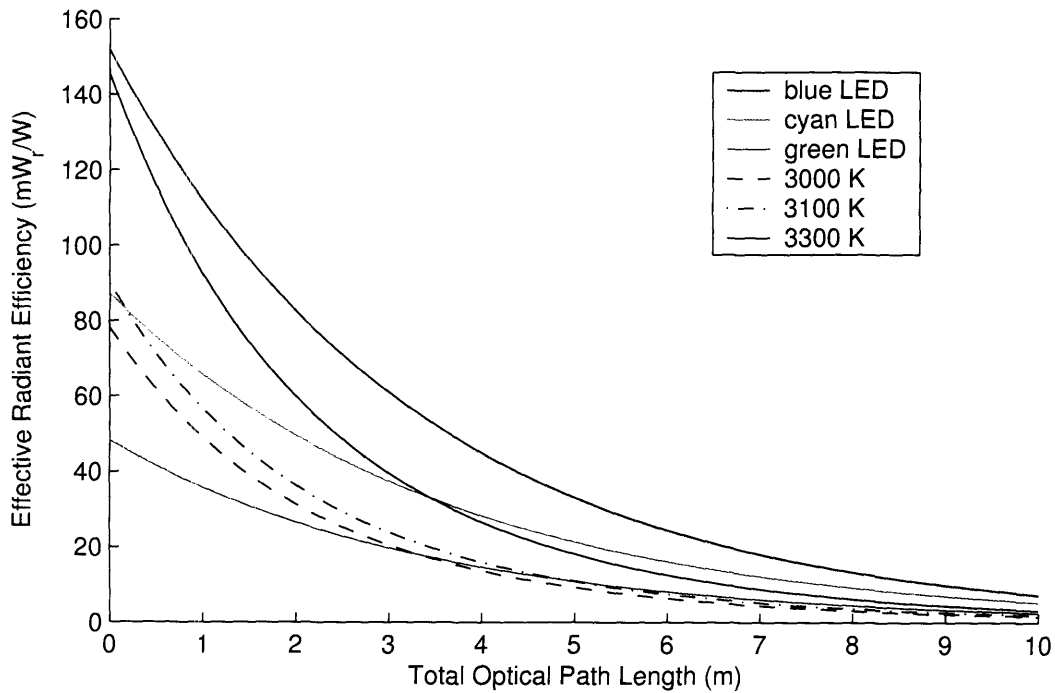
Figure 4-33: Total radiative efficiency of Luxeon 5W LEDs and simulated Halogen lights after propagating through simulated coastal ocean water similar to that seen at Woods Hole, MA.

Chapter 5

Conclusions

Final conclusions are divided into four sections. Presented are a review of performance of Luxeon 5W LEDs themselves based on experiments and simulations, the implications of the in-water testing, an analysis of the proposed LED Candle application, and guidelines for LED illumination applications in the future.

5.1 Luxeon 5W LED Light Review

When a persistent light source is required by an AUV or other imaging platform, the Luxeon 5W LEDs, by any standard of measure, proved to be a good choice for underwater illumination. They are efficient compared to halogen lights and to other LEDs, their light output is concentrated at the wavelengths of minimum attenuation, their package size is very small and can be made waterproof without a special housing, and they scale well at low output light levels.

5.1.1 Efficiency

Compared to the Nichia LEDs used by Rosser [13], the Luxeon 5W LEDs show a minimum of a factor of 2 luminous power efficiency over an equivalent Nichia array (Table 4.2 shows a minimum power consumption of 9.5 watts for a Nichia array compared to 5 watts for the Luxeon 5W LEDs). For an AUV, or other low-power application, this could be very

134

significant. Component costs are also less (Luxeon 5W LEDs retail for about $25.00 while the Nichia LEDs retail for around $1.00 each, and at least 90 would be needed to construct an array comparable to a single Luxeon 5W LED) before even considering the added costs of building the Nichia array.

Compared to the Halogen lights, the Luxeon LEDs fared well. Using Table 4.8 as a reference, compared to only the proven halogen bulbs available from DeepSea Power & Light (DSPL), both the cyan and green LEDs provided higher initial luminous efficiency based on the manufacturer's specifications for luminous output. Using blackbody curves to simulate halogen outputs, the cyan LED was comparable to both DSPL halogens in terms of initial radiative efficiency, which is a better metric for gauging the LED's performance with a CCD camera. The blue LED had a higher initial radiative efficiency than even the high-color-temperature Oreil 6333 halogen used for illumination standards.

When the lights were simulated propagating through water, the efficiency advantage of the Luxeon LEDs is clear. As shown in Figures 4-30 through 4-33, the blue LED starts out more efficient than any other light source, and suffers the least of all in deep ocean water. Cyan has a slight advantage in loss minimization in WHOI water. As the propagation length increases, the LED lights become more and more efficient, comparatively, with cyan overtaking the 3300 K Oreil light after 5 meters in deep ocean water, and 3.5 meters in WHOI water.

However, LEDs remain the best choice only when a persistent light source is required. The Canon S230 camera, used as the basis of many of the tests, is capable of generating at best two images per second. Even assuming long exposure times of 1/10th of a second, the camera would only require light 20% of the time. For an AUV that will be carrying its light source (instead of making use of an off-the-vehicle light source) and can synchronize its still camera with that source, a strobe light is far and away the best choice in terms of efficiency. An LED, however, can also be made to turn on and off almost instantaneously, so for a small AUV which may not have room for a strobe light, LEDs are a good option. For video applications though, for example a survey vehicle or an ROV, LED lighting is the best choice.

5.1.2 Package size

The Luxeon LEDs have a clear advantage when package size is considered. A single Luxeon V Star 5W LED is smaller than a quarter. The Emitter by itself, which Singh [26] is using in his array, is only 7 mm in diameter and the aluminum structure of the array itself becomes the heatsink. As a function of their construction, LEDs can be used bare, exposed to high-pressure sea-water, with only a protective coating on their electrodes. This is a great advantage over conventional lighting sources, which require bulky pressure vessels.

LEDs also have the ability to scale to meet an application need. Whereas a 50W halogen light has less than half the luminous output of a 100W light, and much less than half of its radiative output, ten LEDs put out exactly one half of the output of twenty. This means that for AUVs or other applications that are extremely power limited, a single LED could be used, while a 5W halogen bulb isn't even worth turning on. In the other direction, even a 10W halogen light would require the same waterproof housing as the 100W bulb. Not counting connectors for either type of light source, two LEDs, even with small reflectors, would take up less than 2% of the volume occupied by the DSPL halogen housing.

Small package size enables creative LED placement as well. A traditional pressure vessel light source is very limited in how it can be attached to a vehicle. With some aluminum for a heatsink, reflectors, and electrical contacts, a 47 element, 235 watt array can be made using Luxeon Emitters and be about the size of a sheet of paper. For an AUV or ROV with an aluminum frame, the frame rails themselves could be the heatsink, enabling very compact light sources incorporated into the structure of the vehicle itself.

5.1.3 Camera Compatibility

As can seen in Appendix section B.1 and in the optimum film speed equivalents of the Canon S230 camera shown in Table 4.5, the camera's response to blue LED light was higher than the camera anticipated with its auto-exposure values. This is both good and bad. The good news is that the assumption of a fairly flat radiative response curve of the CCD is valid. The higher film speed equivalents for the blue LED correlates well with its higher total radiative output given in Table 4.8.

The bad news is that to operate autonomously, the camera must be tricked into under-exposing the image (that is to say correctly exposing the blue channel, drastically underexposing the green channel). The camera's cue for auto-exposure is based primarily on green light sensitivity, so in an environment where green light is attenuated at a much different rate than blue (for example, see Figure 4-30), the required exposure compensation may vary for different total optical path lengths.

The camera's auto-exposure was fairly accurate for the cyan and green LEDs, with an advantage going to cyan for yielding lower exposure times. So, for totally autonomous operation with this particular camera, the cyan LED appears to be the best choice. The Canon showed that it would expose accurately for this LED, and generate two color channels of useful data. However, with exposure compensation, or perhaps a different camera that has a blue-tuned lightmeter, the blue LED is far superior. Its higher radiative output and lower required exposure times make it the best choice if some degree of CCD camera control and compensation can be achieved, and especially if an unmasked, unfiltered black & white CCD camera is used instead of an off-the-shelf consumer camera.

5.2 Wet Testing Conclusions

A great volume of data was generated as a result of the underwater tests. Only one measure of contrast data was extracted from these images. By using other points to measure contrast, or applying an IQM scheme that works, much additional data may remain in these images. The Towtank water proved to be too clear to truly simulate the coastal water encountered at WHOI, so the contrast results were not as dramatic. However, even in the Towtank and especially at WHOI, two noteworthy trends emerged. Placing the light source close to the target, minimizing the incident optical path length, is always preferable. Related to this, minimizing the illuminated water volume will yield better images.

The plotted contrast vs. incident optical path length (OPL) results in Sections 4.4.2, 4.4.3, and B.2 clearly show improved contrast in images resulting from closer illumination. This corresponds with Mertens' [27] guidelines for underwater photography quoted in Section 2.7: "Supplemental light sources placed relatively close to the subject can provide illumi-

nation that is less diffuse and will increase the contrast at the subject." This goes beyond simply properly exposing the image with sufficient light. The camera's auto-exposure should compensate for that effect, and as is shown in B.1, it does so reasonably well, and with a flat contrast response for changing illumination level. Therefore the effect shown is real. In WHOI water especially, where backscatter is a major concern (debris could be seen floating past the ROS Navigator display during the test), placing the light source closer to the target than the camera yielded better results.

This advantage for minimizing the incident OPL seems to be directly related to the illuminated water volume. If all of the water column is illuminated between the target an the camera, backscattered light has more opportunity to adversely affect the image. As the illuminated water volume is minimized, contrast is increased. With a carefully aimed light, the illuminated water volume can be reduced provided there is a large source/receiver separation. For an AUV, however, not only is the maximum separation limited, an aimed system would have to be re-aimed for different fly heights. Also, highly oblique angles of incidence tend to reduce the efficiency of the lighting, as R is not constant but decreases with increased angle of incidence.

An additional advantage to minimizing the OPL is, of course, to reduce the attenuation loss due to propagation through water. The shorter the total OPL can be kept, the more efficient the light source. This means that both the light source and the camera should be close to the target. In a situation where the location of the imaging vehicle cannot be controlled, illumination efficiency will still benefit from placement of the light source near the target.

To summarize, placing the light source close to the target, closer than the camera, has many advantages. It reduces the attenuation loss by minimizing the incident optical path length. The illuminated water volume is minimized which should reduce backscatter. Target contrast is maximized by having a less diffuse light source that better enhances shadows. The implication for AUVs is that anything that can be done to move the light source further from the camera and closer to the target is worthwhile. Whether this be an independent off-the-vehicle lighting system, a partner AUV, or simply placing the light source on a pole, placing the light source closer to the target than the camera appears to improve image contrast and

overall light efficiency. Due to their small package size, LEDs have a great advantage achieve this goal without a lot of bulk.

5.3   LED Candle Suitability

Figure 5-1 shows an LED Candle prototype (production version requires a reflector, and a potted battery pack). Totally disposable, should last about 2-4 hours, and cost less than $50- in materials (retail).

Figure 5-1: LED Candle Prototype

One of the original motivations for this work was to determine whether LED candles could be used by a survey vehicle. Rather than having an AUV carry it's own light source, can it first seed the area with inexpensive and disposable LED candles containing, for example, a single Luxeon 5W LED and a small battery pack.

The results of footprint diameter simulation shown in Figures 4-26 and 4-27 and in Tables 4.6 and 4.7 make it clear that even assuming fairly long exposure times and the optimal ($R = 0.3$, perfectly uniform illumination, etc) case, *for this camera*, namely for the Canon S230, large field illumination using LED candles is not viable. Far too many candles would be needed to cover even a small patch of bottom.

139

However, LEDs are continuing to improve. More importantly, the use of the Canon S230 camera is not a requirement. Using better optics (for example, a lens with a lower f-stop number) and an unmasked, black & white CCD (for example, the type used for astrophotography) that is tuned to take advantage of the blue LED's higher radiative output, much larger footprints would be possible with the same light source.

One additional problem, though, is that as footprint size increases, the height of the LED above the bottom must be increased or else the incident light angle α becomes much too steep at the perimeter, and far too much light is lost to specular reflection. As the LED height is increased, the incident optical path length increases, decreasing the effective illumination as more light is attenuated, not to mention increasing the illuminated water volume. In other words, while LEDs themselves do, LED candles do not scale linearly. Doubling the output of the candle (or doubling the sensitivity or light-gathering ability of the camera), does not double the area of the illuminated footprint.

All is not lost in the LED candle arena, however. LED candles can be used sparingly, one target at a time, rather than as field illumination. Even assuming the worst case, $R = 0.1$, the footprint diameter for a 0.1 second exposure with the blue LED, 1.38 meters, is fairly respectable. A hovering AUV capable of moving slowly enough to make use of such a long exposure time could conceivably drop a single LED candle to mark a target of interest, for example an amphora or a mine. Depending on the level of complexity of the LED candle, it could simply illuminate the target for imaging by the HAUV, or it could have additional functionality, like a one-way LED communication system.

Adding a second LED to act as a pulsed transmitter, a simple one-way LED communication system could be added, making the LED candle into a marker beacon or navigational benchmark that displays a few kilobytes of information to whatever other AUVs pass by. By encoding what AUV left the candle, what it thought the target was, and where it thought it was at the time, the candle could become a waypoint for a network of cooperative AUVs, or for a followup classification survey by a single HAUV. A two-way communication system added to a lighthouse system could be used to selectively illuminate a larger wreck site, for example, allowing the light to be turned off to save power or aimed in a particular direction.

5.4 Summary and Proposed Applications

Due to their small package size, scalability, and efficiency in real ocean water compared to halogen lights, LEDs should be considered as a viable replacement wherever a persistent light source is required. LEDs can be waterproofed leaving their bulbs bare, reducing package size tremendously over light sources that require pressure housings. With the addition of a properly designed reflector, the Luxeon 5W LEDs should be used for AUV applications anywhere a conventional incandescent light is used now.

If a camera can be found to accurately gauge the correct exposure, the Luxeon 5W blue LED appears to be the clear choice for AUV applications, be they vehicle mounted or off-the-vehicle. For use with the Canon S230 camera, the cyan LEDs are the best operational choice, as the camera is capable of properly auto-exposing images using this LED, making autonomous picture-taking easier. However, this combination fails to make use of much of the total radiant output of the LED, as the light is filtered with the CCD mask, and split across two channels. A black & white CCD camera, with better optics and tuned to correctly auto-expose with blue Luxeon 5W LED light, is the best choice for AUV applications.

Although LEDs can be shown to be more efficient than conventional halogen lights, they are still only a viable option when *persistent* light is required, or when backscatter dictates an off-the-vehicle solution. Strobe lights are more efficient for taking individual images, but require synchronization. LED efficiency will similarly benefit from being turn on only during the exposure time of the camera, but this is difficult to predetermine.

Minimizing the illuminated water volume viewed by the camera is cruicial to limiting backscattered light. Using the Odyssey IIc as an example, the light source should be placed on the nose, or even on a boom extension beyond the nose (the small size of LEDs helps make this possible), and aimed straight down to minimize the optical path length and the maximum angle of incidence. Reflectors should be utilized to limit stray light, ensuring that only the target itself and a cone above it is illuminated. The camera should be aimed forward and placed as far back in the vehicle as possible.

To place the light source even closer ot the target, LEDs are the best option for unsynchronized, off-the-vehicle applications, ranging from LED candles to large lighthouse arrays.

Underwater Lighting Application	Suggested Light Source
Persistent light source	Luxeon 5W LEDs
AUV, *B&W* video	Luxeon 5W blue LEDs
AUV, *color* video	Luxeon white LEDs
AUV, still photography	Strobe or switched LEDs
Small AUV, still photography	Luxeon 5W LEDs
AUV, Canon S230	Luxeon 5W cyan LEDs
ROV (video)	Luxeon white LEDs
Off-the-vehicle light	Luxeon 5W LEDs

Table 5.1: A table of suggested lighting sources for different underwater applications.

Though of little use to a survey vehicle, LED candles may be used to mark single targets. A larger AUV, for example a survey vehicle that has onboard processing to identify targets, may be used to drop single LED candles at targets of interest. These LEDs would provide illumination for photographic target classification by additional AUVs, or may serve as navigational benchmarks.

LED technology is continuing to improve. White LEDs have seen the most rapid advancement. For applications where attenuation loss is of less concern, white LEDs may be used to generate true color images using off-the-shelf consumer color digital cameras[1]. Table 5.1 summarizes these results, with suggested light sources depending on application.

The future is looking bright for LEDs. Over the next decade, they will likely make inroads into all manner of industrial and consumer lighting. AUVs will benefit from the many advances in this field and LED lighting will likely replace all manner of conventional persistent light sources.

---

[1]Though not investigated, white LEDs have many of the advantages of monochromatic LEDs. Due to the way the LEDs activate the phosophor compound, the current generation has a radiant output spike in the blue range, bad for photopic response, but actually good for LED applications with CCD cameras. True color images could be taken in clear water. In dirty water, as attenuation loss accumulates, the blue radiant energy still gets through LED defaults to a slightly less efficient monochromatic blue LED.

Appendix A

Comparative Light Specifications

A.1 Nichia LED Specifications and Results

In addition to the Luxeon 5W LEDs, four different Nichia LEDs were tested. These were individual bulb LEDs that had been used in the AUV Lab previously for a number of applications, including UW communications [23] and the LED light array constructed by Saul Rosser [13]. They have a lens base diameter of 5.3 mm and typically operate at 3.5 V at 30 mA. Table A.1 shows the manufacturer's specifications for these bulbs.

The viewing angle, $2\theta_{1/2}$, refers to the total angle subtended where the brightness is above one half of the specified value. In other words, at an angle α measured off the zero axis, where $\alpha = \theta_{1/2}$, the brightness is 50% of the maximum value specified. A good approximation of the total luminous output of the LED is then to assume that the brightness is constant at the specified brightness through the swath subtended by $2\theta_{1/2}$, and zero elsewhere. Using the solid angle Equation 2.3, an approximation of the effective luminous output can be

Nichia LED	Abbrev.	Wavelength Peak (nm)	Brightness (cd)	Viewing angle $2\theta_{1/2}$ degrees	Luminous Output estimate (lm)
NSPE500S	E500	505	9.20	15	0.495
NSPE510S	E510	505	3.92	30	0.839
NSPG500S	G500	525	11.60	15	0.624
NSPG520S	G520	525	2.76	45	1.320

Table A.1: Specifications of four Nichia LEDs

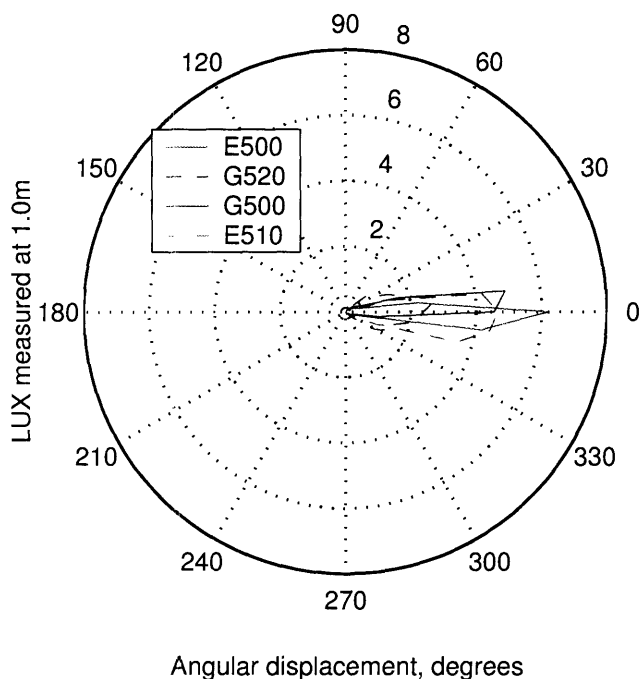calculated. These lumen output estimates are what are shown in Table A.1.

Figure A-1: Measured illumination at 1.0 meters for the four Nichia LEDs tested

Figure A-1 shows the measured illumination pattern of the Nichia LEDs. In a more useful format, Figure A-2 shows the normalized radiative outputs measured for the four Nichia LEDs. This data was used to calculate the measured luminous output given in Table 4.1. This table, and a comparison between the Nichia LEDs and the Luxeon 5W LEDs, is included in Section 4.1.

A.2 Halogen Light Specifications

In order to compare the Luxeon 5W LEDs performance to another real-world system, specifications for three halogen light bulbs were used to generate simulated light sources. Two of the lamps were those supplied by DeepSea Power & Light (DSPL) for use in their Multi SeaLite. The 50W DSPL bulb has been used in the Odyssey IIc vehicle when operated by the MIT Sea Grant AUV Lab. The other lamp was an Oreil model 6333 lamp, used primarily for test instrument calibration. However, it did have a very high color temperature for its

144
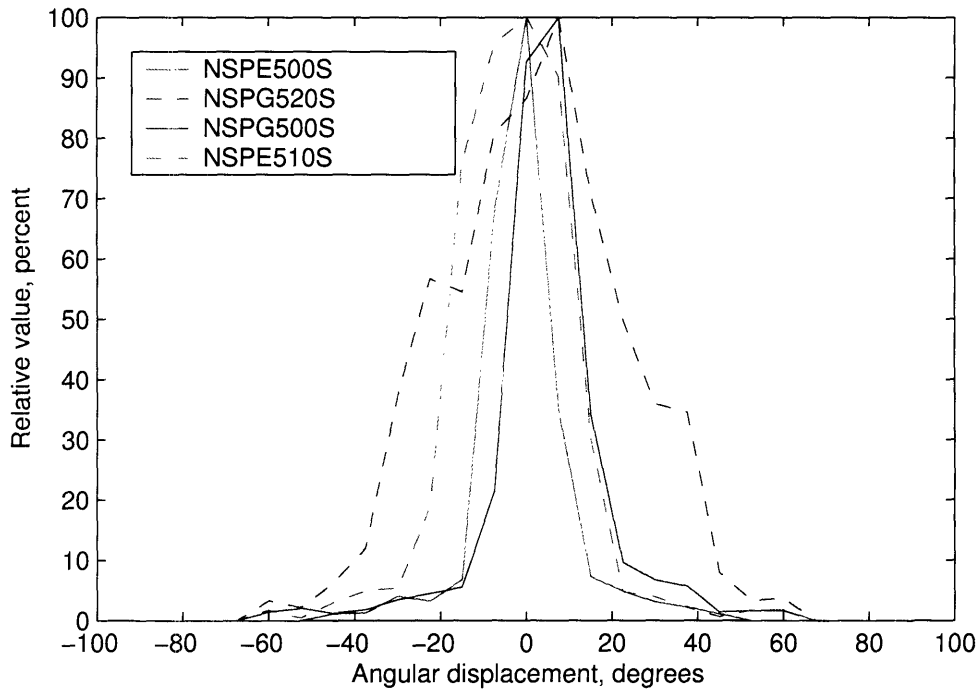
Figure A-2: Normalized output for the four Nichia LEDs tested.

Halogen Lamp	Volts	Watts	Color Temp	Lumens
DSPL BP-12/50	12	50	3000	950
DSPL BP-12/100	12	100	3100	2200
Oreil 6333	12	100	3300	3600

Table A.2: Specifications of the three halogen light sources used to compare to the Luxeon 5W LED lights.

size.

Table A.2 shows the specifications of the lights used for simulations. These lights are almost always referred to by their color temperature, so the 3300 K light would mean the Oreil 6333.

Appendix B

Contrast and Exposure

B.1   Canon S230 Analysis

The single most useful test of the relationship between LED illumination and the Canon camera's performance was one conducted in the MIT Strobe Lab. As described in section 3.3.2, the Canon S230 repeatedly imaged the test target under different light levels. Figure B-1 shows an example image captured during this experiment.

Figure B-1: Test target for contrast and exposure consistency test, illuminated by 5W Cyan LED

Luxeon 5W LED	Current mA	Voltage V	Power W	Target Illumination, lux	Zero exposure time, seconds
Blue	6	5.3	0.32	1.35	0.30
Blue	4	6.8	0.24	5.76	0.07
Blue	700	8.2	5.74	10.21	0.05
Cyan	7	5.3	0.37	3.64	0.60
Cyan	30	6.6	1.98	12.53	0.13
Cyan	700	8.3	5.81	22.40	0.05
Green	8	5.3	0.42	3.53	0.80
Green	30	6.6	1.98	14.44	0.17
Green	700	8.3	5.81	25.40	0.08

Table B.1: Operating voltages and current of the LEDs used in the contrast linearity experiment and the resulting illumination level measured at the center of the target. Zero exposure time refers to the exposure time recommended by the Canon S230 camera. Exposures were bracketed plus and minus two stops from that point in 1/3 stop increments.

The input current to the LEDs was varied in three steps up to its maximum value of 700 mA, dependent on the input voltage. By doing so, the luminous output of the LED could be varied without changing any other parameters (including, most importantly, the beam pattern of the LED, and the shape of the incident light field on the target). At each illumination level, many exposures were taken at different exposure times[1] , so each scene was imaged repeatedly. Table B.1 shows the LED output current, voltage, power, and illumination level at the center of the target.

In order to compare the many images, the total pixel values in regions of neighboring black and white target areas were determined. As described in Section 4.4.1, by differencing the average pixel values in white and black regions, a measure of the total contrast of the image can be determined. This contrast can be measured for each of the channels of the JPEG image, red, green, and blue, as well as for the MATLAB determined grayscale, which combines the three color channels.

Plotted in Figures B-2, B-3, and B-4 are the results of this contrast analysis. For each of the channels of the original JPEG image, as well as for the MATLAB generated grayscale map (which combines the red, green, and blue channels together), the exposure compensation

---

[1]This is known as "bracketing" exposures. The Canon S230 provides exposure time compensation of ±2 stops in 1/3 stop increments. This translates to exposure time of up to four times as long or one fourth as short as what the camera suggests as the optimum exposure time.

(stop) dependent contrast is plotted. Because black and white sections of the target are being compared, absolute contrast varies from 0 (no difference) to 255 (maximum difference). The contrast results are normalized by this 255 factor.

The most important thing to note is that the same basic curve is repeated for each of the three illumination levels (denoted by the three different kinds of lines) within one color channel (denoted by the different line colors). This curve similarity proves that the contrast is independent of the absolute duration of exposure time. In other words, exposure time scales linearly with the inverse of the illumination level, and there is no contrast penalty for extra long or short exposures. The similarity in heights of the peaks of the contrast curves prove that the camera has a linear contrast response. The overlapping nature of the curves also proves that the camera's autoexposure is consistent (in the case of blue LED illuminated scenes, it overexposes the image, but does so consistently. Contrast linearity and autoexposure consistency become very important when comparing the contrast of images taken at different exposure times for different illumination levels.

Another important result that is seen in these plots is the relationship between the color of the illuminating LED and the effective contrast of the resulting image. In many images taken under blue light, The blue channel of the camera saturates. That is to say, white pixels reach a value of 255, as do off-white pixels, creating a plateau of pixel values. See Section 2.6.2 and Figure 2-10 for an explanation of overexposure saturation with a CCD camera. When this occurs, data is lost. Note that this saturation begins to occur in Figure B-2 at the peak of the blue channel curve, at about -1 stop exposure, and worsens for the remaining exposures up to +2 stops. This loss of data is visible as a falloff in contrast. Also, perhaps as a side effect of this overexposure, the red channel begins to register. This may be due to either a bug in the Camera's hardware, or in the way the resulting JPEG image is encoded, but in any case, the red channel appears to hold the "overflow" data from the overexposed blue channel[2]. In an AUV environment, this overexposure is important because it shows that the blue LEDs are not suited to full auto-exposure with the Canon S230 camera.

The peaks of the curves shown in Figures B-2, B-3, and B-4 can be used to estimate

---

[2]When asked about the specifications of the camera's CCD response, Canon stated that it does not publish them.

Exposure Time Based On	Film Speed ASA/ISO Equivalent		
	Blue LED	Cyan LED	Green LED
Blue Channel	1543	103	42
Green Channel	389	184	119
Auto-exposure	709	202	129

Table B.2: The ASA/ISO film speed equivalent response of the Canon S230 digital camera. The response is listed for the camera's blue and green channels as well as its auto-exposure setting for each of the three 5W Luxeon LEDs tested.

the camera's response. Assuming each peak is the "optimum" exposure time for that particular lighting condition, and assuming the reflectance of the target $R = 1.0$ for exposures in air, Equation 2.23 may be used to determine the camera's equivalent film speed. The other quantities (f-stop and luminance, based on illumination level) are known or may be estimated. Table B.2 shows the camera's effective film speed response using exposure times given by the peaks of the blue and green channels, as well as the camera's auto-exposure.

Simulations described in Section 4.5.1 use the optimal ISO film speed equivalents. the blue channel response is used for the blue LED, and the auto-exposure value is used for the cyan and green LEDs, as shown in Table 4.5. The implication of this is that even with a lower luminous output for the blue LED (30 lm, vs 120 for cyan and green), when properly exposed, the Canon S230 will still require shorter exposure times for scenes illuminated with the blue LED, though only one channel of useful data will result. Section 4.5.1 shows graphically.
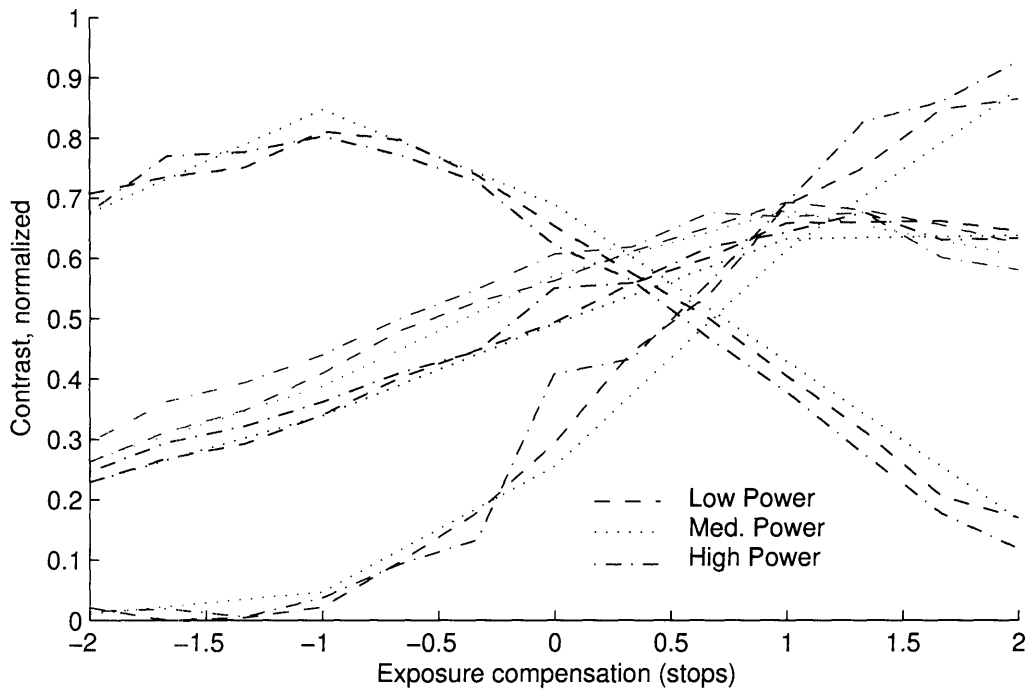
149

Figure B-2: Contrast for three illumination levels (low, medium, and high) for target illuminated by Blue 5W Luxeon LED at bracketed exposures about the camera's recommended exposure. Target illumination is 1.35, 5.76, and 10.21 lux. Colors correspond to color channel of JPEG image (red, green, blue, and grayscale).
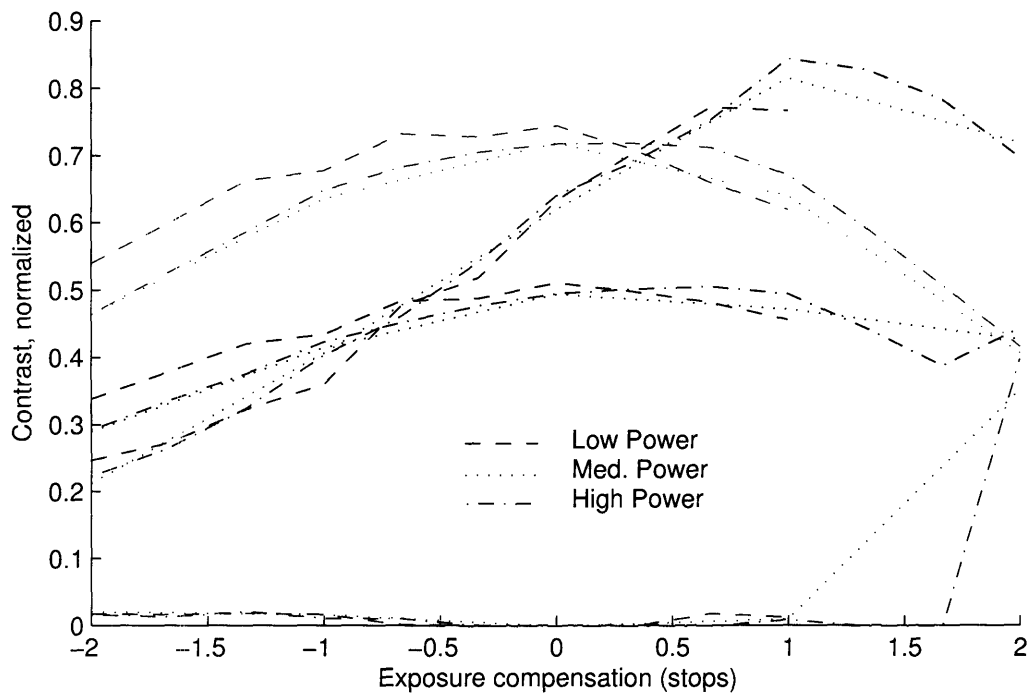
Figure B-3: Contrast for three illumination levels (low, medium, and high) for target illumi-
nated by Cyan 5W Luxeon LED at bracketed exposures about the camera's recommended
exposure. Target illumination is 3.64, 12.53, and 22.40 lux. Colors correspond to color
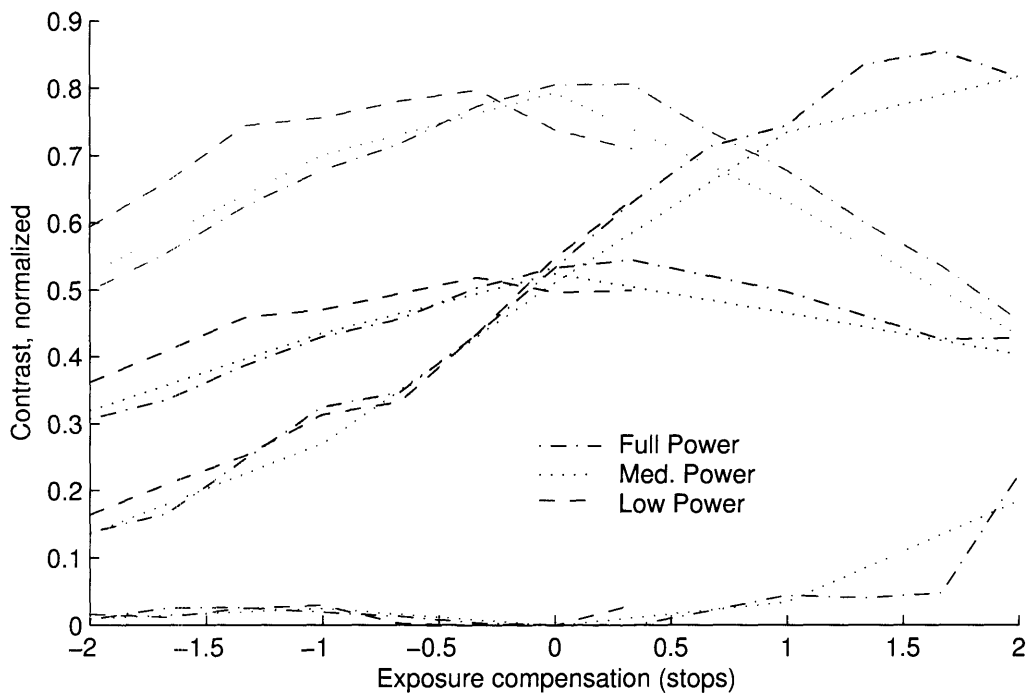channel of JPEG image (red, green, blue, and grayscale).

Figure B-4: Contrast for three illumination levels (low, medium, and high) for target illuminated by Green 5W Luxeon LED at bracketed exposures about the camera's recommended exposure. Target illumination is 3.53, 14.44, and 25.40 lux. Colors correspond to color channel of JPEG image (red, green, blue, and grayscale).

B.2 Additional Contrast Results

Much more data was generated than could easily be placed in Chapter 4. Additional contrast results not shown in Sections 4.4.2 and 4.4.3 are placed here.

B.2.1 WHOI

Figures B-5 and B-6 show the normalized contrast vs. the incident light angle, α, for the green and blue color channels at the most distant camera position. Data from these two plots was used to generate Figure 4-14. Note that the blue LED contrast response at 13° in Figure B-6 is due again to saturation of that channel.
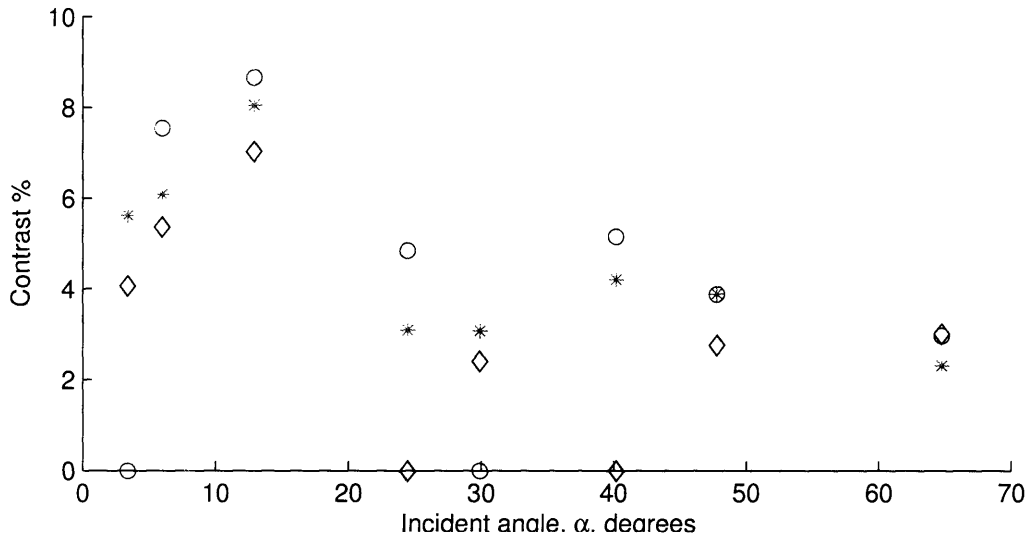

Figure B-5: Green channel contrast response vs. incident angle of illumination, α, at WHOI, of Canon S230 camera for three Luxeon 5W LEDs, blue (diamonds), cyan (stars) and green (circles). Camera is located 2.44 m from the target at an angle $\beta = 26.0°$ from perpendicular.
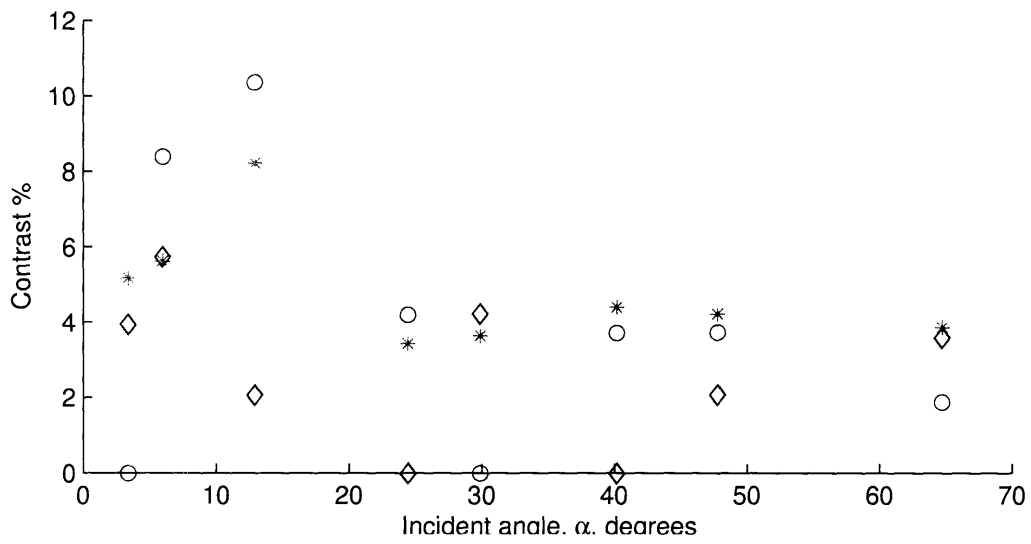
Figure B-6: Blue channel contrast response vs. incident angle of illumination, α, at WHOI, of Canon S230 camera for three Luxeon 5W LEDs, blue (diamonds), cyan (stars) and green (circles). Camera is located 2.44 m from the target at an angle $\beta = 26.0°$ from perpendicular.

B.2.2 Towtank

Figures B-7 through B-13 show the combined blue and green channel contrast response of the Canon S230 digital camera for underwater scenes at the MIT Towtank illuminated by a Luxeon cyan 5W LED. Data from four different camera locations are presented for both the bare cyan LED and the LED with a reflector. Note that the contrast % scale changes in range from one plot to the next.

This data in these figures is analyzed and presented in Table 4.4 and Figure 4-23 in Chapter 4.
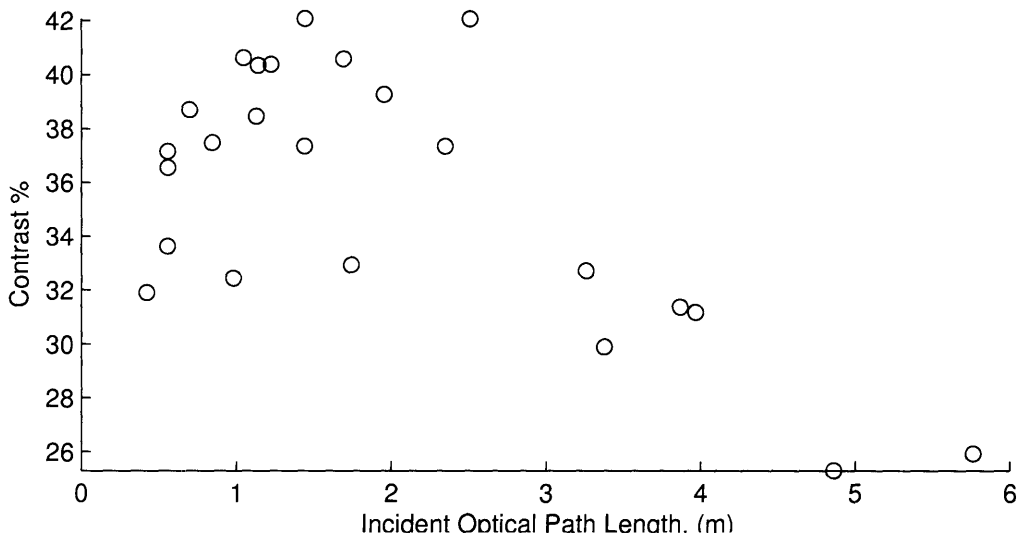

Figure B-7: Combined blue and green channel contrast response vs. incident optical path length of Canon S230 camera for *bare* Luxeon 5W cyan LED, in the MIT Towtank. Camera is located 5.69 m from the target at an angle $\beta = 2.0°$ from perpendicular.
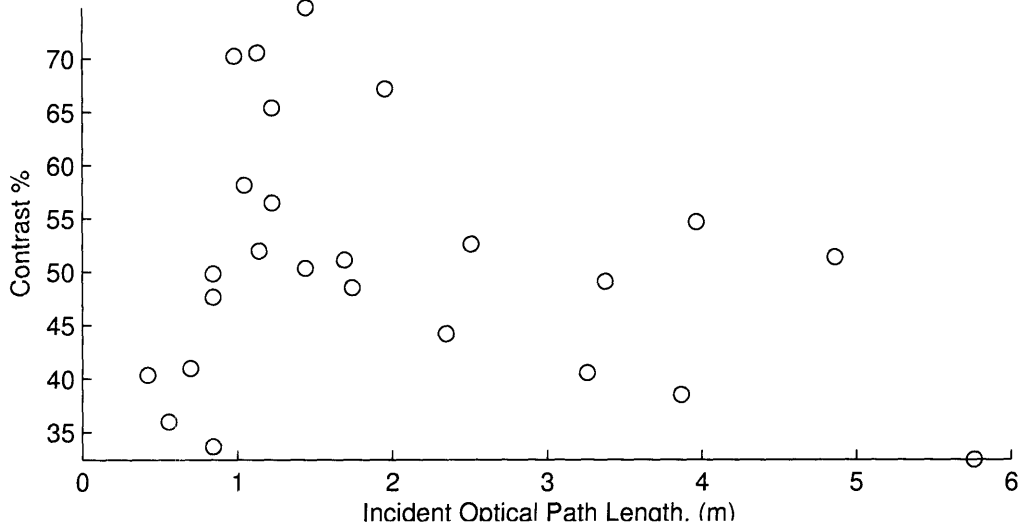
Figure B-8: Combined blue and green channel contrast response vs. incident optical path length of Canon S230 camera for Luxeon 5W cyan LED, with *reflector*, in the MIT Towtank. Camera is located 5.69 m from the target at an angle $\beta = 2.0°$ from perpendicular.
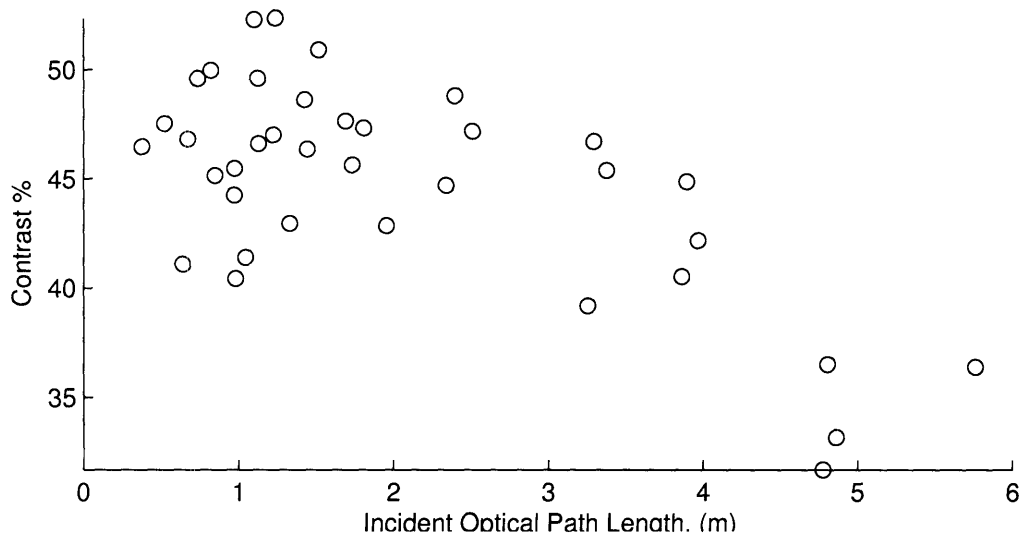

Figure B-9: Combined blue and green channel contrast response vs. incident optical path length of Canon S230 camera for *bare* Luxeon 5W cyan LED, in the MIT Towtank. Camera is located 3.87 m from the target at an angle $\beta = 3.0°$ from perpendicular.

Figure B-10: Combined blue and green channel contrast response vs. incident optical path length of Canon S230 camera for Luxeon 5W cyan LED, with *reflector*, in the MIT Towtank. Camera is located 3.87 m from the target at an angle $\beta = 3.0°$ from perpendicular.
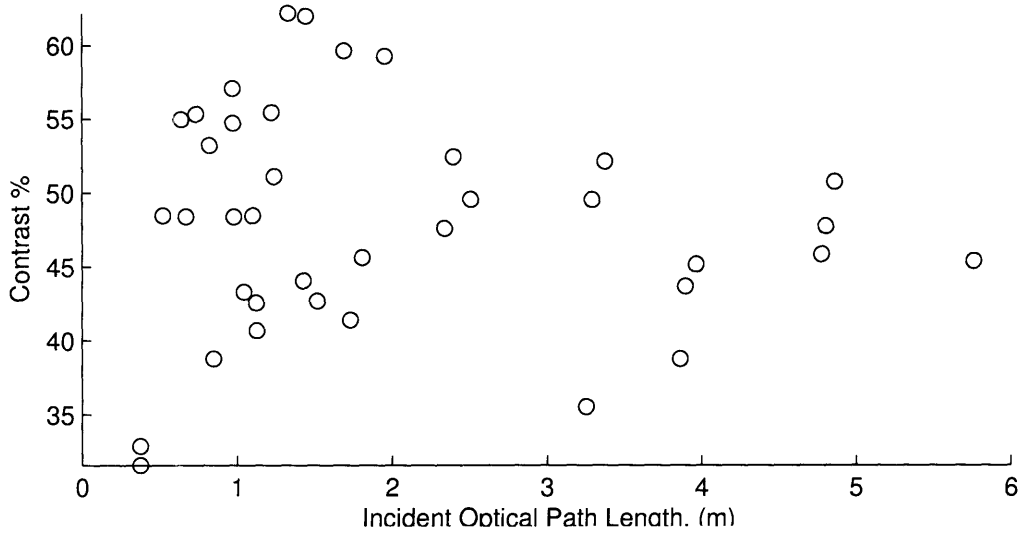

Figure B-11: Combined blue and green channel contrast response vs. incident optical path length of Canon S230 camera for Luxeon 5W cyan LED, with *reflector*, in the MIT Towtank. Camera is located 2.35 m from the target at an angle $\beta = 5.0°$ from perpendicular.

Figure B-12: Combined blue and green channel contrast response vs. incident optical path length of Canon S230 camera for *bare* Luxeon 5W cyan LED, in the MIT Towtank. Camera is located 1.74 m from the target at an angle $\beta = 6.1°$ from perpendicular.
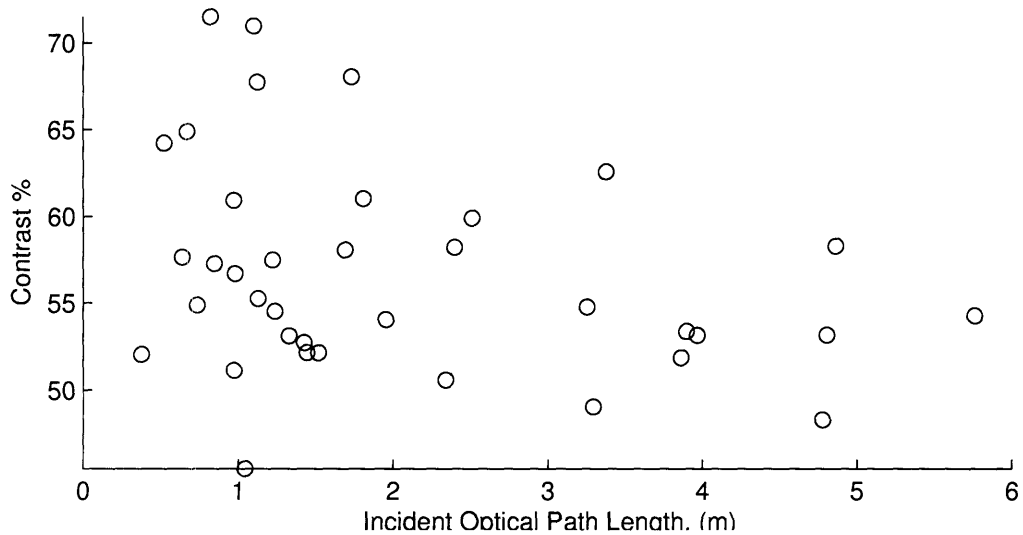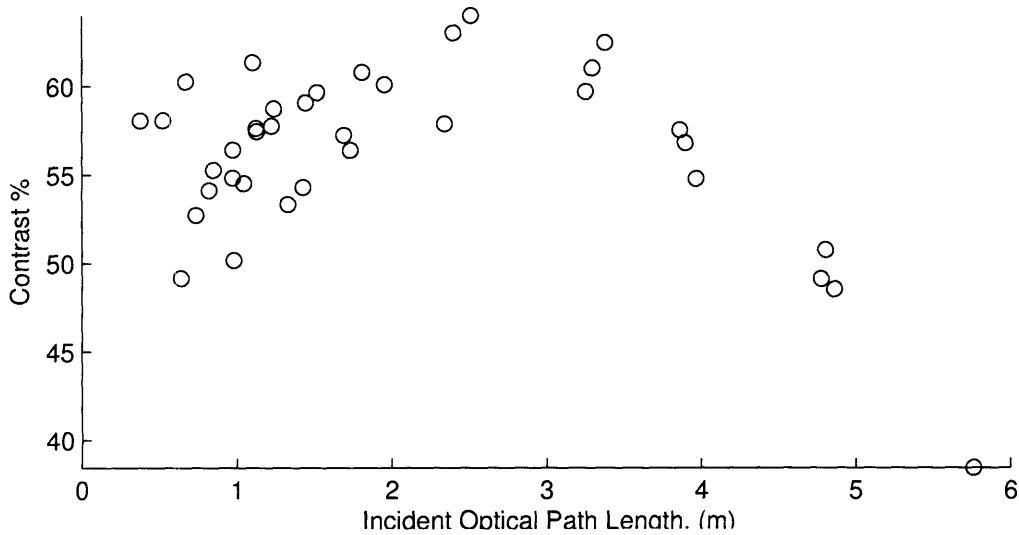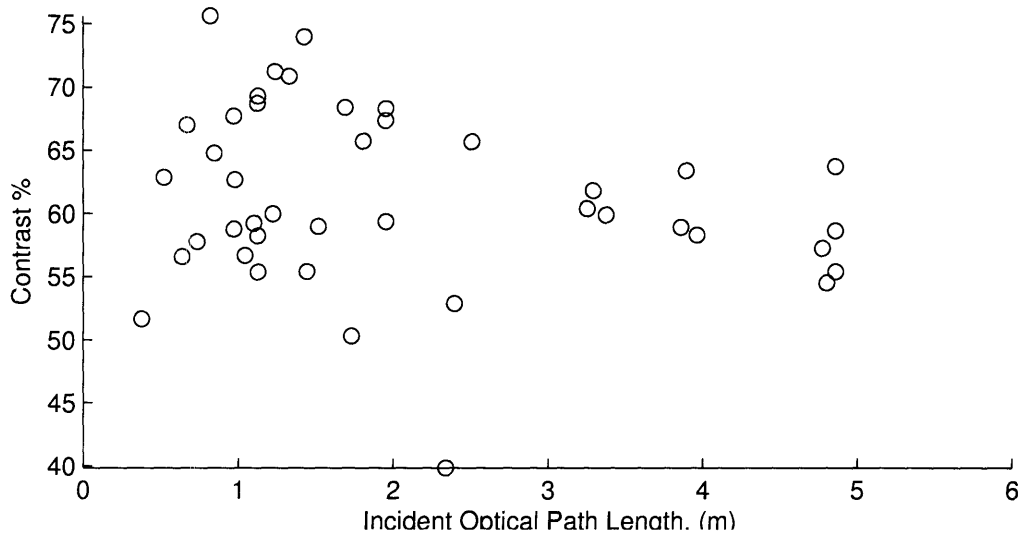

Figure B-13: Combined blue and green channel contrast response vs. incident optical path length of Canon S230 camera for Luxeon 5W cyan LED, with *reflector*, in the MIT Towtank. Camera is located 1.74 m from the target at an angle $\beta = 6.1°$ from perpendicular.

Figures B-14 through B-15 show the combined blue and green channel contrast response of the Canon S230 digital camera for underwater scenes at the MIT Towtank illuminated by a Luxeon cyan 5W LED with respect to α. Data from the closest camera position is presented for both the bare cyan LED and the cyan LED with a reflector. The full range of contrast % (0 to 100%) is shown, making the plot appear fairly smooth. Interestingly, little contrast falloff due to an increase in α is noted, unlike what was noted in Figures 4-15 and 4-18. This may be due to the relative clarity of the water in the Towtank, which tends to minimize the contrast penalty of backscattered light.

Figure B-14: Combined blue and green channel contrast response vs. incident angle of illumination, α, of Canon S230 camera for *bare* Luxeon 5W cyan LED, in the MIT Towtank. Camera is located 1.74 m from the target at an angle $\beta = 6.1°$ from perpendicular.
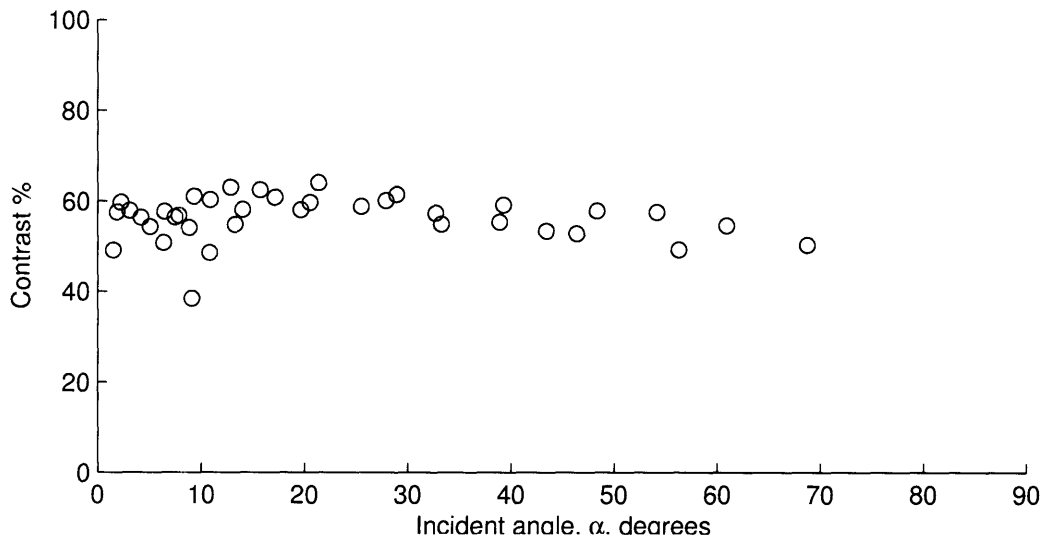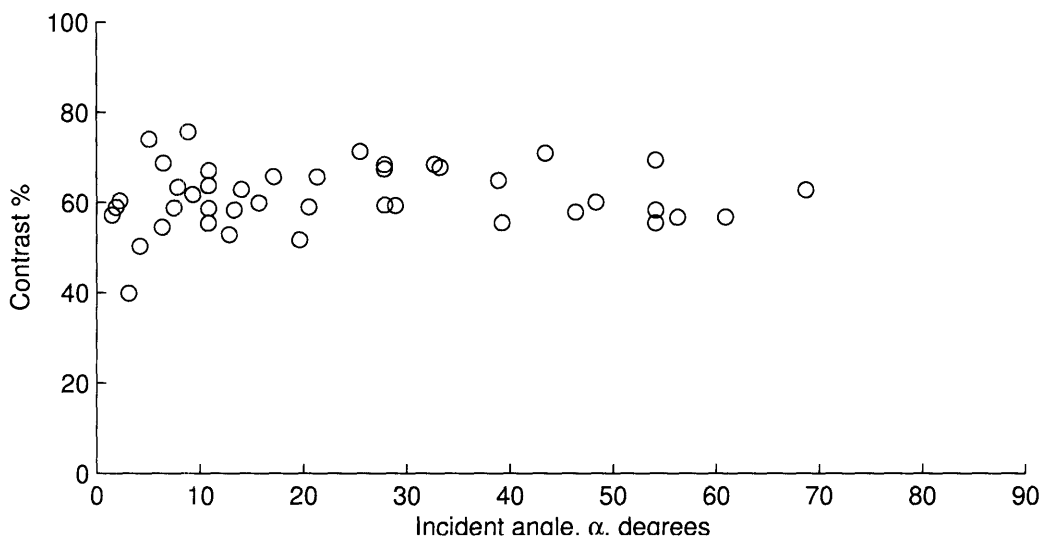
Figure B-15: Combined blue and green channel contrast response vs. incident angle of illumination, α, of Canon S230 camera for Luxeon 5W cyan LED, with *reflector*, in the MIT Towtank. Camera is located 1.74 m from the target at an angle $\beta = 6.1°$ from perpendicular.

Appendix C

Illumination Simulation

In this appendix, background information on the illumination simulations are given. The derivation of the radiative power distribution used as the simulation input is shown. Also shown is the background of the attenuation coefficient curves used for radiative power loss over propagation distance.

C.1   Light Sources

Two types of light sources were simulated. The three Luxeon LEDs, and three 12V halogen bulbs of differing color temperature.

C.1.1   Luxeon LED Lights

In order to simulate the radiative output of the Luxeon 5W LED lights, three probability density functions were employed. Bell curves with a dimensionless integral equal to 1.0 were generated and tweaked by hand to match the curves given in the Luxeon literature.

The simulated curves were then scaled at each wavelength by the IPLF, Equation 2.9. The resulting curve of luminosity vs. wavelength was integrated, with the total integral (which represents the total luminous output) scaled by the specified luminous output of the LEDs shown in Table 3.1. The result was then converted back into radiative units via Equation 2.10.

The resulting radiative power distribution is shown in Figure C-1. This is commonly referred to as the spectral power distribution, though the most proper term is probably the spectral radiative power distribution, as it shows the distribution of radiative power across a spectrum, in this case visible light wavelengths. The relative radiative power distribution for the simulated LED lights is shown in Figure C-2, which corresponds quite well with what is specified by Luxeon and shown in Figure C-3.
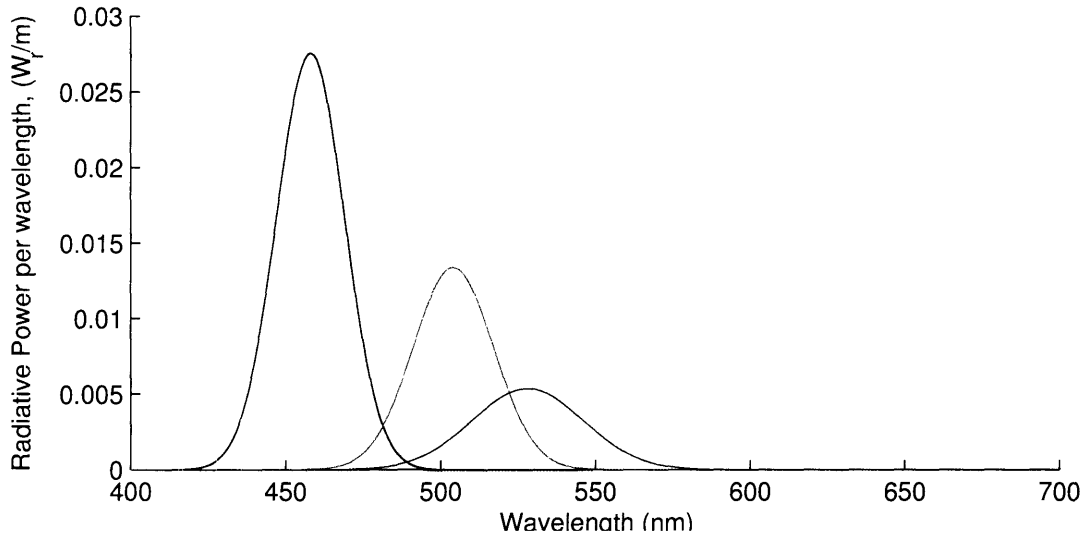

Figure C-1: Absolute radiative power distribution for simulated Luxeon LED lights. From left to right, the curves represent the blue, cyan, and green LEDs

C.1.2 Halogen Lights

For the purpose of comparison, several halogen lights were simulated. The specifications of these lights are given in Table A.2.

The process of generating the simulated radiative power distributions for the simulated halogen lights is very similar to what was done for the Luxeon LEDs. Equation 2.13 was used to create an initial dimensionless distribution. This distribution was converted into lumens per meter by Equation 2.9, and then scaled by the total luminous output given in the manufacturers specifications. The curve was then converted back to radiative units which then had the proper relative values and absolute units.

Figure C-4 shows the absolute radiative power distribution for the three halogen lights
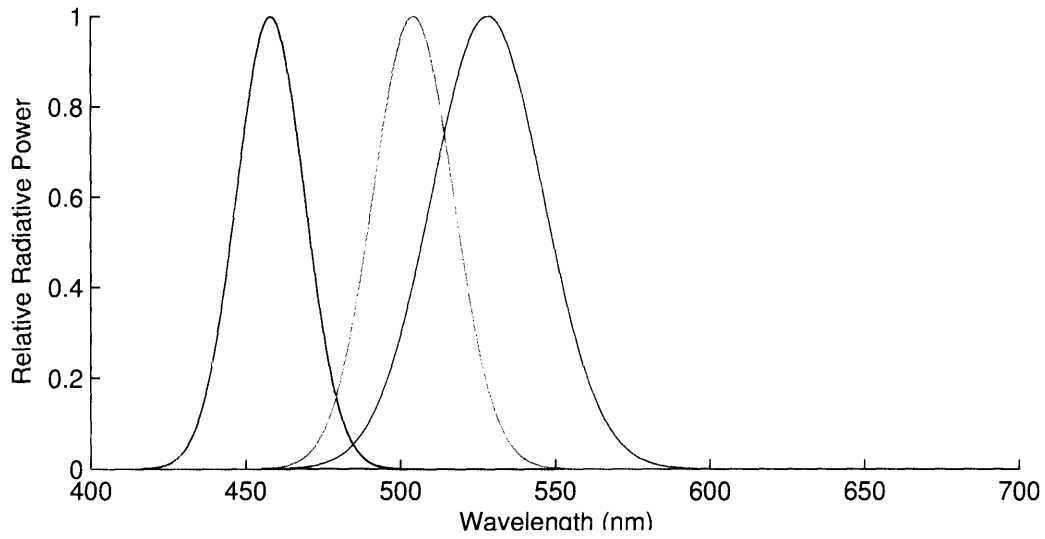
Figure C-2: Relative radiative power distribution for simulated Luxeon LED lights. From left to right, the curves represent the blue, cyan, and green LEDs
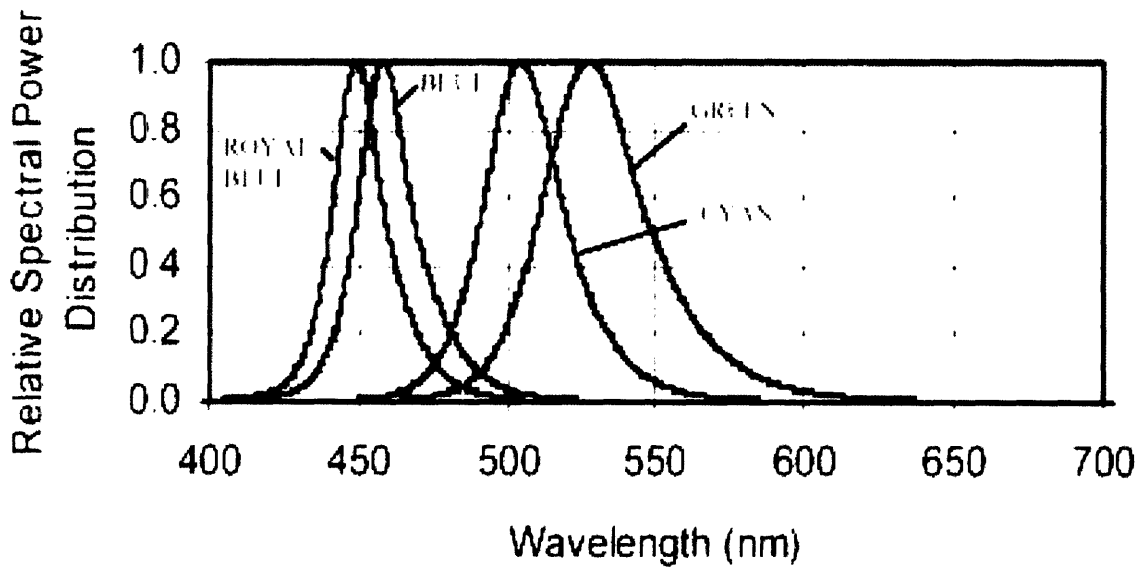
simulated.

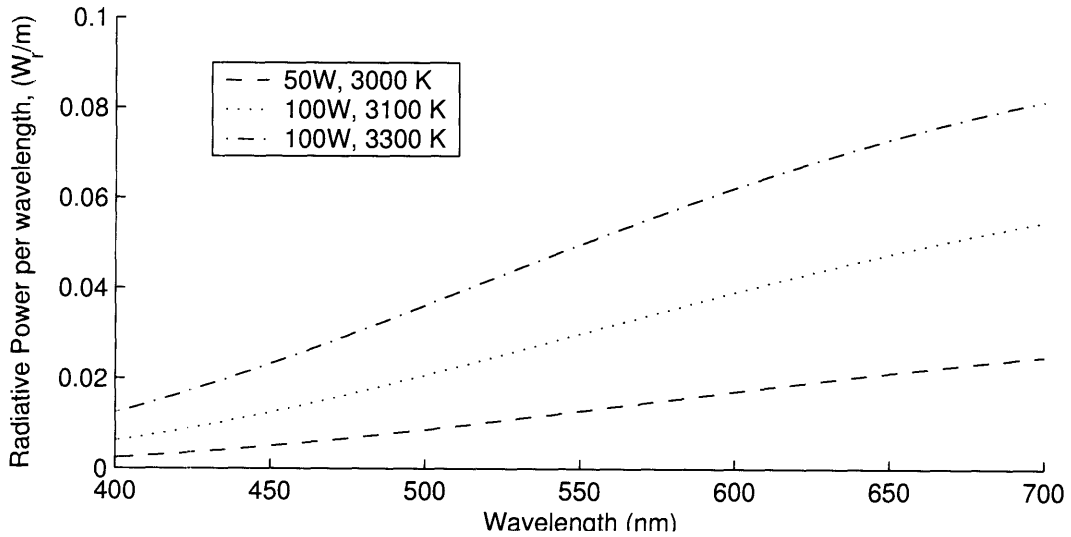Figure C-3: Relative radiative power distribution as specified by Luxeon

Figure C-4: Radiative power distribution for three simulated Halogen lights

164

C.2 Attenuation Coefficient

Two simulated attenuation curves were used. One is similar in appearance to the curve for coastal water given in [9] and used by Palowitch and Jaffe in their simulations [35]. The other is based on the curve for deep ocean water given in [9]. They are similar to curves seen in [27] as well.

In both of the original cases, the wavelengths for which α is given range only from 400 to 600 nm. For the simulations in this work, wavelengths up to 700 nm are desired. In order to fill in the remaining range, an end point value for α at 700 nm was chosen based on the appearance of the distilled water absorption curves. For the simulated WHOI water, the experimentally determined values of α were used, along with the coastal values from Figure 2-6 for the endpoints (α at 400 and 600 nm).

The two curves used for simulations are shown in Figures C-5. Table C.1 displays the values of the attenuation coefficients α_{deep} and α_{whoi} for the simulated water.
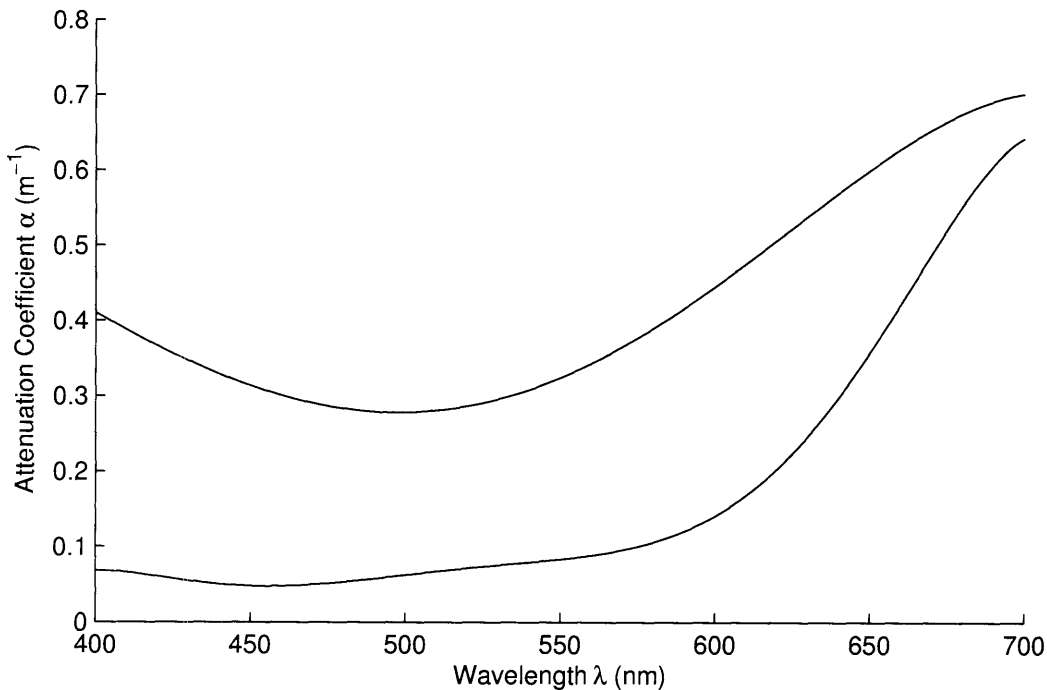

Figure C-5: Attenuation curves of simulated WHOI water(top) and simulated deep ocean water (bottom)

λ (nm)	α_{deep}	α_{whoi}	λ (nm)	α_{deep}	α_{whoi}
400	0.068312	0.41034	555	0.08551	0.33263
405	0.067763	0.39879	560	0.088217	0.34245
410	0.066027	0.38755	565	0.091425	0.35301
415	0.063551	0.37666	570	0.095273	0.36426
420	0.060702	0.36615	575	0.099913	0.37618
425	0.057772	0.35606	580	0.1055	0.38872
430	0.05499	0.34643	585	0.1122	0.40184
435	0.05253	0.33731	590	0.12018	0.4155
440	0.050511	0.32871	595	0.12958	0.42964
445	0.049012	0.32068	600	0.14057	0.44422
450	0.048072	0.31325	605	0.15329	0.45917
455	0.047701	0.30645	610	0.16785	0.47442
460	0.04788	0.30031	615	0.18437	0.48992
465	0.048571	0.29486	620	0.20293	0.50558
470	0.049721	0.29012	625	0.22357	0.52134
475	0.051265	0.28611	630	0.2463	0.53709
480	0.053129	0.28286	635	0.27109	0.55277
485	0.05524	0.2804	640	0.29785	0.56828
490	0.057522	0.27872	645	0.32645	0.58352
495	0.059904	0.27786	650	0.35668	0.59838
500	0.062323	0.27781	655	0.38827	0.61276
505	0.064722	0.2786	660	0.42084	0.62655
510	0.067059	0.28024	665	0.45397	0.63963
515	0.069303	0.28271	670	0.48711	0.65187
520	0.071438	0.28604	675	0.5196	0.66314
525	0.073464	0.29021	680	0.55069	0.6733
530	0.075399	0.29523	685	0.57949	0.68223
535	0.077276	0.30108	690	0.60496	0.68976
540	0.079148	0.30776	695	0.62595	0.69574
545	0.081085	0.31526	700	0.64113	0.70001
550	0.083171	0.32355			

Table C.1: The values of the attenuation coefficients used to simulate deep ocean water, α_{deep}, and ocean water similar to that encountered at WHOI, α_{whoi}, at a wavelength λ, sampled every 5 nm.

Bibliography

[1] Leslie Lamport. *LaTeX: a document preparation system*. Addison-Wesley Publishing Company, 2nd edition, 1994.

[2] H.A.E. Keitz. *Light Calculations and Measurements: An Introduction to the System of Quantities and Units in Light-Technology ant to Photometry*. St. Martin's Press, Inc., 1971.

[3] A. Morel. Optical properties of pure water and pure seawater. *Optical Aspects of Oceanography*, pages 1–24, 1974.

[4] Robert H. Stewart. *Introduction to Physical Oceanography*. Texas A & M University, 2003.

[5] M.R. Querry, D.M. Wieliczka, and D.J. Segelstein. Water (H_2O). In *Handbook of Optical Constants of Solids II*, pages 1059–1077. Academic Press, 1991.

[6] R.M. Pope and E.S. Fry. Absorption spectrum (380–700 nm) of pure water. II. integrating cavity measurements. *Appl. Opt.*, 36:8710–8723, 1997.

[7] H. Buiteveld, J.M.H. Hakvoort, and M. Donze. The optical properties of pure water. In J. S. Jaffe, editor, *SPIE Proceedings on Ocean Optics XII*, volume 2258, pages 174–183, 1994.

[8] K.S. Shifrin. *Physical Optics of Ocean Water*. American Institute of Physics, 1988.

[9] C.J. Funk, S.B. Bryant, and P.J. Heckman Jr. *Handbook of Underwater Imaging System Design*. Naval Undersea Center, Ocean Technology Department, 1972.

[10] William DesJardin and Stephen Kosman. True two-phase ccd image sensors employing a transparent gate. Technical report, Eastman Kodak Company, Microelectronics Technology Division, Rochester, New York, 1999.

[11] E.J. Meisenzahl, W.C. Chang, W. DesJardin, H.Q. Doan, J.P. Shepherd, and E.G. Stevens. A 3.2 million pixel full-frame true 2ϕ ccd image sensor incorporating transparent gate technology. Technical report, Eastman Kodak Company, Image Sensor Solutions, Rochester, New York, 2001.

[12] Jim Bales. MIT Edgerton Center, Cambridge, MA. personal communication.

[13] Saul Rosser. Underwater photographic lighting using light emitting diodes. Master's thesis, Massachusetts Institute of Technology, 2003.

[14] Alex Ryer. *Light Measurement Handbook*. International Light, 1998.

[15] Hugh D. Young. *University Physics*. Addison-Wesley, eigth edition, 1992.

[16] M.S. Twardowski, E. Boss, J.B. Macdonald, W.S. Pegau, A.H. Barnard, and J.R.V. Zaneveld. A model for estimating the bulk refractive index from the optical backscattering ratio and the implications for understanding particle composition in case i and case ii waters. *Journal of Geophysical Research*, 106(7), July 2001.

[17] N.G. Jerlov. *Marine Optics*. Elsevier Scientific Publishing Company, 1976.

[18] Siebert Q. Duntley. Light in the sea. *Journal of the Optical Society of America*, 53, February 1963.

[19] D.A. Steigerwald, J.C. Bhat, D. Collins, R.M. Fletcher, M.O Holcomb, M.J. Ludowise, P.S. Martin, and S.L. Rudaz. Illumination with solid state lighting technology. *IEEE Journal on Selected Topics in Quantum Electronics*, 8(2):310–320, 2002.

[20] David Talbot. Leds vs. the lightbulb. *Technology Review*, 106(4), May 2003.

[21] R. Scott Kern. Light-emitting diodes in automotive forward lighting applications: materials engineering solutions to fundamental challenges. Presentation to sae conference, Lumileds Lighting, 2004.

[22] J.W. Bales and C. Chryssostomidis. High-bandwidth, low-power, short-range optical communication underwater. Technical report, MIT Sea Grant College Program.

[23] Damien Sanoner. Underwater wireless light communication. Technical report, MIT Sea Grant AUV Lab, 2003.

[24] Dwight F. Coleman, James B. Newman, and Robert D. Ballard. Design and implementation of advanced underwater imaging systems for deep sea marine archaeological surveys. *Institute for Exploration*, 2000.

[25] Dwight Coleman. Institute for Exploration, Mystic, CT. personal communication.

[26] Hanumat Singh. Woods Hole Oceanographic Institute, Woods Hole, MA. personal communication.

[27] Lawrence E. Mertens. *In-Water Photography, Theory and Practice*. Wiley-Interscience, 1970.

[28] Willard H. Wells. Loss of resolution of water as a result of multiple small-angle scattering. *Journal of the Optical Society of America*, 59, 1969.

[29] Jules S. Jaffe. Computer modeling and the design of optimal underwater imaging systems. *IEEE Journal of Oceanic Engineering*, 15(2), April 1990.

[30] Norman B. Nill and Brian H. Bouzas. Objective image quality measure derived from digital image power spectra. *Optical Engineering*, 31(4):813–825, April 1992.

[31] Zhou Wang, Hamid R. Sheikh, and Alan C. Bovik. No-reference perceptual quality assessment of jpeg compressed images. In *IEEE International Conference on Image Processing*, September 2002.

[32] İsmail Avcibaş, Bülent Sankur, and Khalid Sayood. Statistical evaluation of image quality measures. *Journal of Electronic Imaging*, 11, April 2002.

[33] Rafael Garcia, Tudor Nicosevici, and Xevi Cufi. On the way to solve lighting problems in underwater imaging. In *Oceans 2002 Proceedings*, 2002.

[34] Curtis D. Mobley. *Light and Water: Radiative Transfer in Natural Waters*. Academic Press Inc, 1994.

[35] Andrew W. Palowitch and Jules S. Jaffe. Computer model for predicting underwater color images. In *SPIE Proceedings, Underwater Imaging, Photography, and Visibility*, volume 1537, pages 128–139, 1991.

[36] Katsumi Tadamura and Eihachiro Nakamae. Modelling the colour of water in lighting design. In *Computer Graphics: Developments in Virtual Environments*, pages 97–114. Academic Press, 1995.

[37] E. Cerezo and F.J. Seron. Synthetic images of underwater scenes: A first approximation. In *Ninth International Conference in Central Europe on Computer Graphics, Visualization and Interactive Digital Media (WSCG 2001)*, Plzen, Czech Republic, 2001.